Characterization of *DAP1*/*YPL170W*: the *Saccharomyces cerevisiae* Membrane Associated Progesterone Receptor (MAPR) Homologue

A Dissertation
Presented To
The Academic Faculty

By

Chris Banna

In Partial Fulfillment
Of the Requirements for the Degree
Doctor of Philosophy in Molecular Biology

Georgia Institute of Technology
December 2004

Characterization of *DAP1*/*YPL170W*: the *Saccharomyces cerevisiae* Membrane Associated Progesterone Receptor (MAPR) Homologue

Approved by:

Dr. Jung H Choi
School of Biology
Georgia Institute of Technology

Dr. Dwight H. Hall
School of Biology
Georgia Institute of Technology

Dr. Thomas G. Tornabene
School of Biology
Georgia Institute of Technology

Dr. Donald F. Doyle
School of Biology
Georgia Institute of Technology

Dr. Yury O. Chernoff
School of Biology
Georgia Institute of Technology

Date Approved:

January 2005

ACKNOWLEDGEMENTS

I would like to thank my advisor Dr. Jung H. Choi for his patience and support over the course of this study. I would like to thank the members of my committee; especially Dr. Thomas G. Tornabene for his constant help and encouragement, Dr. Yury O. Chernoff, Dr. Dwight H. Hall, and Dr. Doyle, for investing their time and energy reviewing this thesis and providing helpful advise. I would, also, like to especially thank Dr. Gunther Holzer, for his great insight, help, teaching and wisdom with the GC and the MS interpretation.

I would like to acknowledge the following people for their help and insight over the years: Gary Newman, for providing strains, plasmids, reagents, and insights into yeast biology; Dr. Renee Wegrzyn, for her friendship and her helpful suggestions on working with yeast; Dr. Phillip Gray and Dr. Hosoon Choi who taught me the basics of molecular biology. The undergraduates who worked for me and provided much help, Vincent Scoglietti and Sherman Ku, much luck in the future. I would also like to thank all the faculty who graciously allowed me to use their equipment and provided me with useful suggestions.

I would like to thank my climbing peeps who have provided a much needed getaway from the rigors of academic life.

Finally, I would like to dedicate this thesis to my parents and my brother, whom have been very supportive and without their constant help, love and encouragement, none of this would have been possible.

TABLE OF CONTENTS

LIST OF TABLES

LIST OF FIGURES

LIST OF SYMBOLS AND ABBREVIATIONS

25-Dx: Rat homolog of the human MAPR, 25-KDa protein induced by dioxin

ADP : Adenosine DiPhosphate

ATP : Adenosine TriPhosphate

Atmp: Arabidopsis thaliana membrane progesterone receptor

CHO: Chinese Hamster Ovary

CMV: Cytomegalovirus

CNS: Central Nervous System

Dap1: Damage response protein related to membrane progesterone receptor

Dg6: Human membrane associated progesterone receptor component 2

EGFP: Enhanced Green Fluorescence Protein

ER: Endoplasmic Reticulum

F_1F_2 ATP synthase : Adenosine TriPhosphate synthase

$GABA_A$: gamma-aminobutyric acid receptor A

GFP: Green Fluorescence Protein

Gpd: glyceraldehyde-3-phosphate dehydrogenase

HEK: Human Embryonic Kidney cells

HeLa: Henrietta Lacks, immortal mammalian cell line

$HERC_2$: Human protein, guanine nucleotide exchange factor

Hpr6.6: Human Progesteron Receptor

IZAg: Inner Zonal Antigen

LiAc/PEG: Lithium Acetate/PolyEthylene Glycol

MAPR: Membrane Associated Progesterone Receptor

mPR: membrane Progesterone Receptor, porcine

Nfs^- : Yeast unable to grow on non-fermentable source

P_i : inorganic phosphate

PBS: Phosphate Buffered Saline solution

PCR: Polymerase Chain Reaction

RFP: Red Fluorescence Protein

RFP2: Red Fluorescence Protein 2

SD: Synthetic Dropout yeast media

SLAD: Synthetic Low Ammonium Dextrose

SPD: Synthetic Proline Dextrose

TE: Tris-EDTA

URA: Uracil

Vem-1: *Caenorhabditis elegans* orthologue of Ventral midline antigen-1

VEMA: Ventral Midline Antigen

YPD: Yeast Peptone Dextrose media

YPG: Yeast Peptone Glycerol

Ypr118w: Yeast systematic name for protein, 5-methylthioribose-1-phosphate isomerase

SUMMARY

Steroid production requires an enormous energy requirement from the cell. The pathway responsible for the production and metabolism of cholesterol in mammalian systems is complex and is the focus of intensive study. Steroids in multicellular organisms are thought of classically to have one primary cellular effect: alteration of nuclear transcription characterized by a latency period between signal and effect. Classical steroid binding proteins are members of the nuclear receptor superfamily. They bind to steroids in either the cytosol or nucleus, dimerize, then migrate to the nuclear genome and act as transcription factors. Recent research suggests some steroids may be involved in a rapid onset of cellular effects not caused by an alteration in gene expression. Membrane binding sites for progesterone have been described and, at least in part, characterized in tissues or cells exhibiting non-genomic progesterone actions, thus pointing to a link between putative membrane receptors and rapid steroid effects.

MAPRs (Membrane Associated Progesterone Receptors) have been implicated in mediating a number of rapid cellular effects not involving changes in gene expression. MAPRs have no significant sequence similarity to classical steroid receptors. The MAPR homologues as a group have been suggested to play widely varying roles from axon guidance, to steroid hydroxylation and steroid metabolism, to influencing reproductive behavior. Their specific role has not yet been clearly demonstrated in any organism.

Dap1p is the yeast homologue of MAPR. Although yeast do not produce steroid compounds they do produce sterols, which are precursor to steroids.

Statement of the Problem

Deletion of *DAP1* in haploid strains produced an altered sterol profile. The goal of this study was to further characterize this protein genetically and biochemically in order to try and better understand the role Dap1p performs in sterol metabolism.

Specific Objectives

The first objective was to characterize the growth rate of the *dap1*Δ mutant strain and the *ypr118w*Δ mutant strain in various media and determine how these rates compared to the growth rate of the control strain. Also, the strains were grown in competition experiments against the control in YPD medium, SLAD medium, and SPHD medium. The data demonstrated there is no significant difference in growth rates in YPD medium. In SLAD medium (nitrogen starvation) the *dap1*Δ mutant strain outcompeted the control strain, and the control strain outcompeted the *ypr118w*Δ mutant strain. In SPHD medium (nitrogen limiting), there was no significant difference in the growth rates between the *dap1*Δ mutant strain and the control stain, but the *ypr118w*Δ mutant strain exhibited a slower growth rate as compared to the control strain.

The second objective was to determine and characterize the localization pattern(s) of Dap1p and Ypr118wp. The Dap1p-GFP fusion protein localized to lipid particles. The Dap1p-GFP fusion protein also localized peri-nuclearly, suggesting it also localizes to the ER. The Ypr118w-RFP2 fusion protein localized to lipid particles and co-localized with Dap1p-GFP when expressed in the same cell.

Upon addition of MMS to cells transformed with *DAP1*-GFP, the Dap1p-GFP fusion protein still localized to lipid particles, but the protein exhibited a higher percentage to localize peri-nuclearly.

The third objective was to determine the localization pattern exhibited by Hpr6.6p-GFP under normal growth conditions and also in the presence of MMS in HeLa cells. Hpr6.6p-GFP localized to the ER in HeLa cells under normal conditions and upon addition of MMS.

The fourth objective was to show if the *dap1*Δ mutant strain was sensitive to MMS as compared to the control strain. The *dap1*Δ mutant strain exhibited a higher sensitivity to YPD plates supplemented with MMS as compared to control, the *ypr118w*Δ mutant strain did not exhibit any increased sensitivity as compared to the control stain, and the *dap1*Δ*/ypr118w*Δ double mutant strain exhibited sensitivity compable to the *dap1*Δ mutant strain.

The fifth objective was to determine if the *dap1*Δ mutant strain, the *ypr118w*Δ mutant strains, and the *dap1*Δ*/ypr118w*Δ double mutant strain exhibited elevated petite formation as compared to the control strain. The *dap1*Δ mutant strain and the *dap1*Δ*/ypr118w*Δ double mutant strain exhibited increased petite formation, the *ypr118w*Δ mutant strains did not exhibit increased petite formation as compared to the control strain.

The sixth objective was to determine and characterize the free sterol profiles and the steryl ester profiles of the control strain and the *dap1*Δ mutant strain at 1 day old culture and 2 day old cultures. The *dap1*Δ mutant strain exhibited significant altered sterol profile in both the free sterol fraction and the steryl ester fraction as compared to

the control strain. Addition of Dap1p under the control of the constitutive promoter, Gpd, to the *dap1*Δ mutant strain increased total sterol content to levels almost consistent with levels in the control strain, but with significant and, perhaps, elucidating differences between the strains. Upon addition of Hpr6.6p under the control of the copper promoter, CUP1, both the control strain and the *dap1*Δ mutant strain exhibited increased ergosterol production in both the free sterol fraction and the steryl ester fraction when Hpr6.6p was expressed in these strains. These data are consistent with the hypothesis that the primary function of Dap1p is in cellular sterol metabolism. Dap1p localized to lipid particles and to the ER, known sites of sterol biosynthesis. Deletion of *DAP1* resulted in a reduction of ergosterol and accumulation of alternative late-stage intermediates in the ergosterol biosynthesis. Overexpression of either Dap1p or Hpr6.6, the human homolog, in the *dap1*Δ mutant strain resulted in elimination of the alternative intermediates and restoration or dramatic increase in ergosterol levels

INTRODUCTION

Membrane Associated Progesterone Receptors (MAPRs)

Enzymes involved in cellular steroid perception can be broken down into two major categories; those enzymes that bind steroids/steroid precursors that are involved in the production of specific steroids and those enzymes that bind steroids which are involved in mediating a response to the steroids produced. Cholesterol serves as bulk membrane support in mammalian cells. But, cholesterol is also the precursor to steroid compounds in mammals. Cholesterol production, utilization, and enzymatic transformation to steroid compounds in mammalian systems have been intensively studied, yet many questions still remain.

Two different routes of cellular effects are mediated by steroids; genomic and non-genomic. The classical pathway of action of steroid hormones and related compounds is mediated by the binding of the steroid hormone to specific nuclear receptors. These receptors then bind to nuclear DNA, alters the transcription of genes and, thus, affect the eventual alteration of a variety of cellular functions [3,4]. This mode of action is characterized by a latency period between steroid signal reception and cellular effects. The nuclear steroid hormone receptors elicit a response characterized by a substantial delay of a few hours to days [4]. To date, the most rapid steroid hormone effect on transcription is for glucocorticoids effect on mouse mammary tumor virus long terminal repeat in mouse L(tk aprt) cells, in which transcription was detectable within 7.5 minutes after glucocorticoid application [5]. Classical receptors include members of the steroid/thyroid hormone receptor superfamily [9]. These are characterized by a helical

sandwich structure which binds the steroid ligand [10]. These receptors can be located in the nucleus or cytosol. Upon binding of ligand, steroid receptors dimerize and migrate to the nuclear genome, whereupon they act as transcription factors [9].

Recently, there has been great interest focused on the characterization of non-genomic responses to steroid/hormone compounds. Recent observations support the existence of a non-genomic response to steroid compounds, characterized by rapid onset of cellular response. These response times can be anywhere from a few seconds to a few minutes [17]. Progesterone was the first of these examples; it was demonstrated to produce a rapid anesthetic effect in the central nervous system [7]. This has recently been determined to be mediated by an effect progesterone has on $GABA_A$ receptors [15]. Rapid effects have now been described for most classes of steroids [8]. Each steroid seems to be able to produce many different rapid responses. In the individual case of progesterone, such rapid effects include: the previous described anesthetic effect in the CNS, calcium influx and chloride efflux in sperm during the acrosome reaction [11,12], depolarization of rat hepatocytes by decreasing the cell-membrane potassium conductance [13], calcium influx in *Xenopus* oocytes [14], and, more recently, inhibition of the action of oxytocin through direct binding to the uterine oxytocin receptor [16].

The time dependence of different actions of steroid presents a useful way of categorizing different types of steroid action. Very rapid effects like ion fluxes, triggering of action potentials, or discharge of secretory vesicles happen within a timeframe of seconds to minutes. Somewhat slower responses might arise from the activation of enzymes or pumps, whose product would be generated immediately, but would only build up to detectable and functional levels over time. Long-term responses,

such as those that are associated with gene expression mediated by steroid receptors acting as transcription factors, require events that eventually alter functional or structural proteins or their levels. Finally, very long-term events may develop over the maturational time course of the organism to produce permanent developmental tissue remodeling. A number of different novel steroid receptors, or even splice variants, are likely to be involved in mediating these different non-genomic actions of steroid.

A putative membrane-associated steroid receptor (MAPR) with high affinity for progesterone was first identified in porcine liver membranes [25]. This paper and later papers by the same group suggested that MAPRs elicit a non-genomic response to progesterone or derivatives, without providing concrete evidence of actual progesterone binding by MAPRs. This porcine protein, named mPR, was later cloned and sequenced from porcine vascular smooth-muscle cells [18]. CHO cells transfected with the coding sequence for the porcine mPR demonstrated an increase in microsomal progesterone binding, *in vitro* [24]. Antibodies raised against recombinant porcine mPR inhibited the progesterone-initiated Ca^{2+} flux in human sperm [24]. In addition, rabbit antibodies raised against a synthetic peptide, corresponding to the first 15 N-terminal amino acid sequence of the porcine mPR, inhibited the progesterone-initiated acrosome reaction of human sperm, and revealed localization to the plasma membrane [26]. Although these events are very suggestive, no direct evidence for progesterone binding *in vivo* or *in vitro* to mPR has yet been presented. Sub-cellular fractionation studies in porcine hepatocytes and immunofluorescence in HEK cells transfected with porcine mPR identify porcine mPR to be localized on the ER and Golgi apparatus [27].

Subsequently, homologous MAPR sequences in human [19], rat [20], mouse [21], and yeast [22] were cloned. Homologues sequences are also found, but not limited to, and studied in mouse (two sequences), cow, *C. elegans*, *Arabidopsis thaliana* (five sequences), and *Oryza sativa* (two sequences) [23]. These sequences were found to bear no significant sequence similarity to the classical genomic intracellular receptors. But, these sequences of the MAPR family, along with sequences of some fungal chitin synthases and $HERC_2$ proteins, have been identified as being distantly related to the cytochrome b_5 family of proteins, which bind heme [23]. MAPRs do not appear to bind heme or to be involved in redox reactions, since they all lack the pair of heme-coordinating histidine residues [23]. This suggests the heme binding site of cytochrome b_5 may have served as a template for the evolution of novel ligand-binding pockets, such as the steroid binding site in MAPRs.

Two MAPRs are found in humans; Hpr6.6 and Dg6. Hpr6.6 is the human MAPR homologue of the porcine mPR. Hpr6.6 mRNA is expressed predominantly in liver and kidney, whereas Dg6 mRNA is preferentially expressed in placenta [19]. Hpr6.6 has recently been suggested to mediate cell death from oxidative damage via a mechanism that is not typical of the apoptotic pathway [103]. The rat MAPR homologue, 25-Dx, is expressed in the ventromedial hypothalamus of female rats, a region of the brain that plays a role in reproductive behavior mediated by steroid hormones [28]. 25-Dx localized to the plasma membrane in those neurons. The data indicate 25-Dx was down-regulated by progesterone and up-regulated by estrogen in female rat brain. Recently, 25-Dx has been localized to neuronal Purkinje cells and the external granule cell layer [110]. Purkinje cells synthesis progesterone *de novo* from cholesterol only during

neonatal life. The authors suggest that progesterone promotes dendritic growth, spinogenesis, and synoptogenesis via 25-Dx as well as the nuclear progesterone receptor. This same rat MAPR was isolated, in a different experiment setup and by a different group, as a protein specific to the inner zones of the rat adrenal cortex, called inner zone antigen (IZAgI) [30]. IZAg was localized to both the microsomal and mitochondrial fractions. IZag was proposed to have an action on steroid hydroxylation, since monoclonal antibodies raised against IZAg cause a dose dependent decrease in hydroxylation of progesterone in the microsomal fraction and a decrease in hydroxylation of deoxycorticosterone in the mitochondrial fraction. Recently, IZag has been proposed to play a role in adrenocorticol steroidogenesis [106]. When COS-7 cells were transformed with plasmids for appropriate steroidogenic enzymes in the presence or absence of an IZAg expression plasmid and tested for their steroidogenic activities, 21-hydroxylation of progesterone was found to be specifically activated by IZAg overexpression, suggesting the involvement of IZAg in progesterone metabolism. This was the first instance linking the involvement of MAPRs to steroid metabolism. The same rat MAPR was isolated yet again as a ventral midline antigen, VEMA, expressed in the central nervous system of rat embryos [29]. The floor plate is composed of a small group of columnar ependymal cells that reside at the ventral midline of the developing vertebrate CNS. These cells play key roles in pattern formation and axon guidance. *In situ* hybridization analysis demonstrated VEMA mRNA being predominantly expressed at the ventral midline. Thus, the researchers suggest a role for VEMA in regulating axon guidance. The researchers proposed that several lines of evidence suggested VEMA does not bind progesterone and that progesterone is not present within the developing rat

spinal cord [29]. Unfortunately, the researchers did not present what kinds of studies were examined and no data was presented as proof of this claim.

Dap1p is the yeast MAPR homologue. Yeast are unicellular organisms, which obviously have no liver, no neuronal cells, or even a CNS. Yeast do not produce steroid compounds, although they do produce sterols, which are precursors to steroid compounds in higher organisms. Although strains used in the study were haploid, deletion of *DAP1* has been demonstrated to lead to sensitivity to MMS, elongated telomeres by ~100bp, defects in mitochondrial biogenesis, and partial arrest of sterol synthesis [66]. Specifically, the *dap1*Δ mutant strain exhibited decreased levels of ergosterol and zymosterol and increased levels of lanosterol and squalene as compared to control strain. It is uncertain as to whether Dap1p is intimately involved in the MMS induced DNA damage response, telomere maintenance, and mitochondrial biogenesis or if it is a by-product created by the altered sterol profile, or even if they are a result of an unknown secondary mutation, since haploid strains were used.

Previous characterization of diploid homozygous mutant strain has shown a differential sensitivity to alcohol, an altered sterol profile, and a strong yeast two-hybrid interaction with Ypr118wp [22]. Ypr118wp was recently shown to be a methylthioribose-1-phosphate isomerase, an enzyme of the methionine salvage pathway [86]. High-throughput screens have found that Dap1p interacts genetically with Erg11, lanosterol 14α-demethylase [112], co-precipitates with Pma1p (H^+-ATPase) and Guf1 (a GTPase located in mitochondria) [111], and interacts in a yeast two-hybrid screen with Tfb1 (a subunit of TFIIH and nucleotide excision repair factor 3 complexes) [113].

Various microarray experiments have shown that *DAP1* mRNA accumulates in response to nitrogen depletion and as cells enter stationary phase [114]. Dap1p mRNA in haploid a cells peaks 60 minutes after alpha-factor application. In diploid cells undergoing meiosis and sporulation, Dap1 mRNA shows a biphasic induction, at 0.5 h and at 7 h of sporulation. The *Schizosaccharomyces pombe* homologue SPAC25B8.01 also shows an interesting pattern of expression during meiosis; increased expression going through meiosis I and II and marked decreased expression afterwards.

These prior observations do not point to an obvious primary function fro Dap1p or the mammalian MAPR homologues. Rather, they indicate pleitropic effects in different cell compartments, from nuclei to the ER, mitochondria and the plasma membrane, from DNA damage responses to sterol metabolism to a receptor for steroids. Nevertheless, combining the facts that deletion of *DAP1* produces an altered sterol profile with the observation that mammalian MAPRs might be involved in steroid metabolism one can propose that Dap1p plays a direct role in sterol metabolism in the yeast cell. A role in sterol metabolism would be consistent with the genetic interaction of Dap1p with Erg11p. Moreover, sterol biosynthesis involves a number of membrane systems, from ER to lipid particles to mitochondria and the plasma membrane, and sterols affect a variety of cellular functions, including endocytosis, amino acid transport, and the cell division cycle. Therefore, a mutation in a gene in sterol metabolism may will have pleiotropic effects (e.g., ERG6 [115]).

Sterol Metabolism

Sterols are thought to serve a number of functions in yeast. The most important of these include bulk membrane support – relating to membrane fluidity and permeability [48], the cell cycle 'sparking function' [48], involvement in endocytosis and exocytosis [49], and 'lipid raft' formation [50,51]. Recently, preliminary studies have described some physiological properties and effects of sterols on aerobic metabolism [74,75], completion of the cell cycle [76], sterol uptake [77], and sterol transport in mitochondria [65]. Sterols are essential components of the eukaryotic plasma membrane. Sterols are highly enriched in the plasma membrane [37,38,39]; other organelles contain sterols at lower, although still significant quantities [40]. The sterol content of the plasma membrane changes depending upon the nature of the external conditions: heat, pH, ions, EtOH, etc. The mechanism of their transport from internal membranes, where they are synthesized, to the periphery of the cell is still obscure [2]. Ergosterol is the major sterol present in the cell, but there are a number of other sterols present. The structural differences are thought to serve not only a differential function of membrane rigidity and permeability, but might also be important for the electrical potential across each membrane.

Yeast sterols are known to be produced from isopentyl diphosphate, the central intermediate in sterol/isoprenoid biosynthesis. There are at least two known biochemical pathways that produce isopentyl diphosphate [41]. The major pathway and, also, the best understood, is production from acetyl-CoA. But isopentyl diphosphate can also be produced from D-glyceraldehyde-3-phosphate + pyruvate. This pathway is not understood very well, all the enzymes involved and steps are not known, and seems to be

used little. Ultimately, three isoprene units are joined to form farnesyl diphosphate. Squalene synthase catalyzes two consecutive reactions in sterol biosynthesis; the condensation of two molecules of farnesyl diphosphate to form the cyclopropylcarbinyl intermediate presqualene diphosphate, and the subsequent rearrangement and reduction of prequalene diphosphate to form squalene [31]. This reaction is the first pathway-specific step in yeast sterol metabolism. Squalene is then epoxidized by squalene epoxidase, then circulized by lanosterol synthase to produce lanosterol, the first sterol in the ergosterol biosynthetic pathway. Lanosterol then undergoes thirteen enzymatic reactions by ten different enzymes to finally produce ergosterol; this is summarized in Tables 1a and 1b.

These are not all the sterols found in the yeast *Saccharomyces cerevisiae*. Yeast can also produce trace amounts of sterol byproducts during double-bond migration in the conversion of lanosterol to ergosterol [42]. More significantly, yeast can produce traces of aberrant sterols by minor alternate pathways [104]. Also, evidence suggests that minor mutations in the enzymes involved in the production of ergosterol can create sterols not normally observed in yeast. This can be achieved by either binding to a different sterol ligand and performing the correct enzymatic reaction, or by binding to the correct ligand, but catalyzing an aberrant enzymatic reaction [105]. Levels of these abnormal metabolites and related biosynthetic intermediates can increase dramatically when normal metabolism is disrupted by genetic defects [43,44,45] or sterol inhibitors [46,47].

Classically, the site of sterol synthesis is considered to be in the microsomal fraction [56]. Sites of synthesis have been determined to include both the surface of the ER and, recently, the participation of lipid particles, since the localization of the enzymes

involved in the ergosterol biosynthetic pathway are localized to both the ER [52,53] and lipid particles [36,54,55]. All types of eukaryotic cells, such as plants [32,33], mammals, [34], and yeast [35], contain intracellular lipid particles. These particles consist of a highly hydrophobic core formed from neutral lipid particles (triacylglycerols and steryl esters) surrounded by a phopholipid monolayer in which only a few proteins are embedded [36].

Ergosterol biogenesis occurs primarily during exponential growth. When cells start to reach stationary phase and during sporulation, the excess sterols are esterified to produce and accumulate steryl esters [62]. Sterols are esterified with long-chain fatty acids in the ER [63], and steryl esters so formed are stored in lipid particles together with triacylglycerols [1,2,57]. Depending on the growth stage, steryl esters are metabolically interconvertible with free sterols [54,58]. The enzyme catalyzing the hydrolytic cleavage of steryl esters, steryl ester hydrolase, was detected at highest specific activity in the plasma membrane [2]. There are two known steryl ester hydrolases present in *Saccharomyces cerevisiae*, Are1p and Are2p [63]. This spatial separation of enzymes involved in the synthesis of sterols and steryl esters, and in the hydrolytic cleavage of the latter components necessitates several steps of intracellular sterol transport. This holds true for the biosynthesis and metabolism of both the free sterols and the steryl esters. Mechanisms proposed, for sterol translocation, are monomer transport with or without the aid of sterol carrier proteins, or vesicle flow with or without an involvement of the protein secretory machinery [59,60]. Nothing conclusive is yet known about the cellular mechanism(s) leading to the deposition of steryl esters to the hydrophobic lipid particles, or about their export from lipid particles to the plasma membrane during the mobilization

and utilization of this sterol source. Results seem to support the view that ongoing membrane proliferation may be a driving force [61].

Normally, ergosterol accounts for most of the sterol fraction in the cell, but its relative quantity can vary depending upon the metabolic state of the cell. This relative quantity can change widely particularly if there are mutations in enzymes involved in the ergosterol biosynthetic pathway. Erg4p is the last enzyme in the ergosterol biosynthetic pathway; it catalyzes the conversion of ergosta-5,7,22,24(28)-tetraen-3β-ol into ergosterol. Erg4p is localized to the ER [55], therefore ergosterol must be supplied somehow from its location of biosynthesis to it destination membrane. The protein(s) or mechanism(s) responsible for this is unknown.

Lanosterol is the first sterol produced in the ergosterol biosynthetic pathway. It is produced by the addition of oxygen to squalene in which squalene epoxide is an intermediate between squalene and lanosterol. Squalene is converted into squalene epoxide by Erg1p. Squalene epoxide is converted into lanosterol by Erg7p. Both Erg1p and Erg7p localize to both lipid particles and on the ER. Erg1p is mainly localized to the ER, ~62%, with lesser quantities in lipid particles, ~38% [70], whereas Ergp7p is mainly localized to lipid particles with only minor quantities being present in the ER [71]. Interestingly, Erg1p is not active in lipid particles, but partial activity can be activated when lipid particles are mixed with microsomes devoid of Erg1p, indicating that there is a factor in the ER that is necessary for squalene epoxidase activity [73]. Erg1p transcriptional expression is regulated by ergosterol levels in the cell [72]. Since, lanosterol in the first sterol in the pathway, it is a pivotal point for the variations so commonly observed. Thus lanosterol is an excellent indicator sterol that may change

significantly depending upon the physiological state of the cell. A C-14 methyl-group is removed from lanosterol by Erg11p, to produce 4,4-dimethylcholesta-8,14,24(28)-trien-3β-ol. Erg11p has been demonstrated to be located on the ER [78]. Erg11p has been identified by large scale interaction studies to genetically interact with Dap1p [79].

Erg6p catalyzes the conversion of zymosterol into fecosterol. Erg6p has been demonstrated to be located as a surface protein in lipid particles [36]. Erg6p is the first enzymes in the ergosterol biosynthetic pathway to be non-essential for viability in *Saccharomyces cerevisiae* cells. Erg3p catalyzes the conversion of ergosta-5,7,22-trien-3β-ol into ergosta-5,7,22,24(28)- tetraen-3β-ol. It has been demonstrated that mitochondria function as important physiological partners with Erg3p in accumulation of toxic sterol intermediate [80], supplying a connection between mitochondria and ergosterol production. Recent data suggests that Erg27p interacts with Erg7p, facilitating Erg7p interaction with lipid particles and also preventing digestion of Erg7p in the ER and lipid particles [81], providing evidence that this enzyme performs more than one role in the cell. Erg28p has been suggested to tether Erg26p and Erg27p to the ER or to facilitate an interaction between the two proteins [82], suggesting protein complexes form to facilitate the enzymes in the ergosterol biosynthetic pathway. Erg25p is a sterol C-4 methyloxidase, performing multiple enzymatic steps in the ergosterol biosynthetic pathway [73], but it is also required to grow on iron-limiting media [83]. It is localized to both the ER and in minor quantities on the plasma membrane, and data suggests that this protein is not regulated by iron, but by an end product of the ergosterol biosynthetic pathway [83]. It has been well established that ergosterol regulates its own biosynthesis through a feedback mechanism [84].

A major focus of this dissertation is to analyze the sterol profiles in the *dap1*Δ mutant strain for alterations that provide insight into the role of Dap1p in sterol metabolism. Both free sterols and esterified sterols will be analyzed. Because sterol metabolism occurs in multiple membrane systems, we will also localize Dap1p in the cell with GFP fusions.

Table 1a. Ergosterol Biosynthetic Pathway; post-squalene

Sterol	Gene / Enzyme Name
1. 2,6,10,15,19,23-hexamethyl-2,6,10,14,18,22-tetracosahexaene (**Squalene**)	*ERG1* / Squalene epoxidase
2. 2,3-oxidosqualene (**Squalene epoxide**)	*ERG7* / Lanosterol synthase
3. Lanosta-8,24-dien-3β-ol (**Lanosterol**)	*ERG11* / Lanosterol C-14 demethylase
4. 4,4-dimethyl-cholesta-8,14,24-trien-3β-ol	*ERG24* / Sterol C-14 reductase
5. 4,4-dimethyl-cholesta-8,24-dien-3β-ol (**4,4-Dimethylzymosterol**)	*ERG25* / Sterol C-4 methyloxidase
6. 4α-methyl-4β-carboxy-cholesta-8,24-dien-3β-ol	*ERG26* / Sterol C-4 decarboxylase
7. 4α-methyl-cholesta-8,24-dien-3β-one (**4-Methylzymosterone**)	*ERG27* / Sterol C-3 keto reductase
8. 4α-methyl-cholesta-8,24-dien-3β-ol (**4-Methylzymosterol**)	*ERG25* / Sterol C-4 methyloxidase
9. 4α-carboxy-cholesta-8,24-dien-3β-ol	*ERG26* / Sterol C-4 decarboxylase
10. Cholesta-8,24-dien-3β-one (**Zymosterone**)	*ERG27* / Sterol C-3 keto reductase
11. Cholesta-8,24-dien-3β-ol (**Zymosterol**)	*ERG6* / Sterol C-24 methyltransferase
12. Ergosta-8,24(28)-dien-3β-ol (**Fecosterol**)	*ERG2* / Sterol C-8 isomerase
13. Ergosta-7,24(28)-dien-3β-ol (**Episterol**)	*ERG3* / Sterol C-5 desaturase
14. Ergosta-5,7,24(28)-trien-3β-ol (**Ergostatrienol**)	*ERG5* / Sterol C-22 desaturase
15. Ergosta-5,7,22E,24(28)-tetraen-3β-ol (**Ergostatetraenol**)	*ERG4* / Sterol C-24 reductase
16. Ergosta-5,7,22E-trien-3β-ol (**Ergosterol**)	

Table 1b. Ergosterol Biosynthetic Pathway; post squalene

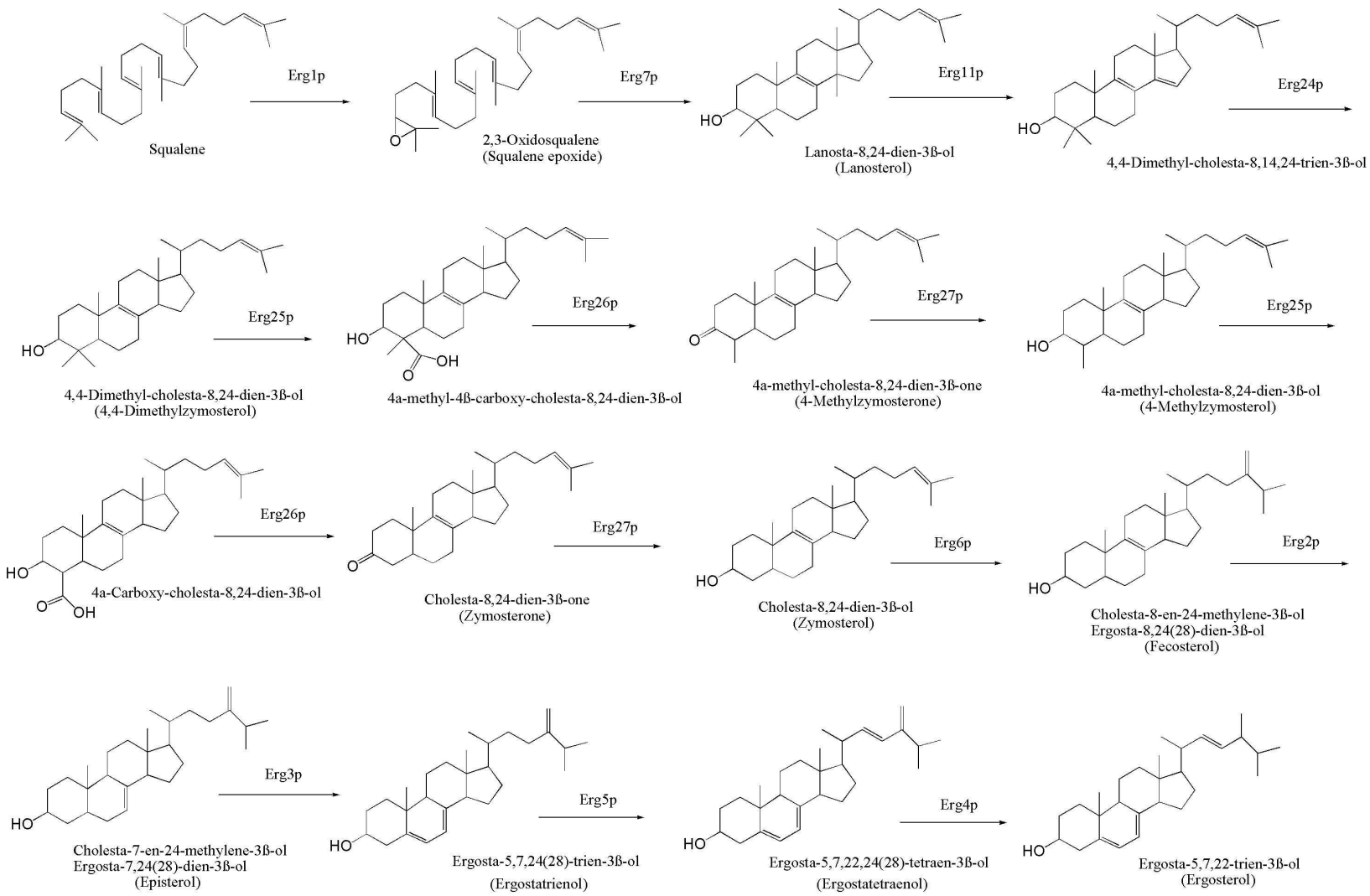

MATERIAL AND METHODS

Media and Growth conditions

Yeast were grown in YPD [1% Bacto-yeast extract, 2% Bacto-peptone, 2% dextrose (or 3% glycerol for YPG), pH 5.8 and 2% agar for plates] (complete) or minimal SD medium (0.17% yeast nitrogen base without ammonium sulfate or amino acids, 0.5% ammonium sulfate, 1x amino acids, 2% dextrose, pH 5.8 and 2% agar for plates) unless otherwise noted.

Low Nitrogen Media

SPD [1g proline, 20g dextrose, 6.7g YNB without amino acids or ammonium sulfate, 1X uracil, histidine, and leucine] + dH_2O to make one liter.

SLAD [6.61mg $(NH_4)_2SO_4$, 20g dextrose, 6.7g YNB without amino acids and ammonium sulfate, 1X uracil, histidine, and leucine] + dH_2O to make one liter.

Growth Curves

Colonies were streaked from glycerol stocks onto fresh selective SD media and incubated at 30ºC for 24 hours. Colonies were removed by scrapping and used to inoculate 10mL YPD at $5x10^5$ cells/mL. Cultures were grown at 30ºC, 220 rpm for 8 hours. Cell concentration was determined by direct cell count on a hemacytometer and used to inoculate a fresh 10mL YPD liquid culture in 50 mL tube with the cap on tight at a concentration of $5x10^3$ cells/mL/strain for a total of $1x10^4$ cells/mL. Cultures were grown at 30ºC with shaking at 220 rpm. At specified time points, aliquots were taken and cells number determined by direct cell count on a hemacytometer.

Competition Experiments

Colonies were streaked from glycerol stocks onto fresh selective SD media and incubated at 30ºC for 24 hours. Colonies were removed by scrapping and used to inoculate 10mL YPD at $5x10^5$ cells/mL. Cultures were grown at 30ºC, 220 rpm for 8 hours. Cell concentration was determined by direct cell count on a hemacytometer and used to inoculate a fresh 10mL liquid culture in 50 mL tube with the cap on tight at a concentration of $5x10^3$ cells/mL/strain for a total of $1x10^4$ cells/mL. Cultures were grown at 30ºC with shaking at 220 rpm. At specified time points, aliquots were taken and spread onto YPD plates and allowed to incubate at 30ºC overnight. Colonies were counted, replica plated onto either SD+geneticin for *dap1*Δ mutant strain selectivity or SD-URA for *ypr118w*Δ mutant strain selectivity, and allowed to incubate at 30ºC overnight. Every seven days, $1x10^5$ cells (total), determined by direct cell count on a hemacytometer, were transferred into 10mL of fresh media.

Yeast Transformation

Transformation of yeast was achieved by the LiAc/PEG protocol. Briefly, one colony was used to inoculate 5mL YPD liquid media, cells were allowed to grow overnight at 30ºC with shaking at 220rpm. The next day, 5mL fresh YPD was added to the solution and incubated 30ºC with shaking at 220rpm for 2-4 hours, to an OD_{600} = 1.0 to 5.0. Cells were spun down for 10min at 4,500 x g and the supernatant discarded. Next, 7mL of 0.1 M LiAc-TE solution was added and the cells incubated at 30ºC with shaking at 220rpm for 60 minutes. Cells were again centrifuged, and then resuspended in 1mL 0.1 M LiAc-TE solution. In a microfuge tube, 100µL of cells, 20µg of carrier

DNA, and 10µg of transforming DNA were mixed and incubated for 30 minutes at 30ºC. Next, 700µL of LiAc-PEG-TE solution was added and incubated for 30 minutes at 30ºC. The cells were then heat shocked at 42ºC for 10minutes, left at room temperature for 60 minutes and plated on selective SD media.

Yeast Strains

All experiments in this study were carried out using homozygous diploid yeast strains of *Saccharomyces cerevisiae*. All yeast strains used in this study are described in Table 2. Strain JCY2 is a strain from the Stanford Yeast Deletion Project (Research Genetics), now available from Invitrogen (San Diego, California), in which the native *DAP1* sequence is disrupted by insertion of the *KanMX6* (an aminoglycoside phosphotransferase), selectable on media containing geneticin. Strain PGY11, created by Dr. Phillip Gray (Georgia Institute of Technology), is a knockout strain, in which the native *YPR118W* sequence was disrupted by insertion of a *URA3* gene, selectable on media lacking uracil. Strain PGY21, created by Dr. Phillip Gray, is a strain created from mating haploids from both the JCY2 strain and the PGY11 strain, in which both genes *DAP1* and *YPR118W* are homozygous disrupted.

Table 2. Strain List.

Strain	Genotype	Background	Source
JCY1	*MAT**a**/α hisD1 leuD20 lys2D0 ura3D0/ hisD1 leuD20 met15D0 ura3D0*	BY4743	Research Genetics
JCY2	*MAT**a**/α dap1Δ::KanMX6/dap1Δ::KanMX6*	BY4743	Research Genetics Record No. 32082
PGY11	*MAT**a**/α ypr118wΔ::URA3/ ypr118wΔ::URA3*	BY4743	Dr. Phillip Gray
PGY21	*MAT**a**/α dap1Δ::KanMX6 ypr118wΔ::URA3/ dap1Δ::KanMX6 ypr118wΔ::URA3*	BY4743	Dr. Phillip Gray

Replica plating

A sterile velvet patch was secured onto a replica block with the plastic ring. The master plate was marked for orientation. The master plate was then placed onto the velvet, colonies facing the velvet, and pressed lightly. A fresh plate, oriented like the master, was lightly pressed onto the velvet for colony transfer.

Petite Experiments

Colonies were streaked from glycerol stocks onto fresh selective SD media and incubated at 30ºC for 24 hours. Colonies were scraped and used to inoculate 10mL YPD at $5x10^5$ cells/mL. Cultures were grown at 30ºC, 220 rpm for 8 hours. Cell concentration was determined by direct cell count on a hemacytometer and used to inoculate a fresh YPD plate at about 150 cells per plate. Cultures were incubated at 30ºC for 24 hours. Colonies were then replica plated onto YPG media to determine number of colonies that contained functional mitochondria. The difference between the number of colonies that grew on the YPD plates and the number that grew on the YPG plates divided by the number of colonies on the YPD plates is the proportion of petite colonies.

MMS Experiments

Sensitivity Assay

Cells were streaked from glycerol stocks onto appropriate selective SD media and incubated at 30ºC for 24 hours. Colonies were removed by scrapping and used to inoculate 10 mL YPD at $5x10^5$ cells/mL. Cultures were grown at 30ºC, 220 rpm for 8 hours. Cell concentration was determined by direct cell count on a hemacytometer. Cells were then serially diluted and spotted onto freshly prepared YPD +MMS plates. The serial dilutions were prepared to deposit a total of 10^5, 10^4, 10^3, 10^2, and 10^1 cells per strain per different MMS concentration. MMS was added to YPD plates to 0.005%, 0.01%, 0.025%, and 0.05%.

Localization Assay

Transformed cells were incubated in a 0.035% MMS solution for the time points listed before fixation and subsequent visualization.

Sterol Extraction, Separation, Quantification, and Identification

Strain growth

Cells were streaked from glycerol stocks onto selective minimal SD media, specific for each strain, and incubated at 30ºC overnight. A fresh colony was then transferred to a microcentrifuge tube containing 1 mL of water, subsequently diluted, and counted on a hemacytometer. Cells were added to 1 L selective SD liquid media, in 2 L wide mouth flasks, to a cell density of $5x10^4$ cells/mL. Cells were grown in SD media, a minimal media, to strictly observe sterol differences between the different strains. Wide

mouth flasks were used to increase aeration, since molecular oxygen is required for sterol synthesis.

Cell Count

At specified time points, in swirling flask, 5 x 1 mL of cells was removed, diluted, and counted directly on a hemocytometer. An average of the 5 cell counts was used to determine total cell number per culture.

Cell harvesting

Cells suspensions were transferred to 150ml Pyrex glass centrifuge tubes, centrifuged at 5,000 rpm for 10 minutes, in a Beckman rotor. The supernatant was discarded quickly to prevent loss of cells, which is also why 10 minutes was used instead of the usual 5 minutes, to create a more compact cell pellet. The process was repeated in the same glass tube until all of the original 1 L cell suspension was used. The cell pellet was resuspended each time additional culture was added for centrifugation. The final cell pellet was resuspended once in 30 mL PBS and centrifuged at 5,000 rpm for 10 minutes. The final cell pellet was resuspended in a minimal of PBS to form a viscous liquid.

Total Lipid Extraction

Lipids were extracted by the Bligh-Dyer (101) method, a more simplified version of the Folch (102) method.

The total amount of resuspended cell volume in H_2O was estimated using identical glass centrifuge tubes with known volumes of water. Distilled methanol and distilled chloroform were added directly to the cell suspension in a 10:5:4 ratio of MeOH:$CHCl_3$:H_2O. This ratio created a miscible solution. If partitioning of layers was

noticed after a few minutes, methanol was added in 0.25 mL increments until no solution partitioning was observed. This was followed by addition of chloroform to correct the MeOH:$CHCl_3$ ratio to10:5. The final volume of each solvent was recorded. At this point, two surrogate standards (1.25 mg each) were added to each sample, estrone and cholesterol acetate. These standards were used because of low price, ready availability, and retention time on the GC column so as to not interfere with sterol peaks. Better standards can certainly be found if price and time are of little importance. Solution was swirled briefly, capped with aluminum foil, sealed tightly with a cap and left to sit overnight.

Solutions were then centrifuged at 10,000 x g for 15 minutes to pellet cell debris. The supernatant was poured into a 250mL separatory funnel. $CHCl_3$ and H_2O was added to bring the final ratio MeOH:$CHCl_3$:H_2O to 10:10:9. The solution was swirled gently in the separatory funnel a few times to insure proper mixing; the glass cap was removed between mixing to release pressure. The separatory funnel was allowed to sit capped overnight. This allowed two distinct layers to form. The chloroform layer, containing the total lipid fraction, being on the bottom, was removed into a round bottom flask. Another extraction was performed adding the same final amount of chloroform as before. Only wait as long as two distinct layers form. The chloroform fraction was removed and added to the first fraction.

The chloroform solvent, containing the total lipid fraction, was evaporated to about 1 mL using a Buchi RE 111 rotavapor. The chloroform solution was then transferred to a test tube. The evaporation flask was washed 5 times with about 1.5 mL chloroform and transferred to the test tube. The test tube, containing the total lipid

fraction, was put in a gently heated water bath 30º-40ºC, so as to not condense water under the evaporating conditions, under a fume hood and evaporated to almost dryness under N_2 gas.

The test tube was then transferred to a desiccation chamber and the solvent was completely removed under vacuum. After complete solvent removal, N_2 gas was slowly allowed to enter the chamber. While keeping the N_2 flowing, and working as quickly as possible the desiccation chamber was opened and the test tube was removed. Two mL of distilled hexane was immediately added to the dry lipid fraction. The process was repeated until all test tubes had been processed.

Sterol Separation

Several glass chromatography columns were set up in a fume hood. Oven dried Unisil (activated salicic acid, 200-325 mesh, Clarkson Chemical Company, INC, Williamsport, Pennsylvania) was added to about a 2 cm depth. The Unisil was packed by gently tapping the column with a rubber stopper. The column was then thoroughly washed inside and out with distilled hexane. The column was tapped gently again to release any trapped gas bubbles in the stationary phase. Before the hexane layer reached the top of the solid phase, the lipid fraction dissolved in hexane was added to the column. The test tube was washed 3 times with about 1.5 mL hexane and added to the column. The mobile phase was allowed to drip into a collection flask. As the top of the mobile phase was about to reach the solid phase about 7 mL of distilled hexane was carefully added to the column. The process was repeated 2 times until about 25 ml hexane was collected.

As the hexane mobile phase was about to reach the solid phase the benzene solution was added to the column. The test tube was again washed 3 times with about 1.5 mL benzene and added to the column. A new collection flask was added to the bottom of the column. As the top of the benzene mobile phase was about to reach the solid phase, 10 mL benzene was carefully added to the column. This process was repeated until about 100 mL of benzene solution was obtained. The process was then repeated with chloroform to about 100 mL and finally methanol to about 25 mL.

The separate fractions were concentrated in a roto-evaporator, transferred to a test tube, taken to dryness under a stream of N_2 at 30º-40ºC and immediately re-dissolved in 0.5 mL distilled chloroform.

The hexane portion contains aliphatic hydrocarbons. The benzene portion contains aromatic hydrocarbons, fatty acid methyl esters, and steryl-esters. The chloroform portion contains free fatty acids, free sterols, triglycerides, diglycerides, and monoglycerides. The methanol portion contains glycolipids and phospholipids. The two surrogate standards added, estrone and cholesterol acetate, partitioned with the free sterol fraction and the steryl ester fraction, respectively.

Determination of Free Sterol vs. Steryl-Ester Separation

To establish that the free sterols were separated from steryl esters, TLC (thin layer chromatography) was performed. Commercially prepared TLC plates were used, Silica Gel G, 20 x 20 cm plates. The plates were heat activated at 120ºC overnight, allowed to cool briefly before use. Separate solvent components were spotted on the TLC plates in the 100-300 µg range. Plates were immediately developed after application of sample.

A glass tank (11 x 21 x 21 cm) with a ground glass cover and lined with filter paper on three sides, to aid in saturating the tank with solvent vapor, was used. Two tanks were prepared, the first, tank #1, with a polar solvent mixture and the second, tank #2, with non-polar solvents. The polar solvent mixture consists of diethylether : benzene : ethanol : acetic acid (45:50:2:0.2), the non-polar solvent mixture consists of hexane : diethylether (96:4).

The polar tank was prepared first and allowed to equilibrate for 30 minutes prior to use. The TLC plate was then placed in tank #1 and the solvent allowed to run about 5/8ths of the way up the TLC plate. The solvent front was marked by making a thin scrape along the edge of the TLC plate. The TLC plate was then dried inside a box flushed with N_2 gas, until no acetic acid could be smelled on the TLC plate. While the TLC plate dried the second tank was prepared and allowed to equilibrate. The TLC plate was then placed in tank #2 and the solvent allowed to run to the top of the TLC plate. The TLC plate was allowed to dry briefly again inside a box flushed with N_2 gas. The components of the TLC plate were visualized by exposing the TLC plate to iodine vapors. This was accomplished by placing the TLC plate inside a glass tank containing iodine crystals. All components of the TLC plate that are potential proton donors will stain a yellowish-orange. A permanent record was obtained by placing a clean glass plate over the chromatogram, tracing the spots with a felt pen, then subsequent photocopying. A typical visualized plate is shown in Figure 1.

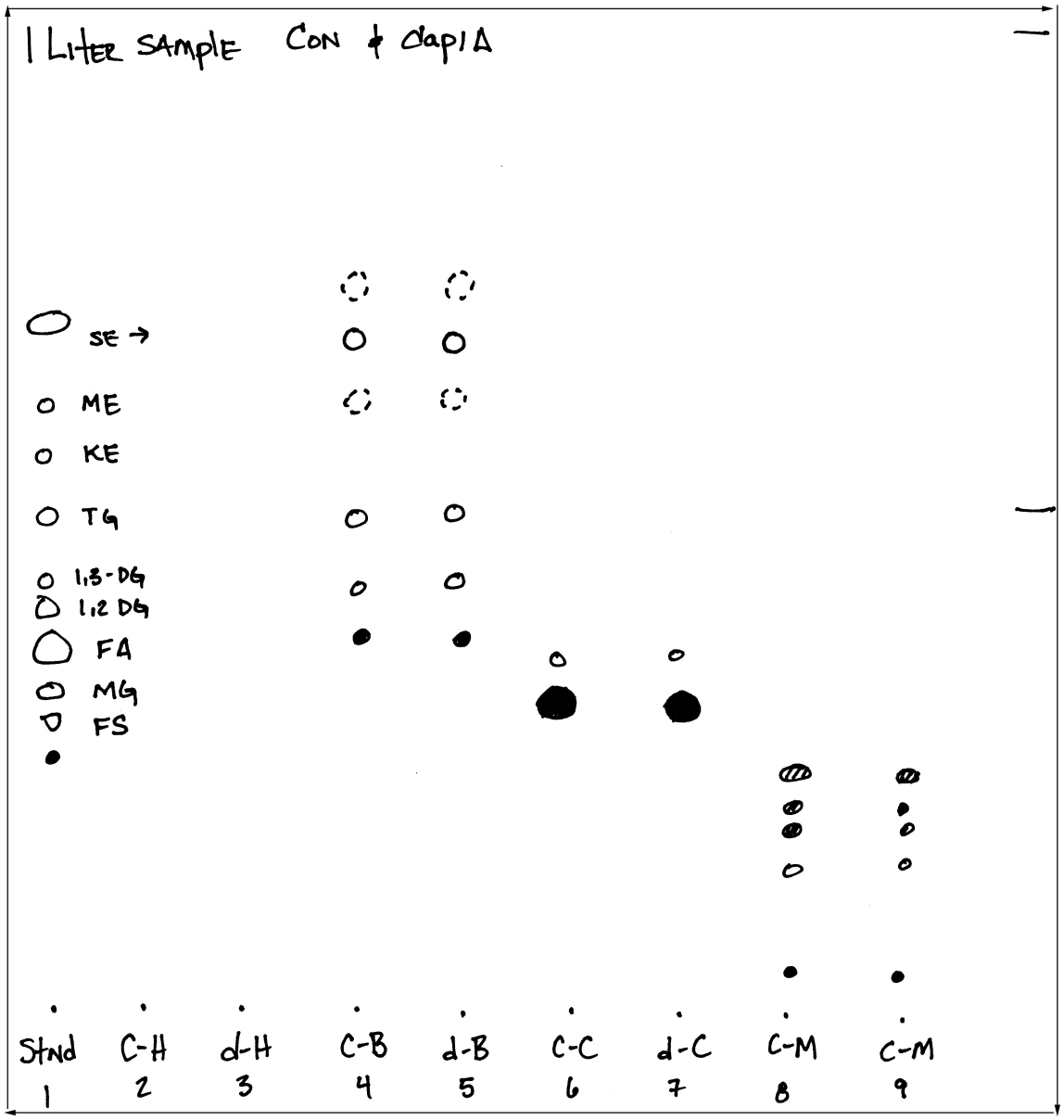

Figure 1. Sample of TLC Sterol Separation. First lane: Standard; 2nd: control-hexane fraction; 3rd: *dap1*Δ-hexane fraction; 4th: control-benzene fraction; 5th: *dap1*Δ-benzene fraction; 6th: control-chloroform fraction; 7th: *dap1*Δ-chloroform fraction; 8th: control-methanol fraction; 9th: *dap1*Δ-methanol fraction.

FS: free sterols; MG: monoglyceride; FA: free fatty acid; DG: diglyceride; TG: triglyceride; KE: ketone; ME: methyl ester; SE: steryl ester.

Saponification of sterol fractions

The benzene portion, containing the steryl-ester fraction, and the chloroform portion, containing the free sterol fraction were reduced to dryness under N_2 gas at 30-40ºC. Next, 2.5 mL of 2.5% HCl:Methanol (W/V) was immediately added to each test tube. The HCl:Methanol was prepared by bubbling 2.5 g HCl gas into 100 ml anhydrous methanol, prepared by distillation. The test tubes were capped tightly and put in an 80º-90ºC oven for 1 hour. The solutions were then dried to almost completion under a stream of N_2 gas at 30º-40ºC, then put into a desiccation chamber and dried to completion under vacuum. Samples were removed from the desiccation chamber as before and the sample was immediately redissolved in 0.5 mL chloroform.

Addition of Internal Standard

Samples in $CHCl_3$ were transferred to 2 mL amber vials with Teflon caps, dried under N_2, and then 0.35 mL chloroform was added immediately to the vials. Next, 0.1 mL of cholesterol (1mg/mL in chloroform) was added to the free sterols samples and 0.1 mL estrone (1 mg/mL in chloroform) was added to the steryl ester samples.

Derivitization of sterol fractions

For derivitization, 0.05 mL of N,N-Bis(trimethylsilyl)acetamide (TMS) was added to each sample. To bring the total volume of each vial 0.5 mL. The caps were put on the vials tightly then placed in an oven set to 80º-90ºC for 15 minutes. Samples were allowed to cool, evaporated under a stream of N_2 gas at 30º-40ºC to about half the original volume. Samples were then run on the GC.

Gas Chromatography

Gas chromatography was performed using a Hewlett Packard 5890 gas chromatograph equipped with an SGE HT5 polyimide clad column (12 m x 0.22mm ID x 0.1 μm), and flame-ionization detector. The detection signal was recorded on an HP3394A integrator. The column head pressure was set to 8psi, the carrier gas (He) was set at 30 psi and all injections were operated in the splitless mode. The injector was set to 300ºC and the FID was set to 320ºC. The program was as follows: oven initial temperature, 200ºC, was increased from 200^{o} to 350^{o} at a rate of 8^{o}/min, and maintained at the upper temperature for 5 min. Based on standards, estrone (Sigma) was known to elute at 10.06 min., cholesterol (Sigma) at 13.83 min., ergosterol (Sigma) at 14.32 min, and lanosterol (Sigma) at 15.44 min. using this particular program. Sterols were identified by comparing the retention times of established commercial standards injected into the GC as well as by GC/MS at the Georgia Tech Mass Spectroscopy Lab. Samples were each injected twice and the average of the quantities was used for data. Each morning before use, the injector column was lightly cleaned with chloroform and methanol and a new septum added to the injector port.

Quantitation of Sterol Content

Quantitization of sterol content was determined by the extraction efficacy based on the area of the surrogate standard peak, area of the internal standard peak, and finally the area of the individual sterol peak.

Difficulties in procedure

One of the serious problems in isolating lipids is the easy acquisition of contaminating material. The most common sources of extrinsic lipids are soap, organic solvents, and plastic products. All glassware were chemically cleaned, thoroughly rinsed with water, methanol, and then dried in an oven reserved for clean glassware. Prior to use glassware was washed with methanol and chloroform and allowed to dry upside down in a fume hood. All solvents were freshly redistilled before use, except benzene, which was considered too hazardous to distill. Most glassware was equipped with tapered joints; screw cap tubes were Teflon lined. Extreme care was exercised with all equipment, chemicals, and glassware to prevent contamination from handling and experimental manipulation during the course of the analyses.

Sterols themselves are degradable. They should not be exposed to oxygen, particularly when in dried form. They should be stored in light restrictive containers. Sterols also have some affinity to stick to glass. Therefore, it was necessary when transferring sterol solutions from one container to another, that the sides of the glass container were washed with solvent at least 3 times, preferably 5 times with the appropriate solvent, usually chloroform. This procedure was most critical immediately prior to injection into the GC. Standard operating procedure was to cap the vial tightly and to place it on top of the GC oven, which heats the chloroform enough for it to evaporate. The chloroform condensed at the top of the vial and droplets formed and roll down the sides of the vial, picking up any residual sterols stuck to the sides.

Consistent results were only obtained when fresh colonies were streaked onto selective synthetic plates from glycerol stocks. Transformation was carried out thusly with fresh colonies and used immediately after transformation.

Mammalian Cell Line Transfection

Hpr6.6 was cloned into the vector pEGFP-N1 (Clonetech) by Dr. Hosoon Choi of our lab, for making EGFP fusion protein under the control of the CMV promoter. The fusion protein plasmid was transfected into HeLa cells using calcium phosphate transfection. Briefly, 9mL of DMEM media [Dulbecco's modified Eagle's medium, 10% fetal bovine serum, 4.5 g/L glucose, 7.42 g/L L-glutamine] was transferred to a 10 cm dish. About $5x10^5$ HeLa cells were added drop-wise into the dish containing sterile 12mm No. 1 glass circle cover slips. The cover slips, with adhered HeLa cells, were moved to 12 well plates 24 hours after plating. 1 mL of DMEM media was added to each well. DNA/$CaPO_4$ mix (2 µg of high purity DNA + 8 µL of 2 M $CaCl_2$, and dH_20 to make total volume 62.5 µL) was prepared in 10mL sterile culture tubes. 62.5 µL of 2X HBS (280 mM NaCl, 10mM KCl, 1.5mM Na2HPO4, 12 mM glucose, 50mM HEPES, pH 7.05) was added to the tube while vortexing. DNA/CaCl2/HBS mixture sat at room temperature for 10 minutes. The mixture was vortexed again, and then the entire mixture was added drop-wise over the plate of cells. The cells were then incubated overnight. The next day, the plates were gently swirled and the media aspirated off. The cells were washed 3 times with PBS, pH 7.4. Fresh media was added and the culture returned to incubation. The next day, cells were washed 3 times with PBS, pH7.4, fixed with 4% formaldehyde, and placed on a glass slide cell side down.

Construction of DAP1 and Ypr118w plasmids

Construction of DAP1 in pUGpd. *DAP1* was PCR amplified using the oligonucleotides YPL170W1 (5'-CGGGCCATGGCACACACACGTACATCGGAAT-3') and YPL170W2 (5'-GGCGGTCGACATAATGTGCGGAGCTCAATCG-3'). The resulting 500 bp fragment was cloned into the T-vector pCR2.1 (In Vitrogen). *DAP1* was removed using *Spe*I/*Xba*I and ligated in the *Spe*I/*Xba*I site of pUGpd (courtesy of Dr. Susan Lindquist), a constitutive expression vector containing the Gpd promoter [85]. Construction was performed by Dr. Phillip Gray, Georgia Institute of Technology.

Construction of YPR118w in pUGpd. *YPR118W* was PCR amplified using the oligonucleotides YPR118W-5' (5'-CTGCTGACAAACCATGGCGTTGG-3') and YPR118W-3' (5'-GGTTATAGTGTTGTCGACTTACAAGG-3'). The resulting 1400 bp fragment was cloned into the T-vector, pCR2.1 (In Vitrogen). *YPR118W* was removed by performing a limited digest with *Spe*I (YPR118w contains a *Spe*I site at 800 bp) and full digest with *Xba*I and ligated in the *Spe*I/*Xba*I site of pUGpd. Construction was performed by Dr. Phillip Gray, Georgia Institute of Technology.

Construction of DAP1 in pHGPD-sGFP. *DAP1* was PCR amplified using the oligonucleotides YPL170W-GFP5' (5'-AAATCTCATCAGCCACACACA-3') and YPL170W-GFP3' (5'-ACGCCAGGCTCTAGAATCAGA-3') containing an *Xba*I site. The resulting 500 bp fragment was cloned into the T-vector, pCR2.1 (In Vitrogen), subsequently removed using *Spe*I and *Xba*I and ligated into the *Spe*I/*Xba*I site of pHGPD-sGFP (courtesy of Dr. Susan Lindquist). The pHGPD-sGFP contains the Gpd

promoter, which allows constitutive expression of the GFP fusion protein. Construction was performed by Dr. Phillip Gray, Georgia Institute of Technology.

Construction of the pUGpd-RFP vector. The MCS and red fluorescent protein were cut out of pDsRed1-N1 (Clontech) using *Bgl*II and *Not*I and cloned into the *BamH*I/*Not*I site of pUGpd. The pUGpd-RFP vector also contains the Gpd promoter, allowing for constitutive expression of RFP fusion proteins.

Construction of YPR118w in pUGpd-RFP. *YPR118W* was PCR amplified using the oligonucleotides 118 RFP 5' (5'- AATATCTACGCCCGGGAAAGT-3') containing a *Xma*I site and 118 RFP 3'(5'-TTCACCACCGGTATTTTTGG-3') containing an *Age*I site. The resulting 1200 bp fragment was cloned into the T-vector, pCR2.1 (In Vitrogen), subsequently removed using *Xma*I and *Age*I and cloned into the *Xma*I /*Age*I site of pUGpd-RFP.

Construction of pUGpd-Ypr118w-RFP2. Since the RFP1 protein had been shown to sometimes aggregate with itself, a construct was made using the new pDsRed2-N1 plasmid (Clontech). The RFP protein was removed from the pUGpd-*YPR118W*-RFP plasmid using *AgeI* and *NotI*, using limited digest since the ypr118wp includes an *AgeI* site. The DsRed2 protein was cut out of pDsRed2-N1 also using *AgeI* and *NotI* and cloned into the AgeI/NotI site of pUGpd-*YPR118W*-RFP.

Construction of ypr118w-RFP2 in pRS315. To allow for co-localization with pHGPD-*DAP1*-sGFP, which contains a *HIS3* marker, in the double mutant strain, the Gpd promoter along with the *YPR118W*-RFP2 fusion construct was cloned into pRS315,

which contains a *LEU2* marker. The Gpd promoter along with the *YPR118W*-RFP2 fusion construct was cut out of pUGpd-ypr118w-RFP2 using *ApaI* and *NotI* and cloned into the already cut *Apa1/NotI* sites of the pRS315 plasmid (courtesy of Dr. Susan Lindquist).

Construction of pmCUP1-Hpr6.6. *Hpr6.6* was PCR amplified from pEGFP-N1 containing full length *Hpr6.6* fused to the N-terminal of EGFP, using oligonucleotide cup1-hpr6.6-fwd (5'-CCGCTCTAGAATGGCTGCCGAGGATGTGGT-3') containing a *NotI* site, and oligonucleotide cup1-hpr6.6-rev (5'-GCGGCGCCTTAATCATTTTTCCGGGCACTCTC-3')containing a *XbaI* site. The PCR product was ligated into pGEM T-vector, cut with *NotI* and *XbaI* and ligated into the *NotI/XbaI* site of pmCUP1 containing a copper promoter.

Construction of pmCUP1-Hpr6.6-GFP. *Hpr6.6* was PCR amplified from pEGFP-N1 containing full length Hpr6.6 fused to the N-terminal of EGFP, using oligonucleotide cup1-hpr6.6-fwd (5'-CCGCTCTAGAATGGCTGCCGAGGATGTGGT-3') containing a *NotI* site, and oligonucleotide cup1-hpr6.6gfp-rev (5'-CTGCGGCCGCCATTTTTCCGGGCACTCTCA-3')containing a *XbaI* site. The PCR product was ligated into pGEM T-vector, cut with *NotI* and *XbaI*, and subsequently ligated into the *NotI/XbaI* site of pmCUP1 containing a copper promoter.

Fluorescence Microscopy

Transformed cells were grown overnight in SD medium, centrifuged, washed with PBS and resuspended in mounting medium (Fluoromount-G, Southern Biotechnology Associates). For DAPI staining, 22.5μg/ml DAPI was added directly to mounting media.

For lipid particle staining, cells were incubated with nile red (Sigma) at 10 μg/ml for 10 minutes, then washed with PBS x 3 prior to resuspension in mounting medium. Images were captured using a Zeiss LSM510 UV confocal laser scanning microscope with either a Zeiss 63X or 100X Plan-Neofluar oil immersion lens (Core Facilities at the Parker H. Petit Center for Bioengineering and Biosciences, Georgia Institute of Technology).

RESULTS

GROWTH CURVES

Cells of the control strain, the *dap1*Δ mutant strain, the *ypr118w*Δ mutant strain, and the *dap1*Δ*/ypr118w*Δ double mutant strain were grown using YPD (Fig. 2-6), SLAD (Fig. 7-8), and SPHD (Fig. 9-10) media, as described in Materials and Methods. Cell counts were determined at specified time points.

Cell Growth in YPD Medium

In YPD medium, no significant differences in growth rate were observed between the strains over 8 days of culture (Figure 2).

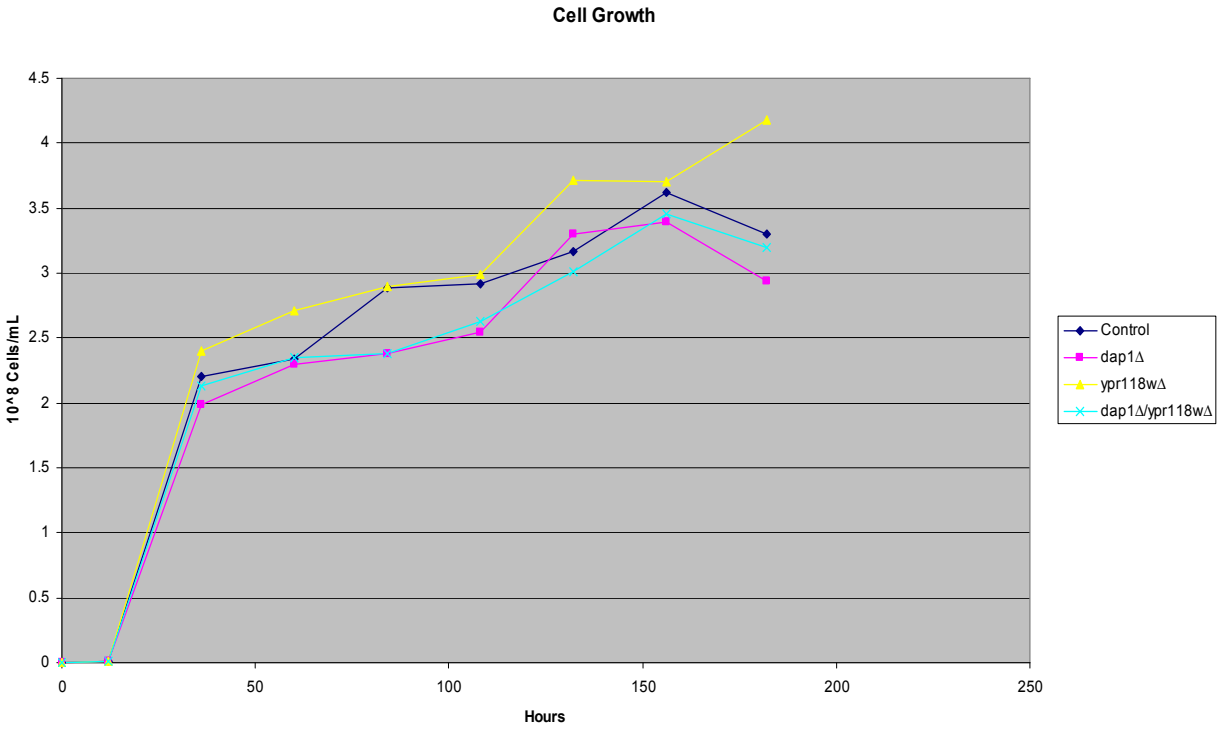

Figure 2. Cell growth in YPD. Graph shows number of cells of the control strain (blue diamonds), the *dap1*Δ mutant strain (pink squares), the *ypr118w*Δ mutant strain (yellow triangles), and the *dap1*Δ/ *ypr118w*Δ double mutant strain (green stars). Cell number was determined by direct cell count on a hemacytometer.

Competition Experiment in YPD Medium

For a more sensitive test of whether the deletion strains have a competitive disadvantage in long-term growth, we performed pairwise long-term competition experiments. Fresh 10mL

In YPD medium, no obvious differences were observed between the control strain and the deletion strains, except at approximately 50 days and beyond, where the deletion strains marginally outgrew the control strain. This was noted in Figures 3 and 4 by a proportional increase ranging from 10-15%. Figures 5 and 6 show that for YPD, in the short term growth period, considered exponential growth phase, there are no considerable differences between the control and the deletion strains. Therefore, neither the *dap1*Δ mutant strain nor the *ypr118w*Δ mutant strain appears to suffer from a growth disadvantage compared to the control strain in YPD, a rich medium.

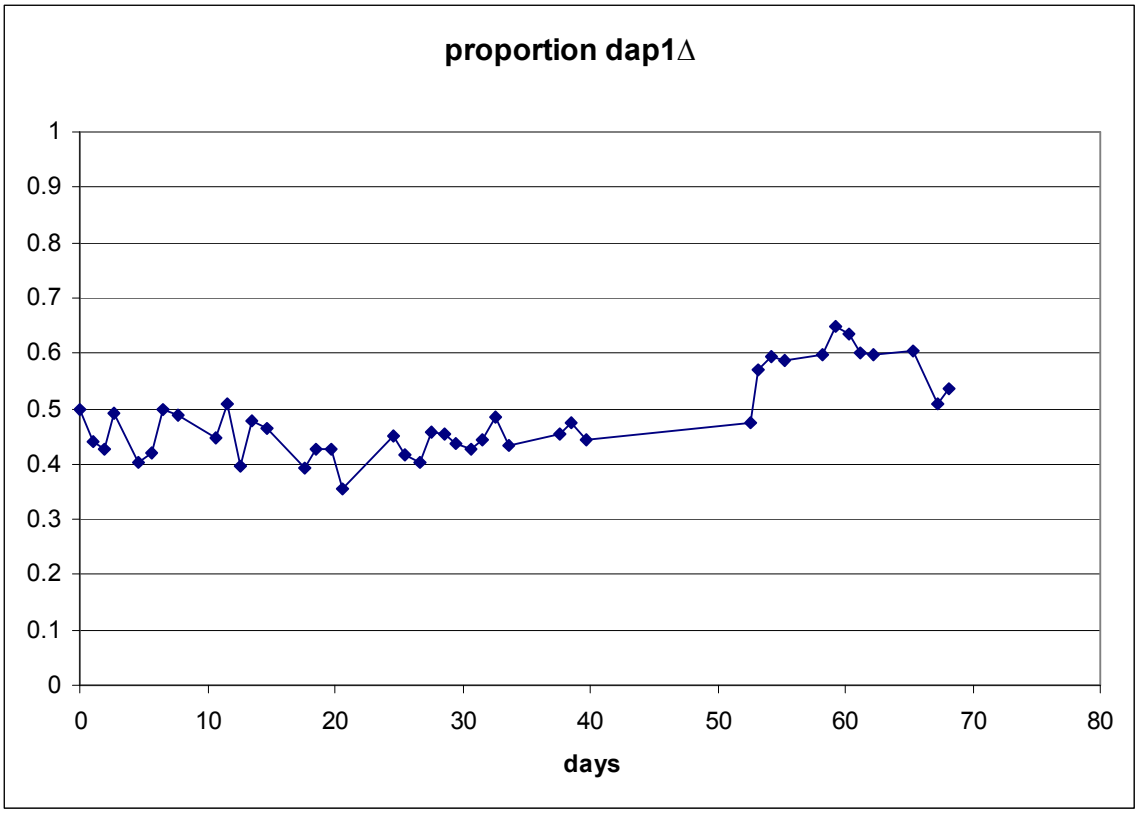

Figure 3. Long term Competition Experiment in YPD: control strain vs. *dap1*Δ mutant strain. Colonies were counted and the proportion determined by the number of *dap1*Δ colonies verses total number of colonies.

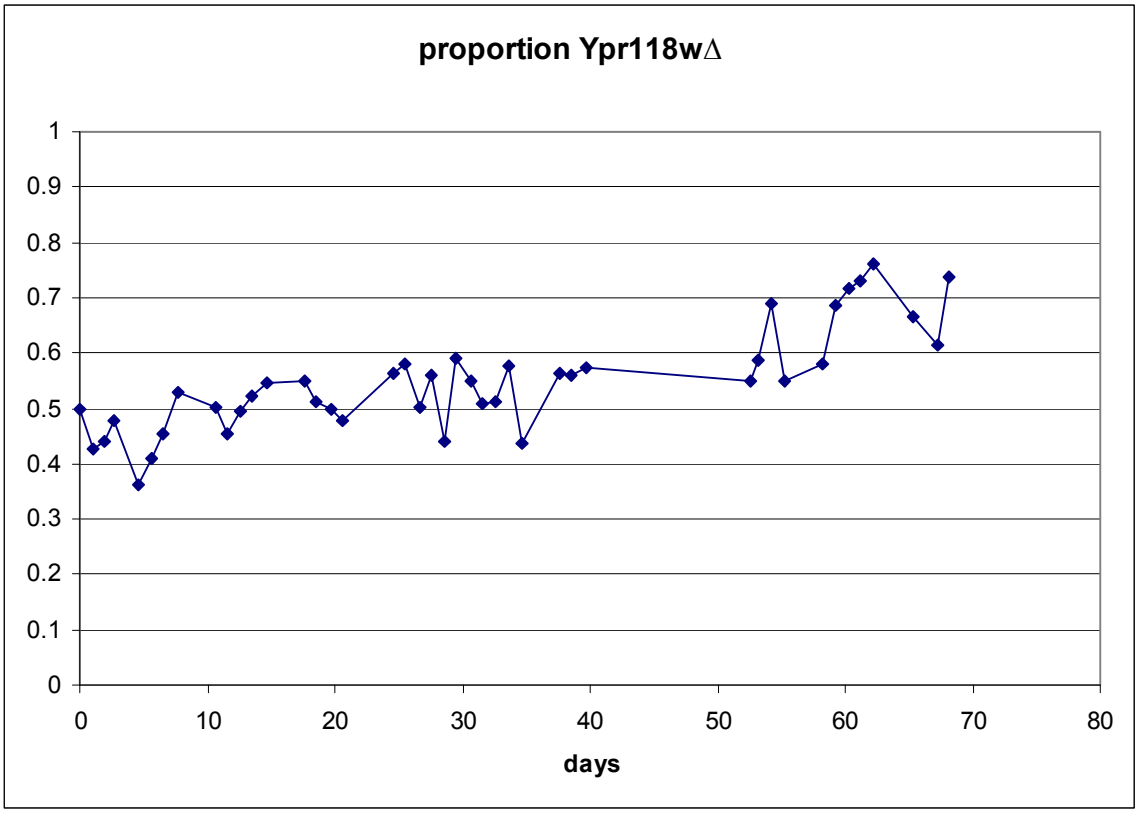

Figure 4. Long term Competition Experiment in YPD: control strain vs. *ypr118w*Δ mutant strain. Colonies were counted and the proportion determined by the number of *ypr118w*Δ colonies verses total number of colonies.

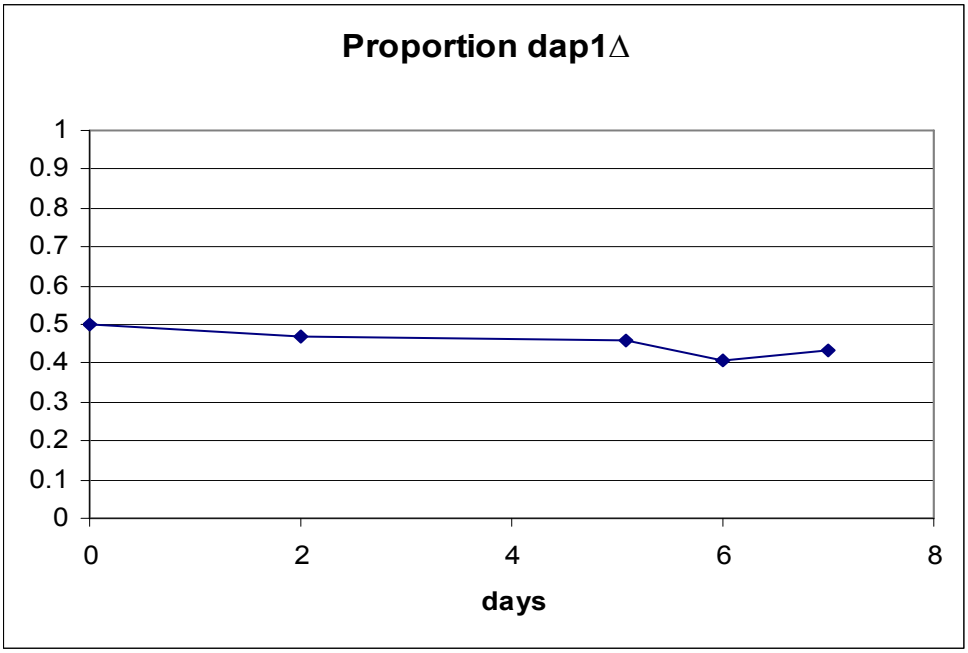

Figure 5. Short term Competition Experiment in YPD: control strain vs. *dap1*Δ mutant strain. Colonies were counted and the proportion determined by the number of *dap1*Δ colonies verses total number of colonies.

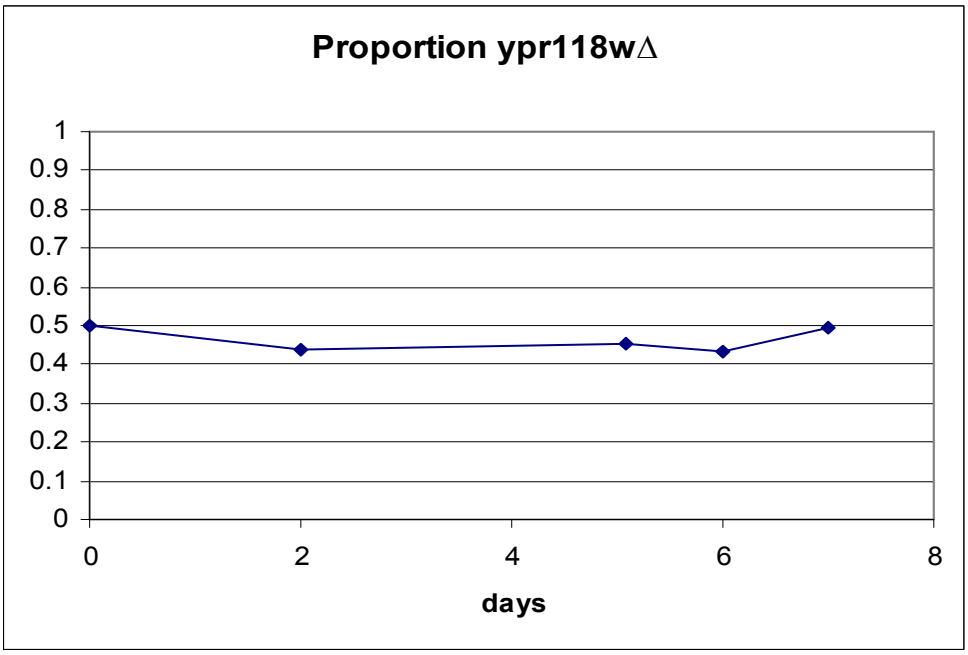

Figure 6. Short term Competition Experiment in YPD: control strain vs. *ypr118w*Δ mutant strain. Colonies were counted and the proportion determined by the number of *ypr118w*Δ colonies verses total number of colonies.

Competition Experiment in SLAD Medium

As a more stringent test, we performed competition experiments in synthetic, nitrogen-limiting media. Nitrogen-limitation was chosen both because yeast in the wild usually face nitrogen limitations, and also because microarray expression data [114] indicated that *DAP1* expression increased during nitrogen-limited growth.

In SLAD (nitrogen starvation) media, no obvious difference was observed between the control strain and the *dap1*Δ mutant strain in the first two weeks of culture, going from exponential growth to late log phase. As the cells are transferred every 7 days to fresh media, this pattern was continued for one more cycle. But between the second and third media change and until the end of the experiment, the *dap1*Δ mutant strain exhibited a competitive advantage over the control strain in the SLAD medium. This is noted in Figure 7 by a proportional increase ranging from 70-95%.

The opposite outcome was observed between the control strain and the *ypr118w*Δ mutant strain. No obvious difference was observed between the control strain and the *ypr118w*Δ mutant strain during the first cycle in SLAD medium. But, during the second and subsequent media cycle changes, the *ypr118w*Δ mutant strain exhibited a much diminished competitive edge as compared to the control strain, in fact going extinct in the culture. This was noted in Figure 8 by a proportional decrease ranging from 30 to 100%. The subsequent identification of Ypr118wp as an enzyme in the methionine salvage pathway would account for the sensitivity of the *ypr118w*Δ mutant strain to nitrogen limitation.

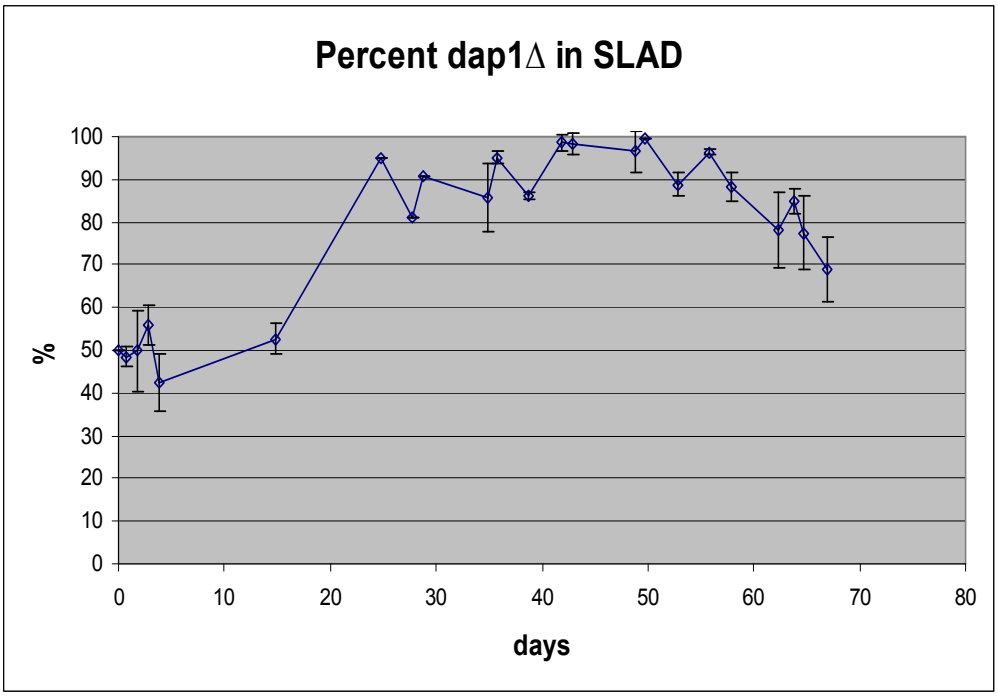

Figure 7. Long term Competition Experiment in SLAD (nitrogen starvation) media: control strain vs. *dap1*Δ mutant strain. Colonies were counted and the proportion determined by the number of *dap1*Δ colonies verses total number of colonies. Points show average of 3 independent experiments, bars represent standard deviations.

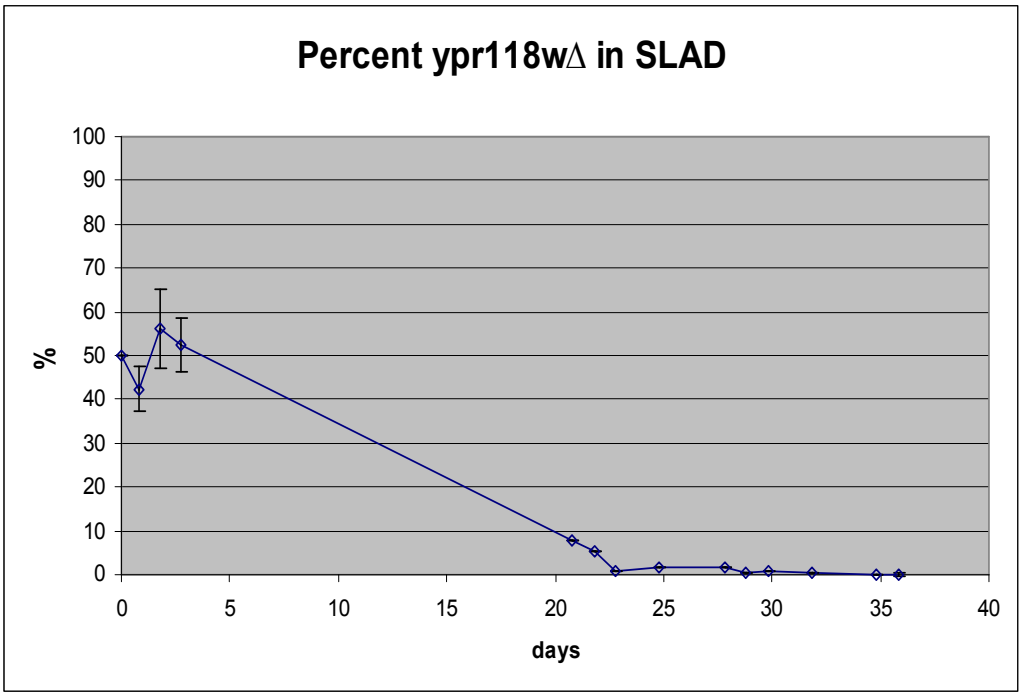

Figure 8. Long term competition experiment in SLAD (nitrogen starvation) media: control strain vs. *ypr118w*Δ mutant strain. Colonies were counted and the proportion determined by the number of *ypr118w*Δ colonies verses total number of colonies. Points show the average of 3 independent experiments, bars represent standard deviations.

Competition Experiment in SPHD Medium

We also performed competition experiments in SPHD, a medium that is less severely nitrogen-limiting than SLAD.

In SPHD media, no obvious differences were observed between the control strain and the *dap1*Δ mutant strain, except at approximately 50 days and beyond, where the *dap1*Δ mutant strains marginally outgrew the control strain. This was noted in Figure 9 by a proportional increase ranging from 10-20%.

In contrast, the *ypr118w*Δ mutant strain was outgrown by the control strain very early in the experiment. The control strain and the *ypr118w*Δ mutant strain seemed to reach and maintain equilibrium of approximately three control strain cells for every one *ypr118w*Δ mutant strain cell. This was noted in Figure 10 by a proportional decrease ranging from 10-25%.

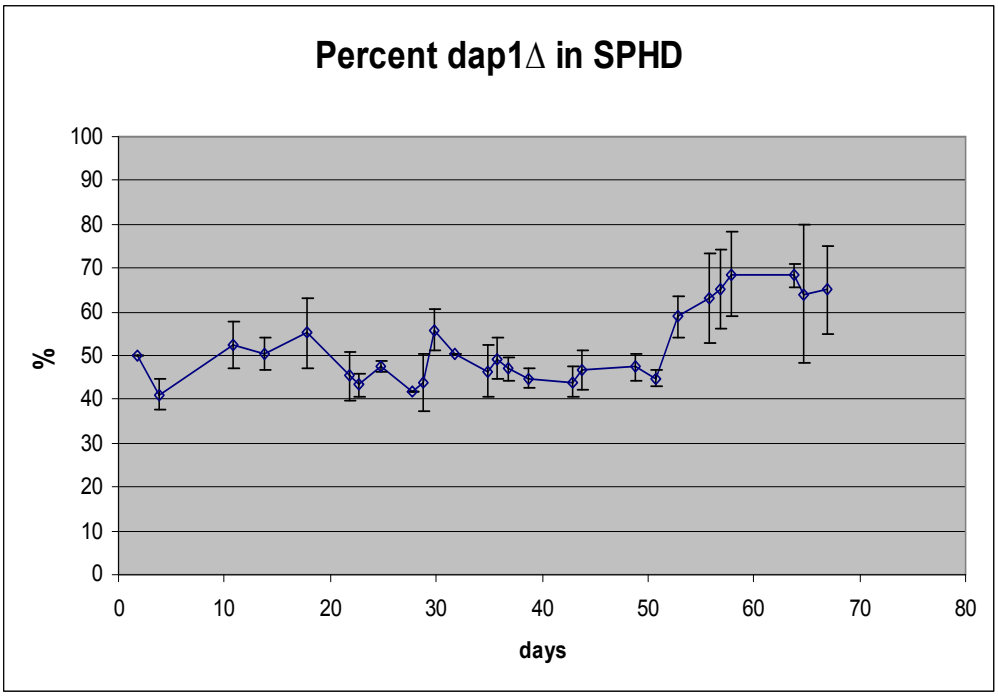

Figure 9. Long term Competition Experiment in SPHD (low nitrogen) media: control strain vs. *dap1*Δ mutant strain. Colonies were counted and the proportion determined by the number of *dap1*Δ colonies verses total number of colonies. Points show the average of 3 independent experiments, bars represent standard deviations.

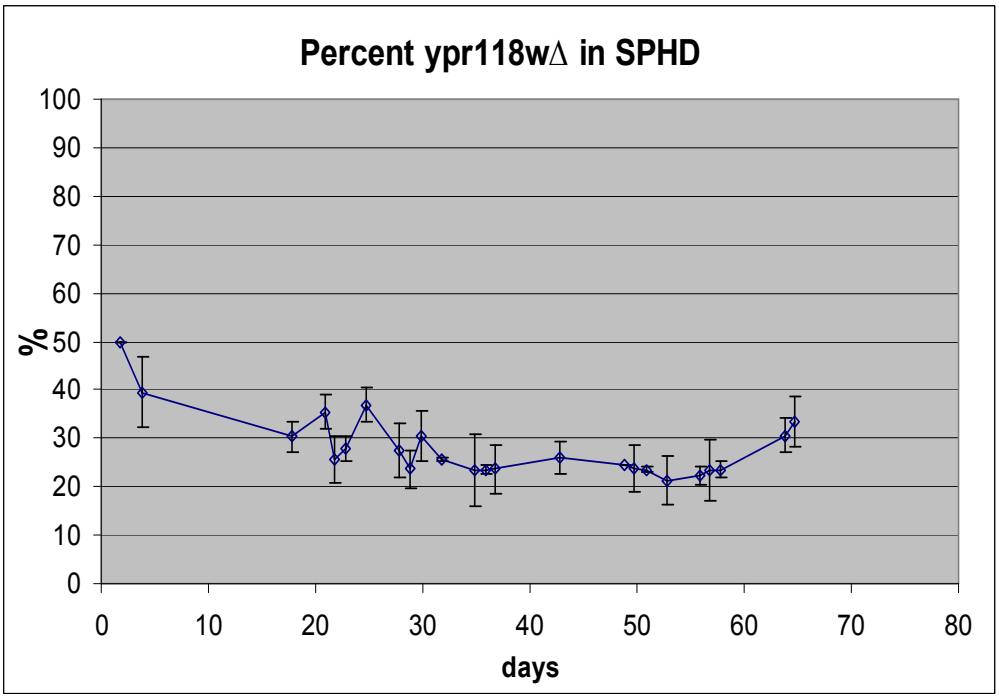

Figure 10. Long term competition experiment in SPHD (low nitrogen) media: control strain vs. *ypr118w*Δ mutant strain. Colonies were counted and the proportion determined by the number of *ypr118w*Δ colonies verses total number of colonies. Points show average of 3 independent experiments, bars represent standard deviations.

PHENOTYPIC GROWTH PATTERNS

Frequency of Petite mutants

It was noticed that the *dap1*Δ mutant strain exhibited an increase in the number of petite colony formation during routine cell streaking from glycerol stock. To determine if the colonies were actually petite or just exhibited prolonged slow growth, cells of the control strain, the *dap1*Δ mutant strain, the *ypr118w*Δ mutant strain, and the *dap1*Δ/ *ypr118w*Δ double mutant strain were grown on YPD plates overnight and then replica plated onto YPG plates. Those colonies that did not grow on the YPG plates were assumed to have lost mitochondrial function and classified as petite. No further studies or characterization of the basis of mitochondrial loss was conducted. Ten random colonies were scraped from the YPG plates, diluted, and used for the subsequent generations.

Petite growth experiment

Colonies of the *dap1*Δ mutant strain and colonies of the *dap1*Δ/ *ypr118w*Δ double mutant strain exhibited a higher proportion of petite colonies as compared to the control in the first generation of culture (see Figures 11 and 13). Subsequent generations exhibited levels consistent with control levels. Colonies of the *ypr118w*Δ mutant strain exhibited petite formation consistent with control levels; as seen in Figures 11 and 14.

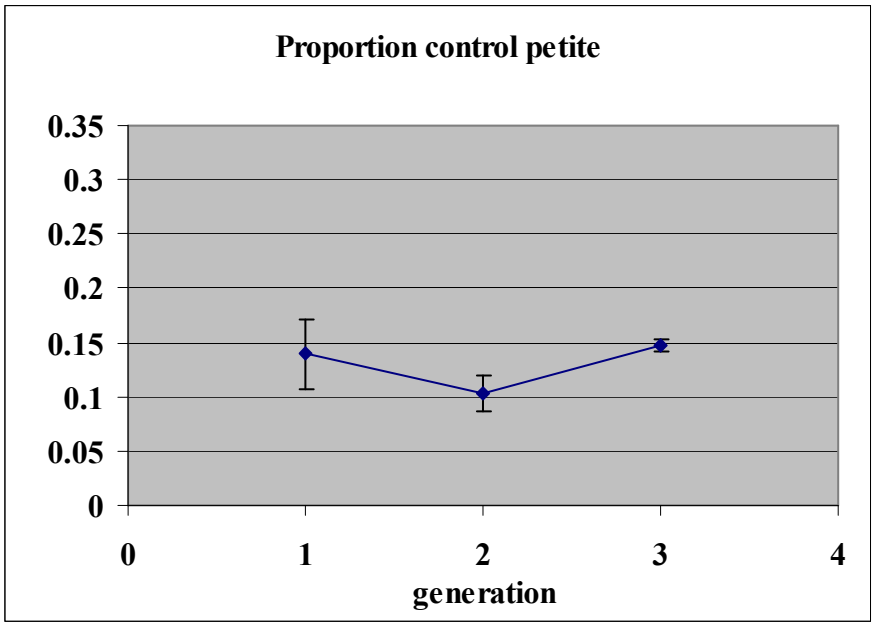

Figure 11. Proportion of Petite Colonies of control strain grown in YPD for 3 generations. Points show average of 3 independent experiments, bars represent standard deviations.

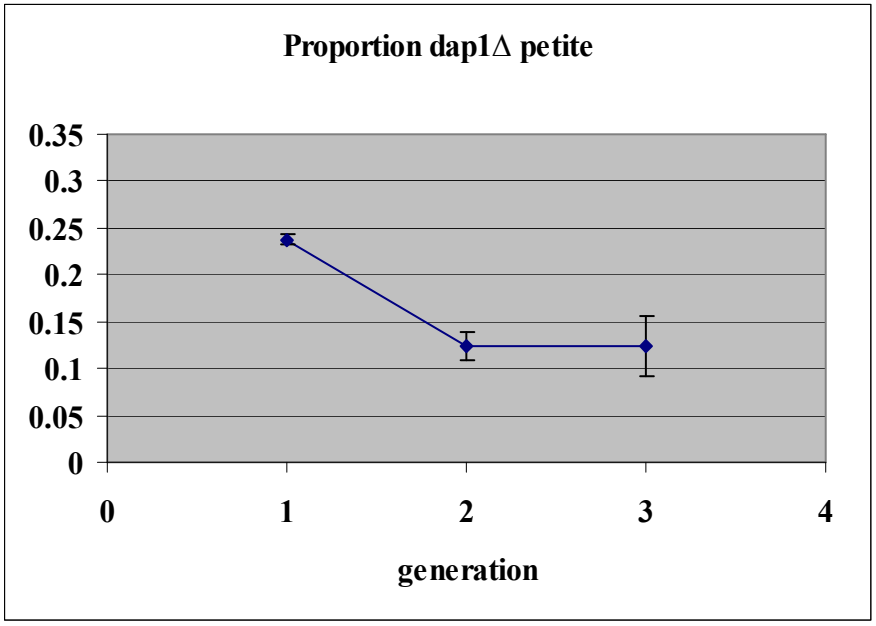

Figure 12. Proportion of Petite Colonies of the *dap1*Δ mutant strain grown in YPD for 3 generations. Points show average of 3 independent experiments, bars represent standard deviations.

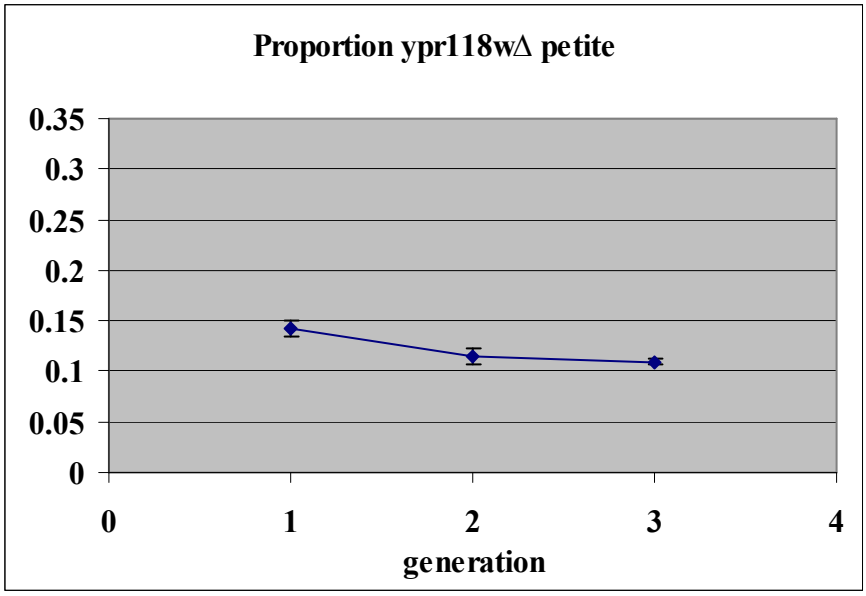

Figure 13. Proportion of Petite Colonies of the *ypr118w*Δ mutant strain grown in YPD for 3 generations. Points show average of 3 independent experiments, bars represent standard deviations.

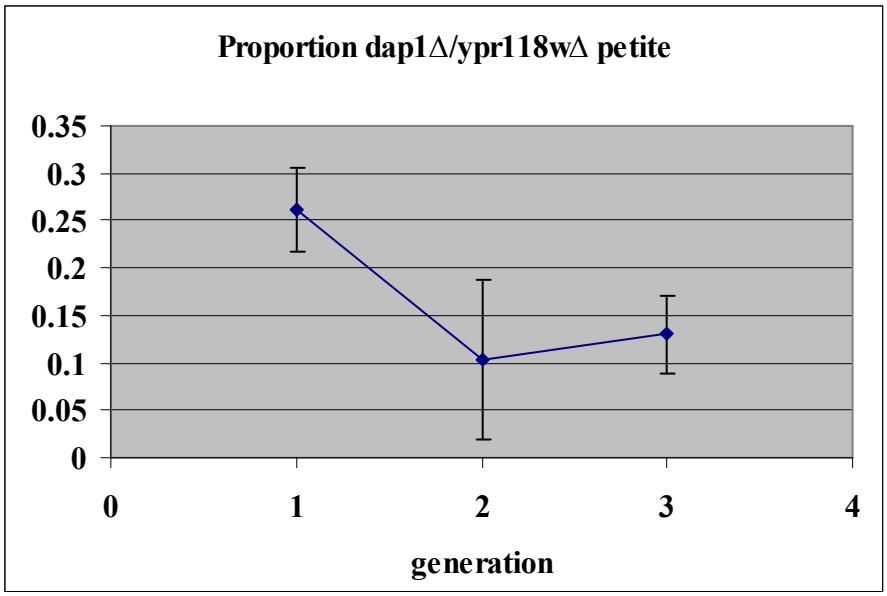

Figure 14. Proportion of Petite Colonies of the *dap1Δ/ypr118wΔ* double mutant strain grown in YPD for 3 generations. Points show average of 3 independent experiments, bars represent standard deviations.

Methyl Methanesulfonate (MMS) Sensitivity Experiment

It had previously been reported [66] that the *dap1*Δ mutant strain exhibited an increased sensitivity to the DNA damaging agent MMS. To verify this and to test the sensitivity patterns of the *ypr118w*Δ mutant strain, and the *dap1*Δ/ *ypr118w*Δ double mutant strain an MMS sensitivity experiment was performed.

The *dap1*Δ mutant strain was more sensitive to MMS treatment than the control strain; this can most readily be seen in Figure 15 plates iii and iv. The *ypr118w*Δ mutant strain acted similar to the control strain in MMS sensitivity; this can most readily be seen in Figure 15 plates iv and v. The *dap1*Δ/ *ypr118w*Δ double mutant strain was more sensitive to MMS treatment than the control strain, but exhibited a slightly less sensitivity than the *dap1*Δ mutant strain; this can most readily be seen in Figure 15 plates iii and iv.

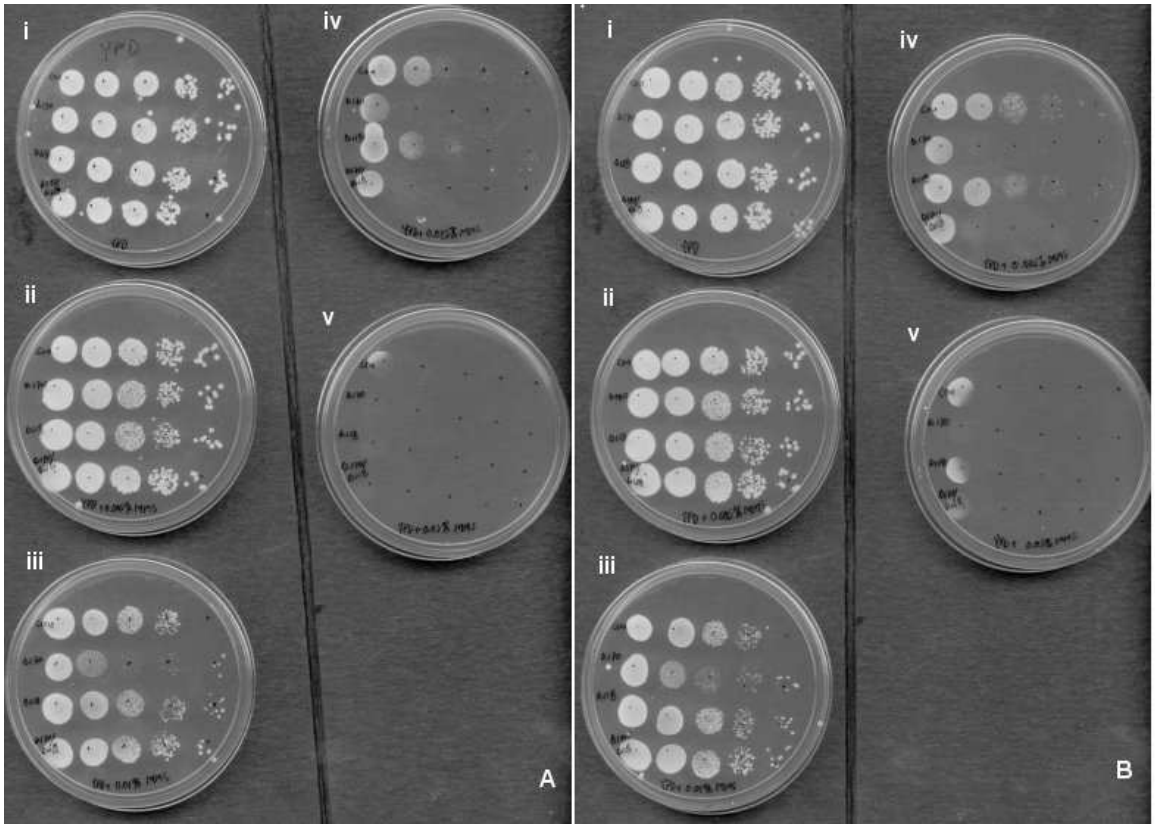

Figure 15. MMS Sensitivity Experiment. Growth of serial dilutions from top to bottom on each plate: control strain, *dap1*Δ mutant strain, *ypr118w*Δ mutant strain, and *dap1*Δ*/ypr118w*Δ double mutant strain on YPD media supplemented with MMS. i) YPD, ii) YPD + 0.005% MMS, iii) YPD + 0.01% MMS, iv) YPD + 0.025% MMS, v) YPD + 0.05% MMS. Set A and B are duplicate independent experiments.

LOCALIZATION OF PROTEINS

DAP1-GFP and *YPR118W*-RFP2 fusions were constructed to monitor the sub-cellular localization of the protein products in cells during vegetative growth. *DAP1* and *YPR118W* were cloned into different vectors with different selectable markers and fused to different colored fluorescent proteins; they were used to monitor their localization simultaneously in the same cell as well as independently in different deletion strains. The *DAP1*-GFP and *YPR118W*-RFP2 fusion proteins were under the control of the constitutive promoter, Gpd.

Dap1p-GFP Localization and Ypr118wp-RFP2 Localization

*Dap1*Δ mutant yeast cells and *ypr118w*Δ mutant yeast cells were transformed by the LiAc/PEG method with the plasmid pHGPD-*DAP1*-sGFP and pRS315-*YPR118W*-RFP2, respectively. Transformed cells were grown overnight in selective SD liquid media, centrifuged at 4,000 x g for 5 minutes, washed once with 1X TE, fixed with 3.7% formaldehyde, and resuspended in mounting media (1mg/ml p-phenylenediamine in 1X PBS 90% glycerol) containing 22.5ug/ml DAPI (4',6-Diamidino-2-phenylindole). Images were captured using a Zeiss LSM510 UV confocal laser scanning microscope with either a Zeiss 63X or 100X Plan-Neofluar oil immersion lens (Core Facilities at the Parker H. Petit Center for Bioengineering and Biosciences, Georgia Institute of Technology).

Both Dap1p-GFP (Fig. 16-17) and Ypr118wp-RFP2 (Fig. 18-19) exhibited discrete particulate localization in the cytoplasm, and it appeared that Dap1p-GFP was also present in the ER.

To further characterize the Dap1p-Ypr118wp interaction, it was tested whether the absence of Dap1p would affect the localization of Ypr118wp-RFP2 and vice versa. Localization of Dap1p-GFP and Ypr118wp-RFP2 were monitored in the *ypr118w*Δ and *dap1*Δ mutant backgrounds, respectively, as well as in the *dap1*Δ /*ypr118w*Δ double mutant background. The results showed the localization patterns of Dap1p-GFP and Ypr118wp-RFP2 are not dependent upon one another (data not shown).

In addition, Dap1p-GFP co-localizes with nile red, a stain specific for neutral lipids, and hence for lipid particles (Figure 20). Lipid particles were also monitored in the *dap1*Δ mutant strain and in a strain over-expressing Dap1p (pUGpd-Dap1), to determine if the absence, or over production, of Dap1p influenced lipid particle formation, number or size. No obvious differences were observed in the appearance or number of lipid particles in either the *dap1*Δ mutant strain, or in the strain over-expressing Dap1p, when compared to controls (data not shown).

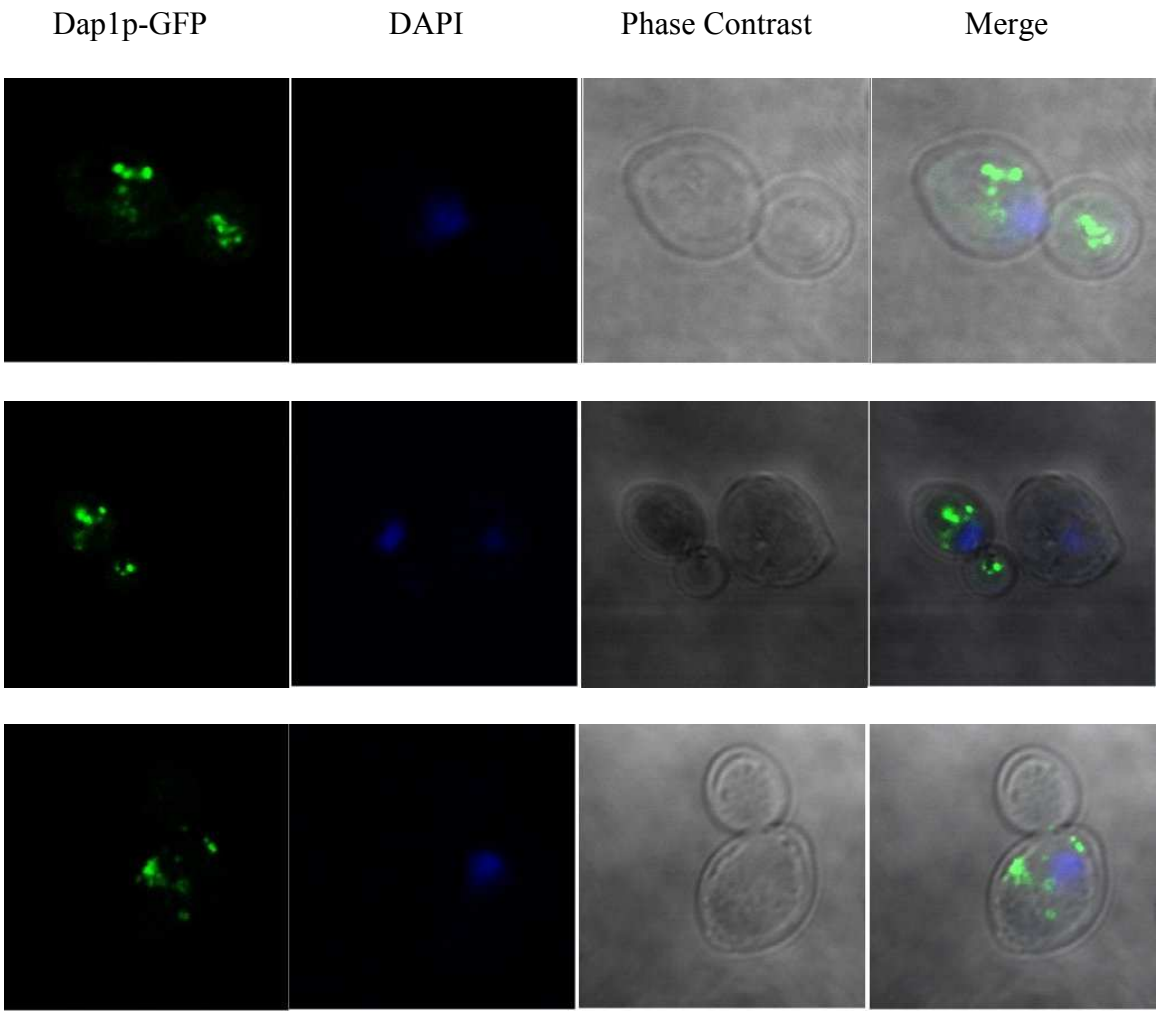

Figure 16. Dap1p-GFP localization experiment. Left column were monitored in the green portion of the spectrum for acquisition of the GFP fluorescence. Second column was monitored in the blue portion of the spectrum for acquisition of the DAPI stained nucleus fluorescing. Third column was monitored in phase contrast for acquisition of cell boundary and cell morphology. These three pictures were merged to form the right column.

A representative picture of the Dap1p-GFP localization experiment is shown below in large format for clearer viewing of localization.

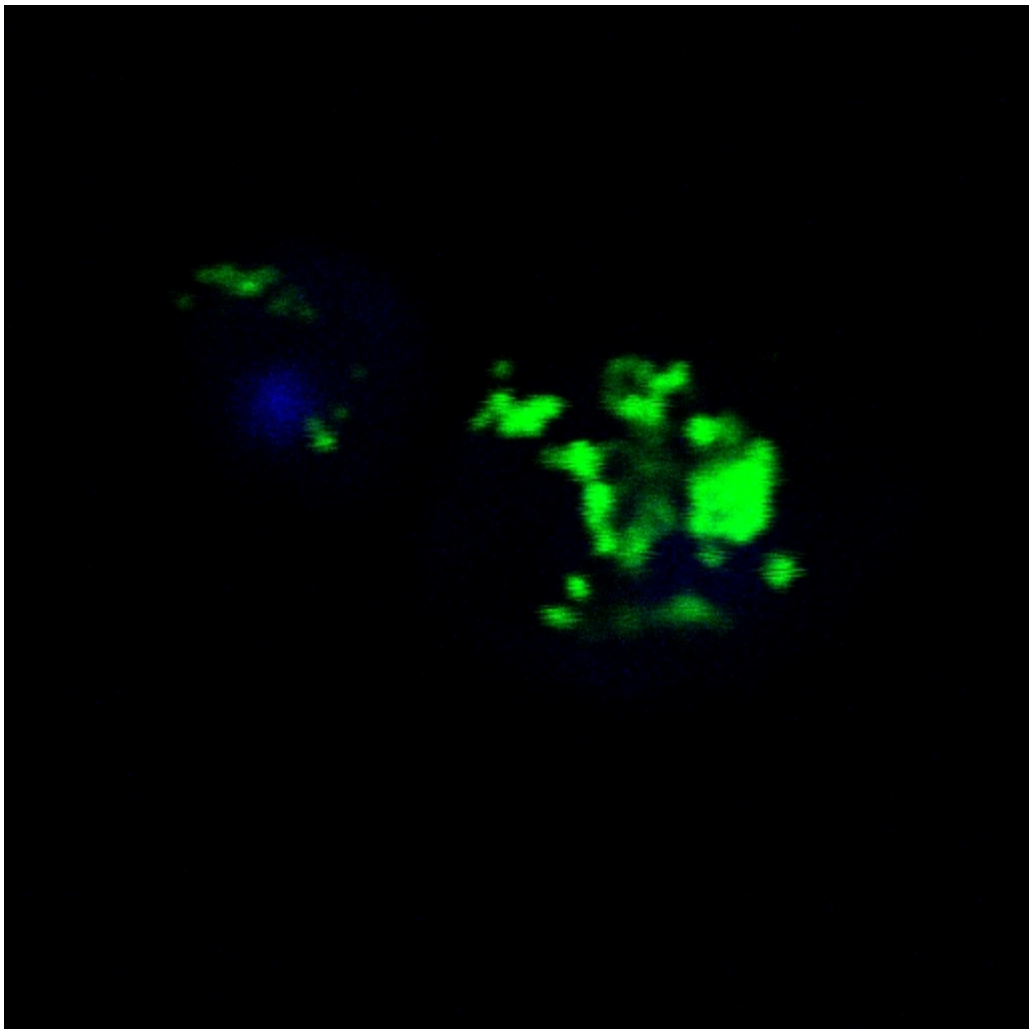

Figure 17. Dap1p-GFP localization experiment, close-up.

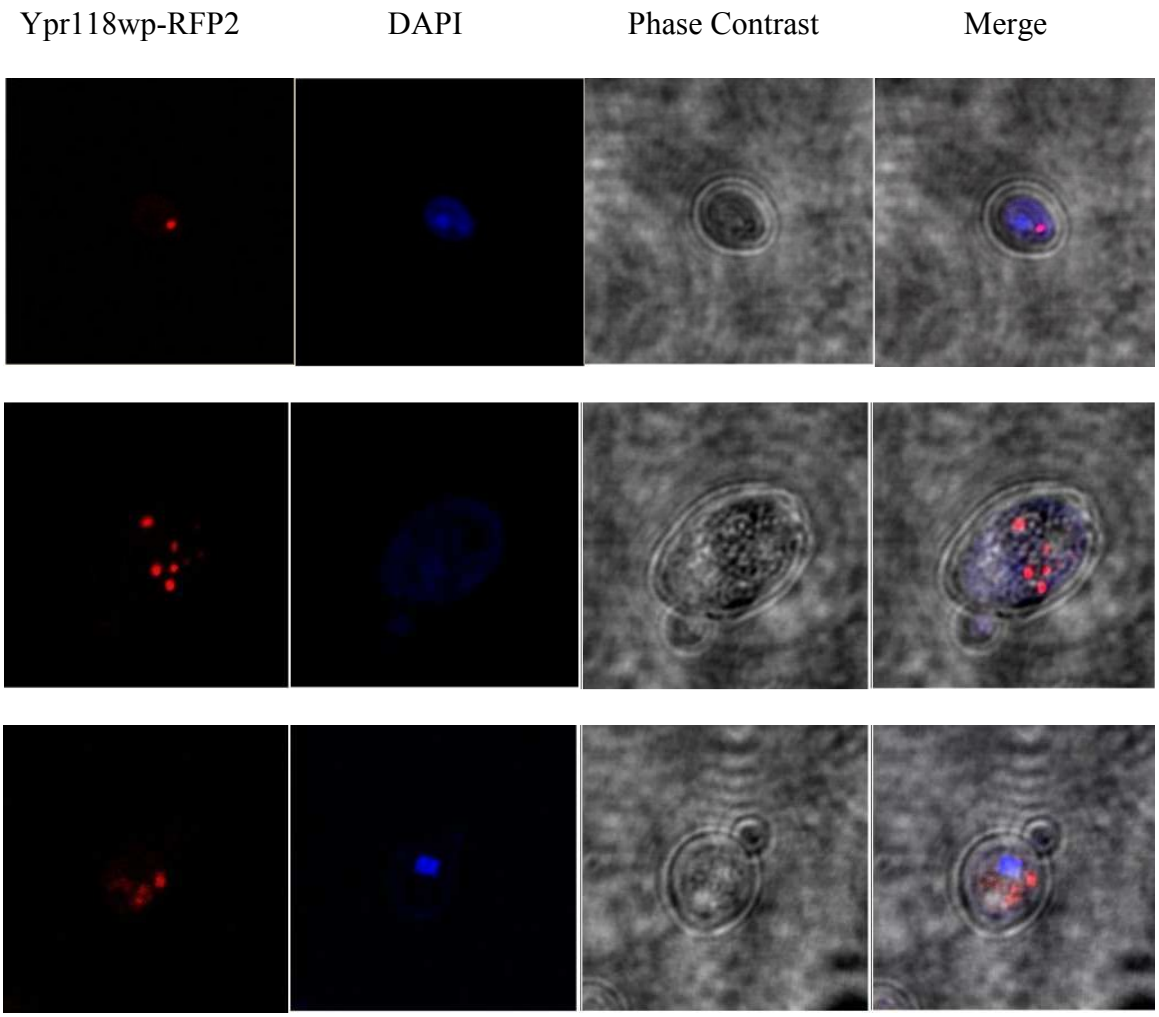

Figure 18. Ypr118wp-RFP2 localization experiment. Left column was monitored in the red portion of the spectrum for acquisition of the RFP2 fluorescence. Second column was monitored in the blue portion of the spectrum for acquisition of the DAPI stained nucleus fluorescing. Third column was monitored in phase contrast for acquisition of cell boundary and cell morphology. These three pictures were merged to form the right column.

A representative picture of the Ypr118wp-RFP2 localization experiment is shown below in large format for clearer viewing of localization.

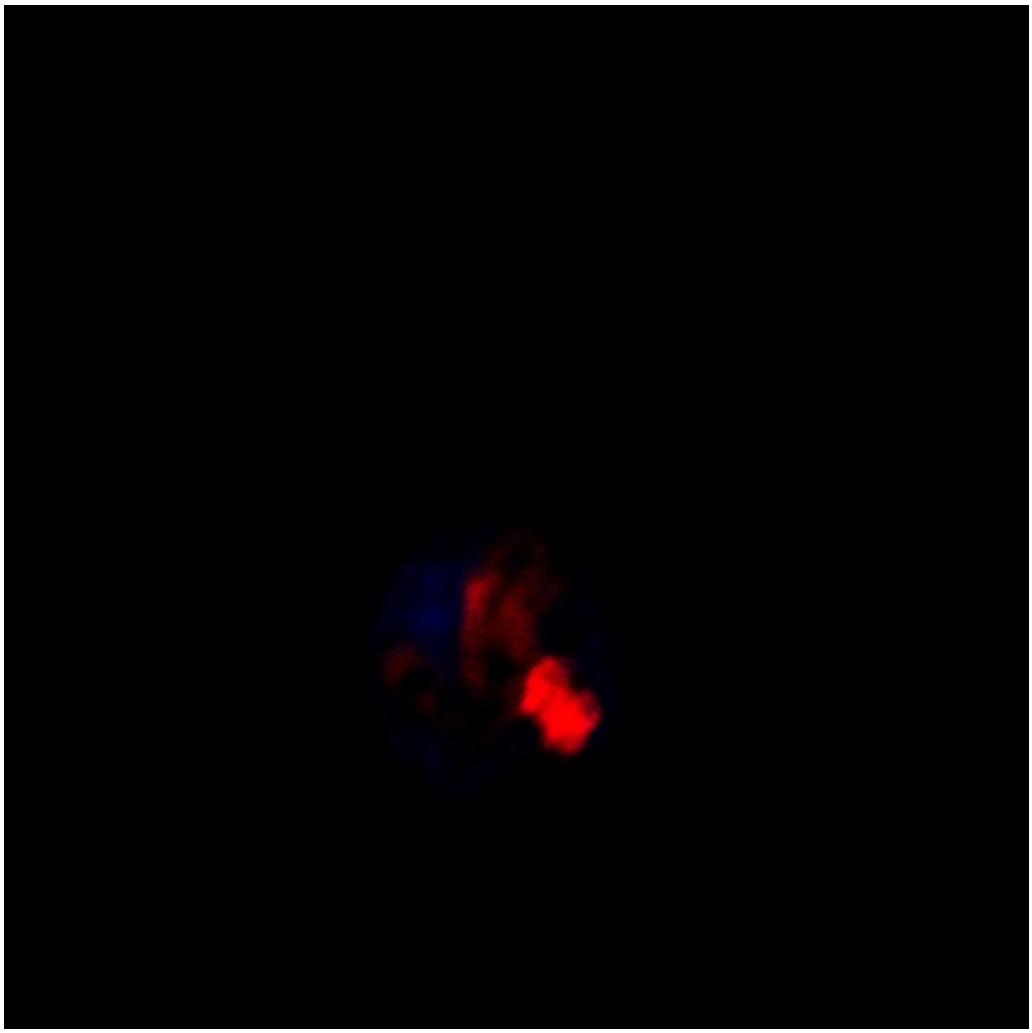

Figure 19. Ypr118wp-RFP2 localization experiment, close-up.

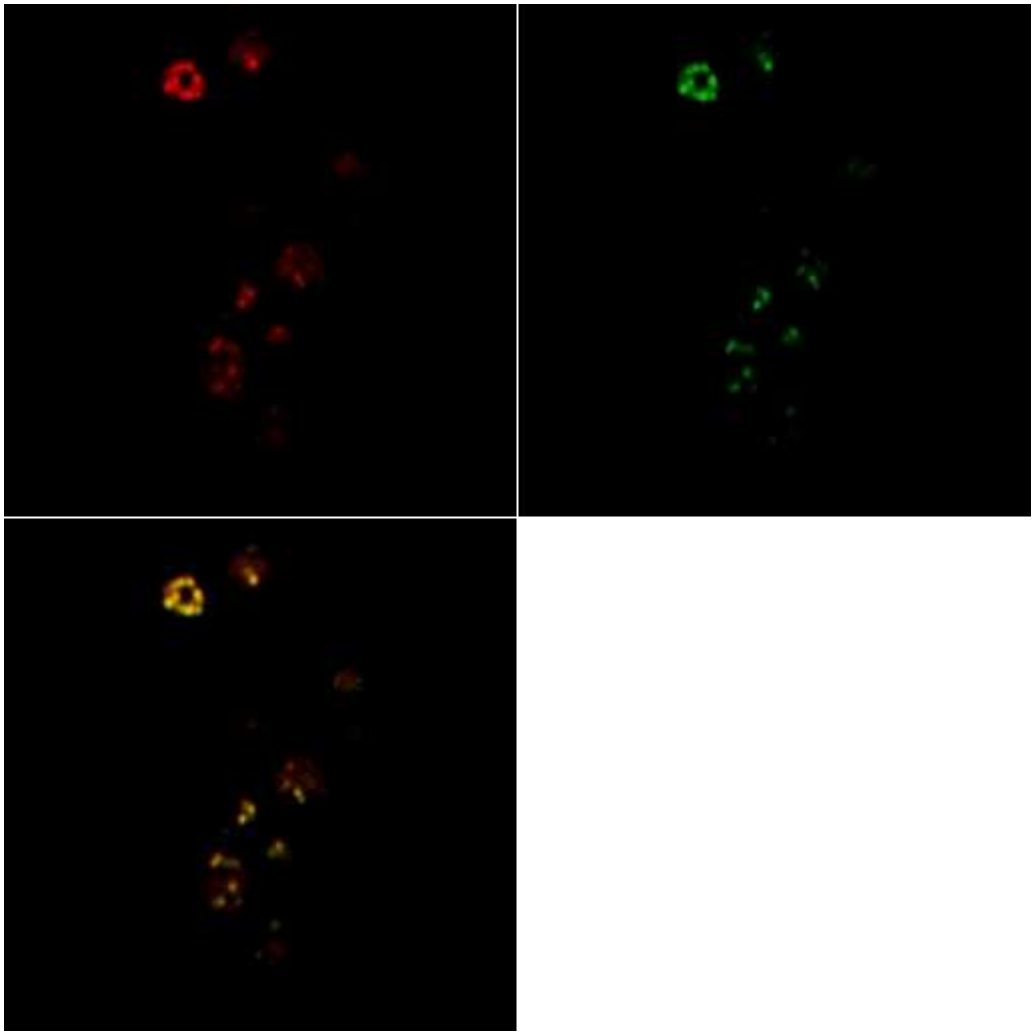

Figure 20. Dap1p-GFP localization with nile red stain. Upper left panel was monitored in the red portion of the spectrum for acquisition of the nile red stain fluorescence. Upper right panel was monitored in green for acquisition of GFP fluorescence. These three pictures were merged to form the lower left panel.

Dap1p-GFP Localization with MMS Treatment

To determine if the Dap1p-GFP fusion protein exhibited differential localization upon addition of MMS (a DNA damaging agent), cells of the *dap1*Δ mutant strain were transformed with the pHGPD-*DAP1*-sGFP plasmid and incubated for various time points in YPD supplemented with 0.035% MMS. The experiment showed an increase in the percentage of the Dap1p-GFP that localized peri-nuclearly (Figure 21 and Table 3).

*Dap1*Δ mutant yeast cells were transformed by the LiAc/PEG method with the plasmid pHGPD-*DAP1*-sGFP. Transformed cells were grown overnight in selective SD liquid media, centrifuged at 4,000 x g for 5 minutes, and washed once with 1X TE. Cells were then resuspended in 1mL YPD containing 0.035% MMS (v/v) for various time points, before being fixed with addition of formaldehyde to 3.7%. Cells were then centrifuged and resuspended in mounting media (1mg/ml p-phenylenediamine in 1X PBS 90% glycerol) containing 22.5ug/ml DAPI. Images were captured using a Zeiss LSM510 UV confocal laser scanning microscope with either a Zeiss 63X or 100X Plan-Neofluar oil immersion lens (Core Facilities at the Parker H. Petit Center for Bioengineering and Biosciences, Georgia Institute of Technology).

About 30 cells expressing the Dap1p-GFP fusion protein were picked at random at each time point for visualization and subsequent data storage. After all data was gathered, pictures were then studied to determine if a merge existed between the blue of the DAPI stain and the green fluorescence of the Dap1p-GFP fusion protein. If any amount of merge existed, the localization of the Dap1p-GFP fusion protein was termed peri-nuclear localized, even if some or most of the Dap1p-GFP fusion protein was localized to the cytoplasm; see Figures 21 and 22.

Between 10 and 15 minutes after the addition of 0.0035% MMS, a greater percentage of the cells expressing the Dap1p-GFP fusion protein showed peri-nuclear localization rather than being exclusively localized to lipid particles as compared to transformed strain without the addition of MMS. This higher percentage persisted for at least 60 minutes; see Table 3.

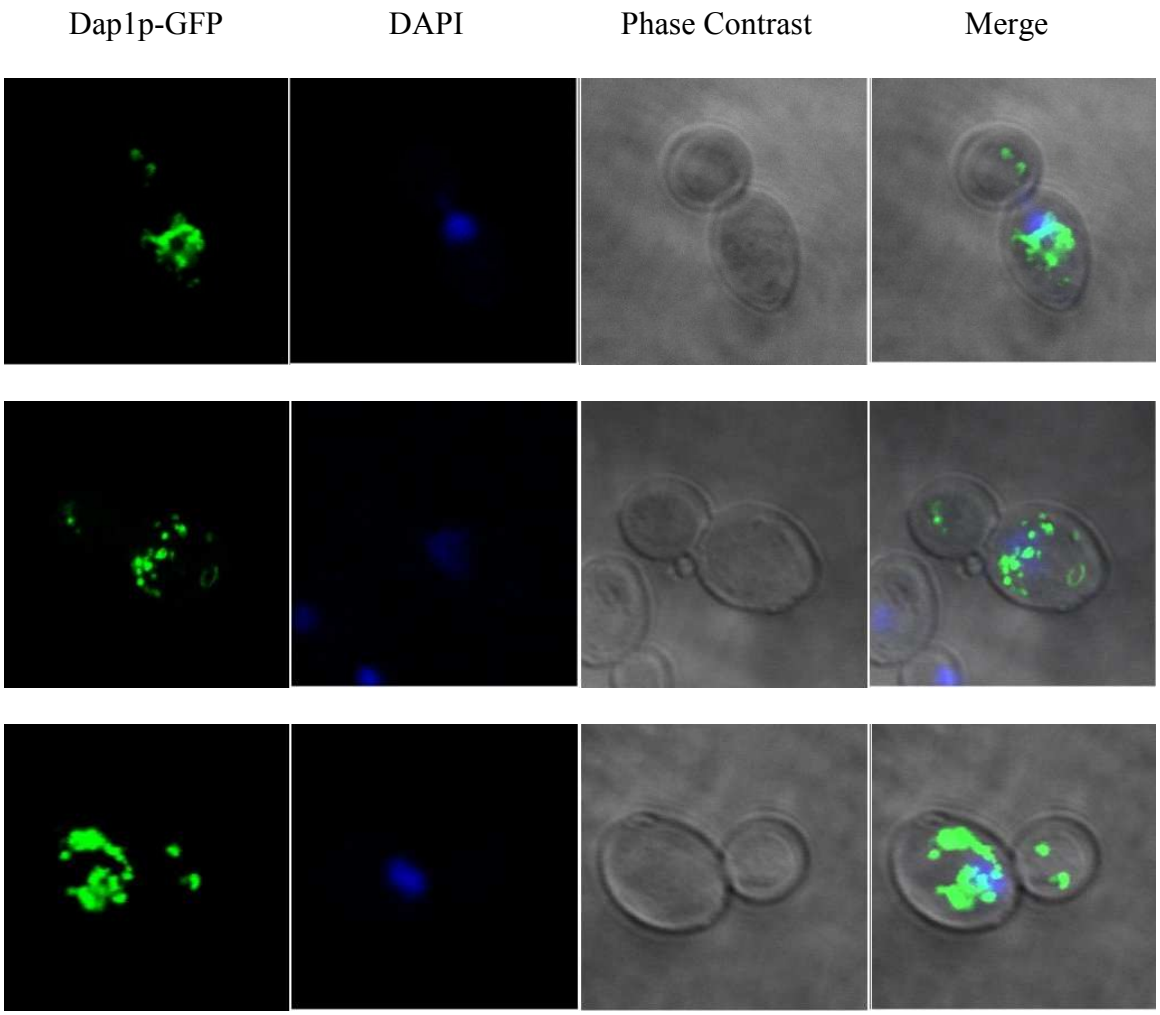

Figure 21. Dap1p-GFP localization experiment with addition of MMS. Left column were monitored in the green portion of the spectrum for acquisition of the GFP fluorescence. Second column was monitored in the blue portion of the spectrum for acquisition of the DAPI stained nucleus fluorescing. Third column was monitored in phase contrast for acquisition of cell boundary and cell morphology. These three pictures were merged to form the right column.

A representative picture of the dap1p-GFP with addition of 0.035% MMS localization experiment is shown below in large format for clearer viewing of localization.

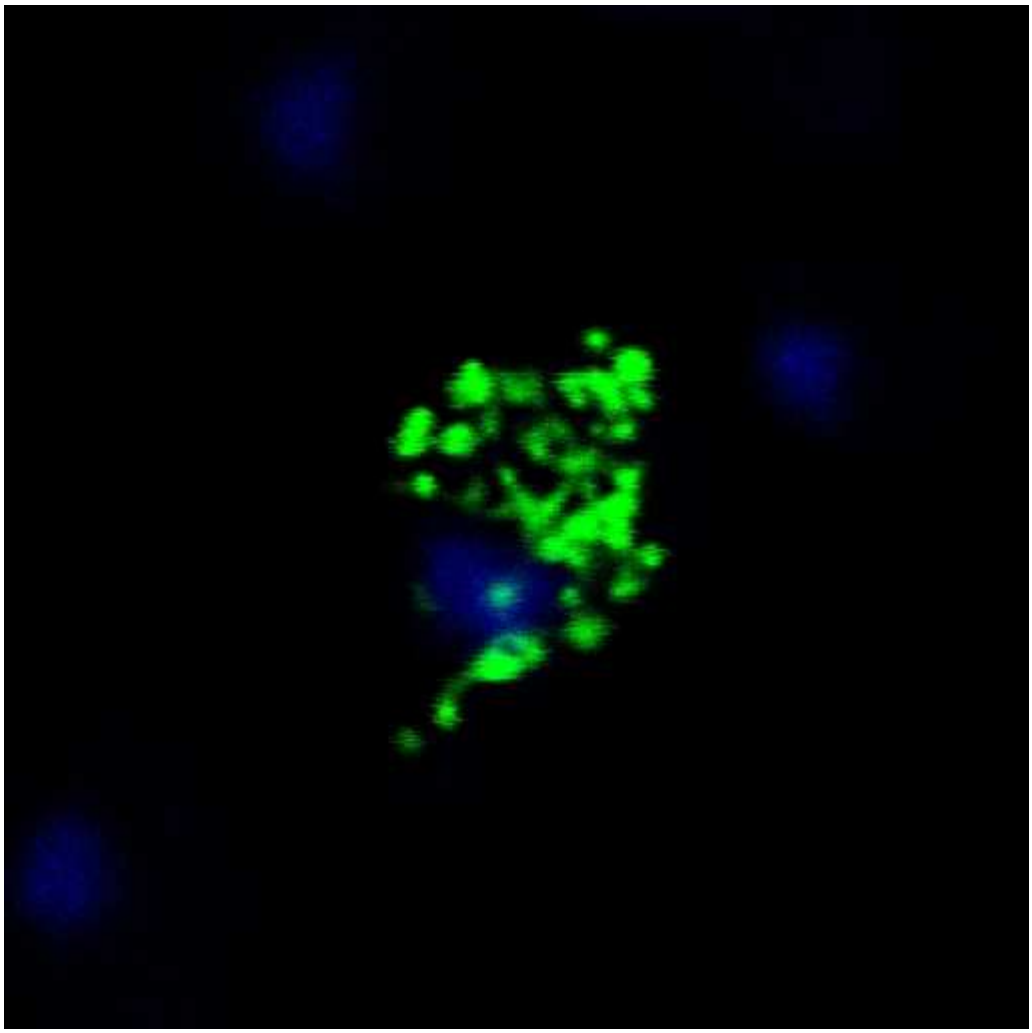

Figure 22. Dap1p-GFP localization experiment with addition of MMS, close-up.

Table 3. Percentage of Dap1p-GFP that show peri-nuclear localization.

Amount MMS(v/v)	Time (min)	Number Cytoplasmic	Number Peri-Nuclear	Total	% Peri-Nuclear
None	0	28	8	36	22
0.035%	1	11	2	13	15
0.035%	5	22	7	29	24
0.035%	10	27	8	35	23
0.035%	15	20	12	32	38
0.035%	30	19	15	34	44
0.035%	60	20	11	31	35

MMS – Methane Methylsulfonate

Dap1p-GFP and Ypr118wp-RFP2 Co-localization Experiment

To reinforce the observation of the two-hybrid protein-protein interaction between Dap1p and Ypr118wp, performed by Dr. Phillip Gray (Georgia Institute of Technology), a co-localization experiment was performed in the *dap1*Δ*/ypr118w*Δ double mutant yeast strain. This experiment showed an overlap of localization between Dap1p-GFP and Ypr118wp-RFP2 (see Figures 23 and 24).

Cells of the *dap1*Δ*/ypr118w*Δ double mutant yeast strain were co-transformed with pRS315-*YPR118W*-RFP2 and pHGPD-*DAP1*-sGFP according to the LiAc/PEG transformation protocol. Transformed cells were grown overnight in selective SD liquid media, centrifuged at 4,000 x g for 5 minutes, washed once with 1X TE, fixed with 3.7% formaldehyde, and resuspended in mounting media (1mg/ml p-phenylenediamine in 1X PBS 90% glycerol) containing 22.5ug/ml DAPI. Images were captured using a Zeiss LSM510 UV confocal laser scanning microscope with either a Zeiss 63X or 100X Plan-Neofluar oil immersion lens (Core Facilities at the Parker H. Petit Center for Bioengineering and Biosciences, Georgia Institute of Technology).

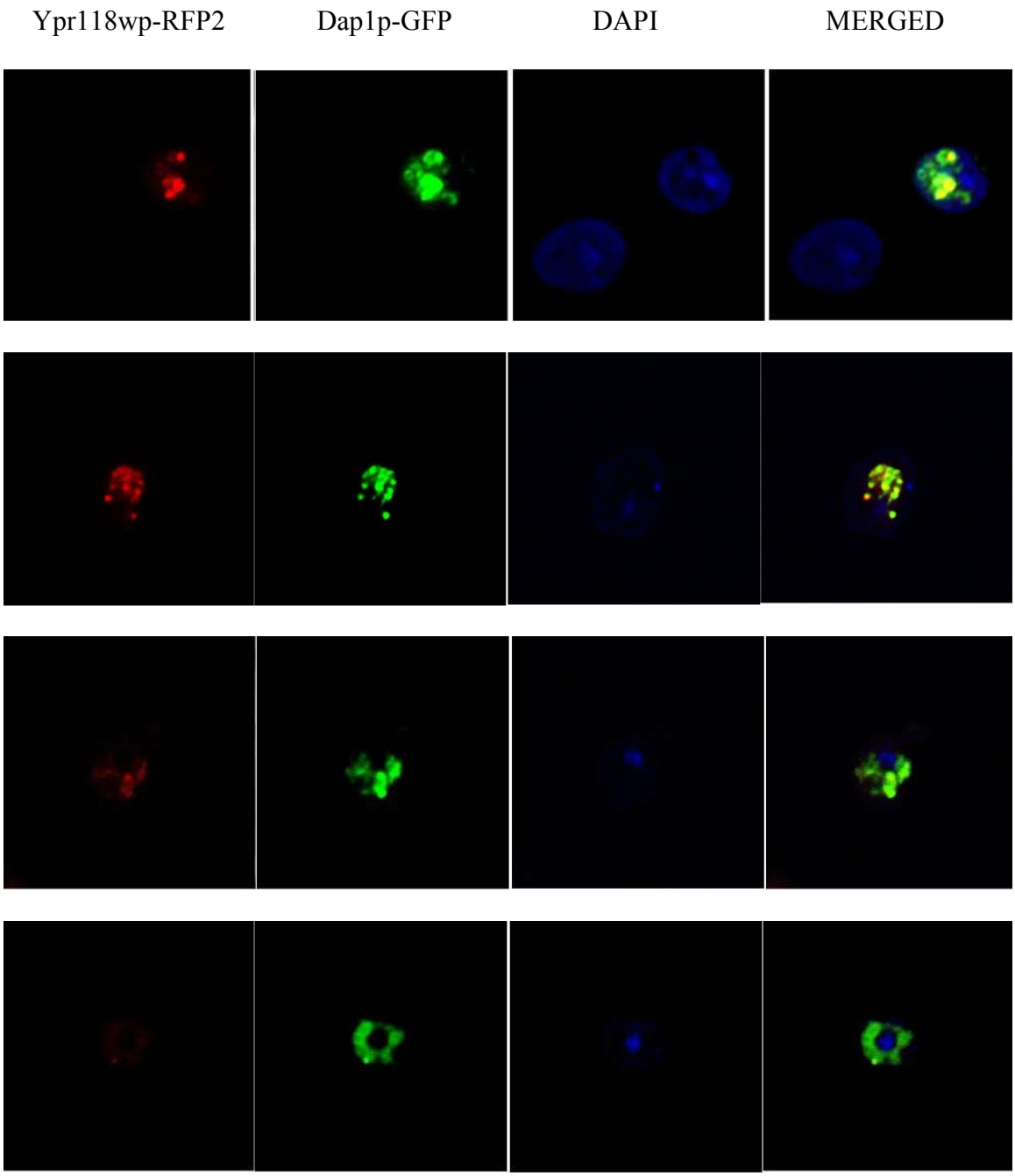

Figure 23. Dap1p-GFP and Ypr118wp-RFP2 co-localization experiment. Four different co-transformed cells are shown to show the differences in protein distribution. First column is detection in the red portion of the spectrum for cells expressing Ypr118wp-RFP2. Second column is detection in the green portion of the spectrum for cells expressing Dap1p-GFP. Third column is detection in the blue portion of the spectrum showing cells stained with DAPI, for DNA localization. The fourth column is a merge.

A representative picture of the co-localization experiment is shown below in large format for clearer viewing of localization.

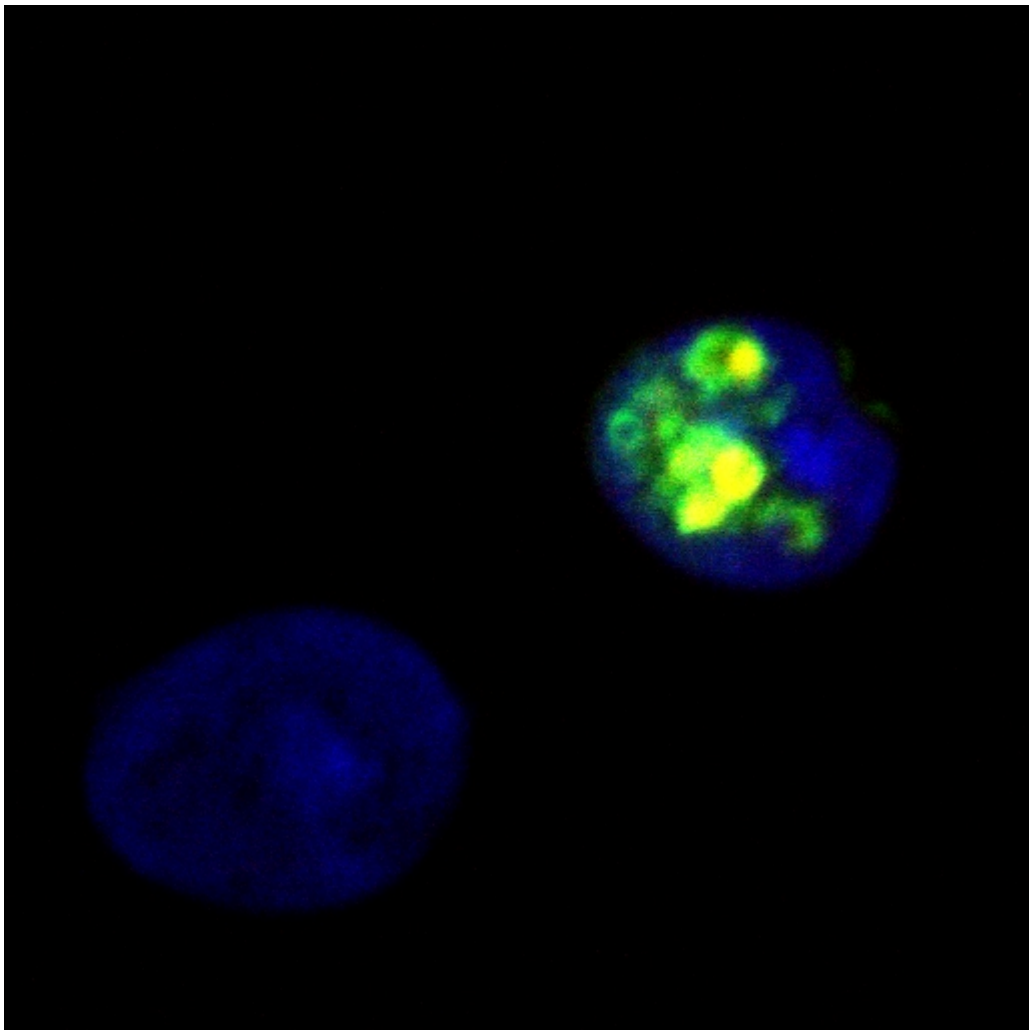

Figure 24. Dap1p-GFP and Ypr118wp-RFP2 co-localization experiment, close-up.

Transfection of HeLa cells with Hpr6.6p-EGFP

Hpr6.6p-EGFP fusion protein was constructed in the pEGFP-N1 plasmid containing the CMV promoter. HeLa cells were transfected with this construct in order to determine the sub-cellular localization pattern of this protein during growth (Figure 25).

Another localization study was done with Hpr6.6p-EGFP fusion protein with the addition of various amounts of MMS (0.05%, 0.1%, 0.5%, and 1%) for various time points (5min, 15min, 30min, 60 min, and 120min). No obvious difference in the localization pattern was seen as compared to cells incubated in media lacking MMS (data not shown). With the highest concentration of MMS for the longer time points, gross cell morphology differences and cell death was observed (data not shown).

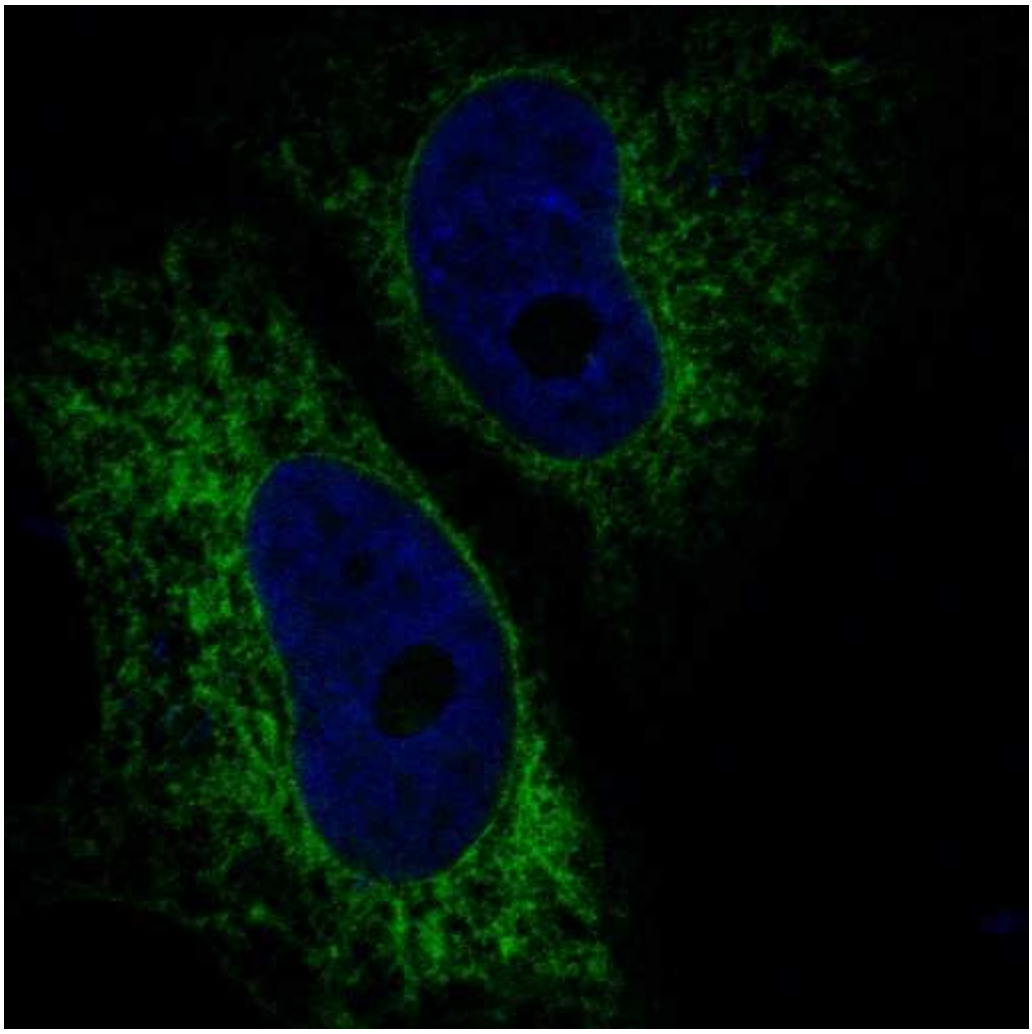

Figure 25. Hpr6.6p-EGFP localization experiment in HeLa cells. HeLa cells were transfected with Hpr6.6p-EGFP. DNA was stained with Hoescht stain. Images were captured using a Zeiss LSM510 UV confocal laser scanning microscope with a Zeiss 63X Plan-Neofluar oil immersion lens (Core Facilities at the Parker H. Petit Center for Bioengineering and Biosciences, Georgia Institute of Technology).

STEROL IDENTIFICATION AND QUANTITATION

Yeast cells of the control strain and the *dap1*Δ mutant strain were grown, total lipids were extracted and free sterols were separated from steryl-esters, see pp. 17-25 in Materials and Methods. Free sterols are sterols with only an alcohol group (hydroxyl) attached to the C-3 carbon in the A ring. Steryl esters are sterol with a side chain, such as a long chain fatty acid or sugar moiety, that has been attached by an ester or glycosidic linkage bond to the C-3 carbon of the A ring and are therefore classified differently from free sterols. The glycosidic sterols were not readily detected; thus no studies were done to quantify or identify the composition of these lipids. After separation into free sterol and steryl esters any side-chain present was cleaved off in HCL: MeOH (15%v/w) leaving all sterols in the free sterol manifestation. Sterol extracts were then derivitized with TMS and separated by gas chromatography. Individual sterol peaks were identified by comparing the retention times to those of established commercial standards as well as by GC/MS at the Georgia Tech Mass Spectroscopy Lab.

Figure 26, page 91, exhibits a representative of the GC runs from each strain, fraction and experiment. Figure 27, page 92, details the GC run between the control strain and the *dap1*Δ mutant strain. The peaks are numbered in Figure 28, page 93, which corresponds to the peak numbers in the sterol tables.

Mass Spectral Interpretation

The mass spectra of a large number of sterol TMS-ether compounds are available from mass spectral databases [107,108] and the fragmentation patterns of selected sterol compounds have been reported [109]. The molecular ion ($M^{+\cdot}$) provides the most

valuable information in the mass spectrum; it mass and elemental composition show the molecular boundaries into which the structural fragments indicated in the mass spectrum must be fitted. The molecular ions of sterol TMS-ethers are very stable and have a high abundance. Characteristic fragments are observed at $(M\text{-}CH_3)^+$, $(M\text{-}TMSOH)^+$, $(M\text{-}CH_3\text{-}TMSOH)^+$, $(M\text{-side chain})^+$ and $(M\text{-side chain-}TMSOH)^+$.

The presence of the 3 -O-TMS group in sterols with a double bond in ring B can greatly enhance the cleavage of the adjacent C-C bond. The scheme below demonstrates the cleavage of the molecular ion into two fragments, each of which can retain the positive charge.

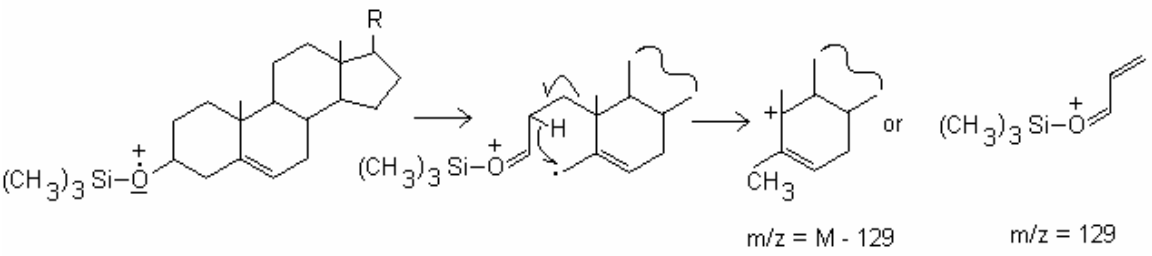

Scheme 1

Only Δ^5 and Δ^6 monounsaturated sterol TMS ethers exhibit the $(M\text{-}129)^+$ ion in higher abundances. In all other double bond isomers the abundance of the $(M\text{-}129)^+$ ion is l% or less.

Di-unsaturated sterol TMS ethers can also form a $(M\text{-}129)^+$ ion. At abundances between 1% and 50%, the fragment is observed in the mass spectra of the following isomers : $\Delta^{5,7}$, $\Delta^{5,8}$, $\Delta^{5,8(14)}$, $\Delta^{5,20(22E)}$, $\Delta^{5,22E}$, $\Delta^{5,24}$, $\Delta^{6,8}$, $\Delta^{7,9(11)}$, and $\Delta^{8,14}$ [109]. Under certain conditions the $(M\text{-}129)^+$ ion can loose $2H^{\bullet}$ to form a tropylium ion derivative as demonstrated in the scheme below.

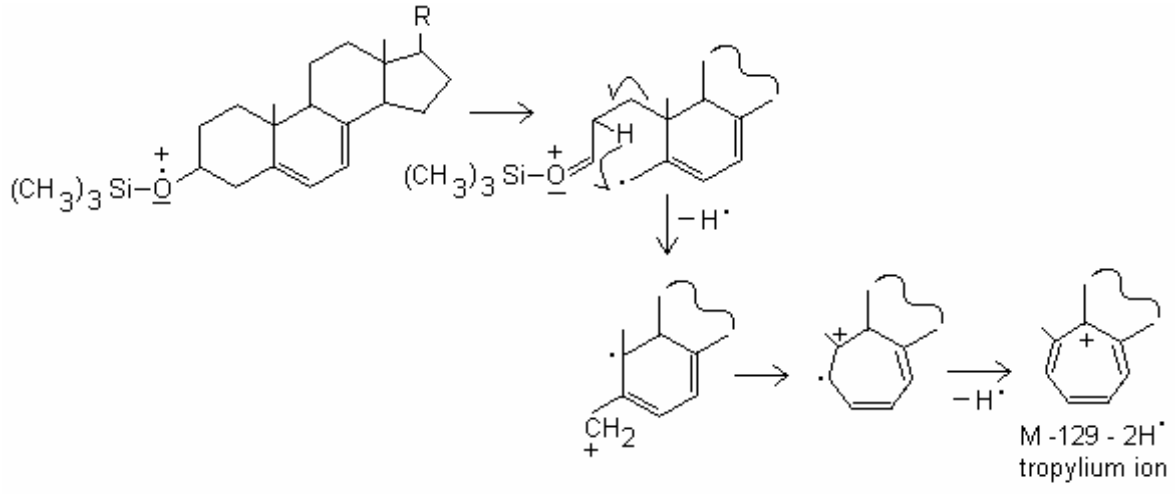

Scheme 2

Since the tropylium ion can only be formed if the two double bonds are located in ring B or in a specific position in rings B and C, the $(M\text{-}129 - 2H^{\bullet})^{+}$ ion is observed in higher abundances only in the mass spectra of four double bond isomers: $\Delta^{5,7}$, $\Delta^{5,8}$, $\Delta^{5,8(14)}$, and $\Delta^{6,8}$.

Peak #1:

The mass spectrum of compound 1 exhibits a molecular ion at m/z = 466. Major fragments are observed at m/z = 376 $(M - TMSOH)^{+}$, m/z = 361 $(M - CH_3 - TMSOH)^{+}$ and m/z = 335 $(M\text{-}129\text{-}2H^{\cdot})^{+}$, formation of tropylium ion (scheme 2). Based on gas chromatographic retention data and comparison with mass spectra of authentic standards, peak 3 was identified as 3-trimethylsilyl-oxy-ergosta-5,7,22E,24(28)-tetraene (Ergostatetraenol).

Peak #2:

The mass spectrum of compound 2 exhibits a molecular ion at m/z = 470, indicating 2 double bonds. Major fragments are observed at m/z = 455 $(M - CH_3)^{+}$, m/z = 380 $(M - TMSOH)^{+}$, and m/z = 365 $(M - CH_3 - TMSOH)^{+}$. The peak at m/z = 341 is

formed by loss of $(M-129)^+$ ion (scheme 1). Among the possible structures for compound 2 are 3-trimethylsilyl-oxy-ergosta-diene with the following isomers: $\Delta^{5,7}$, $\Delta^{5,8}$, $\Delta^{5,8(14)}$, $\Delta^{5,20(22E)}$, $\Delta^{5,22E}$, $\Delta^{5,24}$, $\Delta^{6,8}$, $\Delta^{6,22E}$, $\Delta^{6,24(28),}$,$\Delta^{7,9(11)}$, and $\Delta^{8,14}$.

Peak #3:

The mass spectrum of compound 3 exhibits a molecular ion at m/z = 458. Major fragments are observed at m/z = 441 $(M - CH_3)^+$, m/z = 366 $(M - TMSOH)^+$, and m/z = 351 $(M - CH_3 - TMSOH)^+$. The peak at m/z = 343 is formed by the loss of the side chain + $2H^{\bullet}$. This fragment is observed in TMS sterol ethers which have unsaturation in their side chain. Only after loss of $2H^{\bullet}$ the $(M - \text{side chain})^+$ ion can be stabilized by resonance (scheme 3).

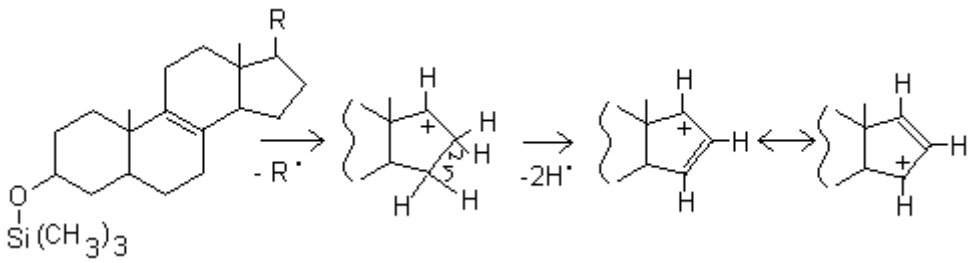

Scheme 3

The position of the double bond in the side chain and the ring skeleton can not be determined from the mass spectrum. Based on gas chromatographic retention data and comparison with mass spectra of authentic standards, peak 3 was identified as 3-trimethylsilyl-oxy-cholesta-8,24-diene (zymosterol).

Peak #4:

The mass spectrum of compound 4, the additional peak in the *dap1*Δ mutant strain, exhibits a molecular ion at m/z = 466. Major fragments are observed at m/z = 451 $(M - CH_3)^+$, m/z = 376 $(M - TMSOH)^+$, m/z = 341 $(M - \text{side chain} - 2H^{\bullet})^+$ and m/z =

251 (M – TMSOH – side chain – $2H^{\bullet}$) $^{+}$. The m/z = 341 peak is formed via scheme 3 and indicates a 9 carbon side chain with two double bonds. The strong fragment at 251 is formed through consecutive loss of TMSOH, side chain and $2H^{\bullet}$. The position of the double bonds in the side chain can be assumed as 22E, 24(28) since ergosta-5,7,22E,24(28)-tetraen-3-ol is the only intermediate in the ergosterol biosynthetic pathway which has two double bonds in the side chain. The positions of the two ring double bonds are uncertain, however, since no (M – 129) $^{+}$ ion (scheme 1) and no tropylium ion (scheme 2) is present. Thus, certain isomers can be ruled out. These restrictions rule out ring A as a double bond carrier as well as ring B having two double bonds. Among the possible structures for compound 4 are 3-trimethylsilyl-oxy-ergosta-7,9(11),22E,24(28)-tetraene or the following isomers in the rings: $\Delta^{6,8(14)}$, $\Delta^{8,14}$, or $\Delta^{7,(14)}$.

Peak #5:

The mass spectrum of the compound 5 exhibits a molecular ion at m/z = 468 and major fragment ions at m/z = 453 (M – CH_3) $^{+}$, m/z = 378 (M – TMSOH) $^{+}$, m/z = 363 (M – side chain – $2H^{\bullet}$), m/z = 337 (M – 129 – $2H^{\bullet}$) $^{+}$ and m/z = 253 (M – TMSOH – side chain – $2H^{\bullet}$) $^{+}$. Based on gas chromatographic retention data and comparison with mass spectra of authentic standards, compound 3 was identified as 3-trimethylsilyl-oxy-ergosta-5,7,22E-triene (ergostosterol).

Peak #6:

The mass spectrum of compound 6 has a molecular ion at m/z = 484 and major fragment ions at m/z = 469 (M – CH_3) $^{+}$, m/z = 394 (M – TMSOH) $^{+}$, and m/z = 379 (M – CH_3 – TMSOH, base peak) $^{+}$. There are no fragments which lost the side chain. The

compound was tentatively identified as 3-trimethylsilyl-oxy- 4,4-dimethyl-cholesta-8,24-diene, based on the comparison of the mass spectrum of a standard compound.

Peak #7 and #8:

The mass spectrum of compound 7 and compound 8 were very similar in nature. They both possessed a molecular ion at m/z = 470 and major fragment ions at m/z = 455 $(M - CH_3)^+$, m/z = 380 $(M - TMSOH)^+$, m/z = 365 $(M - TMSOH - CH_3)^+$, m/z = 343 $(M - \text{side chain} - 2H^{\bullet})^+$ and m/z = 255 $(M - TMSOH - \text{side chain} - 2H^{\bullet})^+$. Based on previously reported GC data on similar columns and retention time compound 7 was assigned as 3-trimethylsilyl-oxy-ergosta-7,24(28)-diene (episterol) and compound 8 was assigned as 3-trimethylsilyl-oxy-ergosta-8,24(28)-diene (fecosterol).

Peak #9:

The mass spectrum of compound 9 exhibits a molecular ion at m/z = 468, and major fragment ions at m/z = 453 $(M - CH_3)^+$, m/z = 378 $(M - TMSOH)^+$, m/z = 363 $(M - \text{side chain} - 2H^{\bullet})$, and m/z = 253 $(M - TMSOH - \text{side chain} - 2H^{\bullet})^+$. Based on gas chromatographic retention data and comparison with mass spectra of authentic standards, peak 3 was identified as 3-trimethylsilyl-oxy-ergosta-5,7,24(28)-triene (ergostatrienol).

Peak #10:

The mass spectrum of the compound 10 exhibits a strong molecular ion at m/z = 474 and fragment ions at m/z = 459 $(M - CH_3)^+$ and m/z = 384 $(M - TMSOH)^+$. The molecular ion suggests a completely hydrogenated sterol. There are no significant ions present at M – side chain or M – TMSOH – side chain. Therefore two structures are

possible for peak 10, each TMS ether deriviatives; 4–methyl-cholestane–3β-ol or a fully hydrogenated ergosterol.

Peak #11:

The mass spectrum of the compound 11 exhibits a molecular ion at m/z = 498, an fragment ion at m/z = 483 $(M - CH_3)^+$ and m/z = 393 $(M - CH_3 - TMSOH, \text{base peak})^+$. Based on gas chromatographic retention times and mass spectral data compound 31 was identified as 3-trimethylsilyl-oxy-lanosta-8,24-diene (lanosterol).

Peak #12:

The mass spectrum of compound 12 exhibited a molecular ion at m/z = 466, and fragments at m/z = 451 $(M - CH_3)^+$, m/z = 376 $(M - TMSOH, \text{base peak})^+$ and m/z = 339 $(M - 127)^+$. This last fragment is a mystery, since with a molecular ion at m/z = 466, there should be 4 double bonds present, with 2 in the side chain. It seems this compound had only one double bond in the side chain and 3 in the ring system. Therefore, the fragment ion $(M-127)^+$ corresponds to $(M - TMSOH - \text{side chain} - 2H^{\bullet})^+$. The latter fragment is typical for sterols with unsaturated side chains. The position of the double bond in the side chain is uncertain, it can be either 22E or 24(28), since both positions are present in the side chain of compounds in the ergosterol biosynthetic pathway. The positions of the three ring double bonds are uncertain, also. Since no $(M - 129)^+$ (scheme 1) and no tropylium ion (scheme 2) are present certain isomers can be ruled out. Component 12 is a 3-trimethylsilyl-oxy-ergosta-tetraene isomer.

Peaks #13 and #14:

Both compounds have similar fragmentation patterns. There was a molecular ion at m/z = 498, and fragment ions at m/z = 483 $(M - CH_3)^+$ and m/z = 393 (M – TMSOH –

$CH_3)^+$. These are the major fragment ions expected from a lanosterol isomer, thus compounds 13 and 14 are ring double bond isomers of 3-trimethylsilyl-oxy-lanosta-24-diene.

Peak #15 and Peak #16:

The mass spectrum of compounds 15 and 16 exhibit very similar spectra both containing a molecular ion at m/z = 472, major fragments at m/z = 457 (M – CH_3, base peak)$^+$ and minor fragments at m/z = 382 (M – TMSOH)$^+$, m/z = 367 (M – TMSOH–$CH_3)^+$, m/z = 345 (M – side chain – $2H^{\bullet})^+$, and m/z = 255 (M – TMSOH – side chain – $2H^{\bullet})^+$. A molecular ion at m/z = 472 gives one double bond, furthermore, the position of the double bond is in the side chain, because of the presence of m/z = 345 and m/z = 255. Therefore, these are positional isomers of each other with one possessing the double bond at 22E and the other at 24(28), these compounds are identified as 3-trimethylsilyl-oxy-ergosta-ene. Since, the position of the double bond in the side chain cannot be determined it is unknown which peak corresponds to which compound.

Peak #17:

The mass spectrum of peak 17 consists of three components, which could not be resolved by the gas chromatographic column. Component 1 has a molecular ion at m/z = 498 and fragment ions typical for lanosterol-TMS, thus component 1 is a ring double bond isomer of 3-trimethylsilyl-oxy- ergosta-22,24(28)-tetraene. Component 2 exhibited a molecular ion at m/z = 472. Fragments are observed at m/z = 457 (M – $CH_3)^+$, m/z = 382 (M – TMSOH)$^+$, m/z = 367 (M – CH_3 – TMSOH)$^+$ and minor fragments at m/z = 345 (M – side chain)$^+$ and m/z = 255 (M – TMSOH – side chain)$^+$. These two fragments establish a side chain with 9 carbons. Since there is no double bond in the side chain, the

two fragments that have lost the side chain are of low intensity. An $(M - 129)^+$ fragment was absent (scheme 1) which ruled out certain positions of the ring double bond. Comparison with the mass spectra of mono unsaturated sterol TMS ethers identified the compound as 3-trimethylsilyl-oxy- ergost-8(14)-ene. Component 3 exhibited a molecular ion at m/z = 530, and fragment ions at m/z = 515 $(M - CH_3)^+$, m/z =.425 $(M - CH_3 - TMSOH)^+$, and m/z = 337. The structural assignment for this compound is unknown.

Table 4. Mass Spectrometric Data of the TMS Derivatives of Extracted Sterols

Ion	m/z(%)															
Peak # →	1	2	3	4	5	6	7	8	9	10	11	12	13	14	15	16
$(M^{+\cdot})$	466	470	456	466	468	484	470	470	468	474	498	466	498	498	472	472
$(M\text{-}CH_3)^+$	455	441	451	453	469	455	455	453	459	483	451	483	483	483	457	457
$(M\text{-}TMSOH)^+$	376	380	366	376	378	394	380	380	378	384	393	376	393	393	382	382
$(M\text{-}TMSOH\text{-}CH_3)^+$	361	365	351		363	379	365	365	363						367	367
$(M\text{-}129)^+$		341														
$(M\text{-}129\text{-}2H^{\cdot})^+$	335				337											
$(M\text{-}SC\text{-}2H^{\cdot})^+$			343	341			343	343				339			345	345
$(M\text{-}TMSOH\text{-}SC)^+$									253							
$(M\text{-}TMSOH\text{-}SC\text{-}2H^{\cdot})^+$	251		253	251	253		255	255	251						255	255

M: molecular ion
TMSOH: trimethylsilyl-hydroxy
SC: side chain
* see text for peak #17, which contains 3 unresolved compounds.

In summary, the major sterol peaks that were identified in this investigation were ergosterol; lanosterol; zymosterol; fecosterol; episterol; ergosta-5,7,22,24(28)- tetraen-3β-ol, ergosta-5,7,22-trien-3β-ol; and 4,4-dimethyl-cholesta-8,24(28)-dien-3β-ol. In addition to the identified sterols, there were numerous compounds that were detected in relative small quantities, with a few exceptions, that could not be identified precisely. The unidentified compounds did not elute with any of the known sterol standard and may be metabolic intermediates of sterols. The fragmentation pattern by GC/MS analysis did not have library matches. The parent ions were in the same range as those of the identified sterols, but without definite fragmentation patterns that support a proposal to identify the molecules. The available evidence suggests that these components are aberrant sterols that have arisen through double bond migration during the sterol synthesis process, or as artifacts created by the hydrolysis and the derivitization procedure.

Sterol Profiles

Tables 5-8 shows the sterol content of the control strain and the *dap1*Δ mutant strain as $\mu g/10^8$ cells and also as a percentage of total sterols. The tables are divided by both strain type and sterol origin (free sterol or steryl ester). Figures 29 - 34 present a graphical representation of the same data in $\mu g/10^8$ cells, whereas Figures 35 and 36 present the data as total sterol content; the addition of the free sterol fraction and the steryl ester fraction. In order to study the total sterol content of each strain the individual sterols for each strain in both the free sterol fraction and the steryl ester fraction were summed. For the control strain this sum was 2.77 and 2.89 $\mu g/10^8$ cells for 1 and 2 day old cultures, respectively. For the *dap1*Δ mutant strain this sum was 2.44 and 2.58

μg/10^8 cells for 1 and 2 day old cultures, respectively. For the *dap1*Δ + pUGpd:*DAP1* strain this sum was 2.71 and 2.81 μg/10^8 cells for 1 and 2 day old cultures, respectively. For the *dap1*Δ + pCUP1:Hpr6.6 strain this sum was 2.68 and 2.82 μg/10^8 cells for low and high copper in 2 day old cultures, respectively. And finally, for the control + pCUP1:Hpr6.6 strain this sum was 2.98 and 3.17 μg/10^8 cells for low and high copper in 2 day old cultures, respectively.

1-day versus 2-day cultures

Looking at the free sterol fraction of the control strain, the relative composition of individual sterols in 2 day old cultures is different from the relative composition in 1 day old cultures. The difference is not highly dramatic showing that, metabolically, there is a conservation of sterol production and distribution. In some cases, such as ergosterol, ergosta-5,7,22,24(28)- tetraen-3β-ol, and ergosta-5,7,22-trien-3β-ol, the relative proportions exhibited a slight increase in proportion from 1 day old cultures to 2 day old culture. Whereas, zymosterol, fecosterol, and 4,4-dimethyl-cholesta-8,24(28)-dien-3β-ol decreases from 1 day culture to 2 days of culture. Similarly, some of the unidentified compounds also varied in relative quantity of the total sterol composition.

In the control strain, the steryl ester fraction represented about 35% of the total sterol pool in 1 day old cultures. This increased to about 41% in 2 day old cultures. The esterified sterols of the control strain are not direct percent conversions to the free sterol fraction. There is an apparent selectivity for which sterols are esterified. Most notably, ergosterol, which accounted for about 33% of the free sterol fraction, accounted only for 8-9% of the steryl ester fraction. Lanosterol and 4,4-dimethyl-cholesta-8,24(28)-dien-3β-

ol made up about 13% each in the steryl ester fraction, while only representing about 5% and 2%, respectively, in the free sterol fraction.

Comparing the steryl esters of the control strain from 1 day old cultures to 2 days old cultures, ergosterol is present in almost equal proportions. This holds true for most of the esterified sterols. However, episterol, fecosterol, and ergosta-5,7,22-trien-3β-ol decrease in relative proportion by about 50%, 35%, and 25%, respectively. Two unidentified compounds increased in relative proportion. An ergosta-ene isomer (unidentified peak #16) increased by about 70%, making up the largest portion of the steryl ester fraction at 15.35% in 2 days of culture. A ring double bond isomer of lanosta-24-diene (peak #14) also nearly doubled from 1 to 2 days of culture. The fact that the relative quantities of the identified sterols in the free sterol fraction of the control strain are quantitatively greater than in the steryl ester fraction makes it unlikely that these differences are due to the methodology, the derivitization process, or from contamination from extrinsic sources.

***dap1*Δ mutant strain versus control strain**

The *dap1*Δ mutant strain exhibited a 10-12% decrease of total sterol content as compared to the control strain. This decrease was due primarily to the steryl ester fraction; a 6-9% decrease occurred in the free sterol fraction, whereas a 16-17% decrease occurred in the steryl ester fraction.

Not only was there a decrease in total sterol content, but the *dap1*Δ mutant strain exhibited a significantly altered sterol profile. The most striking differences were a 50% reduction in ergosterol and the presence of an additional sterol peak, identified as an ambiguous ergosta-traene isomer (peak #4), eluting just before ergosterol and accounting

for 12-13% of the sterols present in the free sterol fraction in the deletion strain. This peak was only seen in the free sterol fraction of the *dap1*Δ mutant strain. It was not detected in the steryl ester fraction, nor was it detected in the *dap1*Δ mutant strain when either DAP1 or Hpr6.6 was overexpressed.

The free sterol fraction of the *dap1*Δ mutant strain exhibited an overall consistency between 1 and 2- day old cultures in the relative proportions of the sterols present, with a few exceptions. The most significant was zymosterol (peak #3) which increased by ~75% from 1 day old cultures to 2 day old cultures. Also, zymosterol was the most abundant sterol present in 2 day old cultures accounting for ~20% of sterols present. This increase in zymosterol was at the expense of 4,4-dimethyl-cholesta-8,24(28)-dien-3β-ol (peak #6) which decreased by ~70%, ergosta-5,7,24(28)-trien-3β-ol (peak #9) by ~45%, ergosterol by ~19%, and a sterol identified either as 4-methyl-cholestane-3β-ol or a fully hydrogenated ergosterol (peak #10), by ~32%. The other sterols maintained a similar relative proportion from 1 day old cultures to 2 day old cultures.

The steryl esters of the *dap1*Δ mutant strain, in contrast, exhibited a greater variability in relative distributions between 1 and 2-day old cultures. Ergosterol and 4,4-dimethyl-cholesta-8,24(28)-dien-3β-ol decreased by about half each. Episterol (peak #7) increased by ~200%, fecosterol (peak #8) increased by ~20%, and lanosterol (peak #11) increased by ~30%. Looking at the ambiguously identified compounds, the most significant was an ergosta-diene isomer (peak # 2), which decreased to about 25% that present in 1 day of culture. Also, a lanosta-24-diene isomer (peak # 14) increased by ~90% and a lanosterol isomer (peak #13) increased by about 60%.

Comparing the free sterol fraction of the control strain to the *dap1*Δ mutant strain, there were significant differences in the sterol distribution pattern. The most striking difference, as mentioned before, was the presence of the additional ergosta-tetraene compound, peak #4, eluting just before ergosterol that accounted for 12-13% of the free sterol present in the *dap1*Δ mutant strain. This peak was present in both 1 and 2 day old cultures only in the *dap1*Δ mutant strain, and only in the free sterol fraction.

Comparing 1 day old cultures of the free sterol fraction of the control strain to the *dap1*Δ mutant strain, the sum of the ergosta-tetraene peak and ergosterol (peak #5) almost matches the amount of ergosterol in the control strain. The deletion strain showed a decrease in episterol and fecosterol by ~40% and ~60%, respectively, compared to the control strain. On the other hand, the relative proportion of ergosta-5,7,24-trien-3β-ol in the *dap1*Δ mutant strain was over twice that of the control strain. Also, ergosta-5,7,22,24-tetraen-3β-ol was present in a small quantity in *dap1*Δ mutant strain, but it was not detected in the control strain. There were only slight differences in the most of the other sterols present.

Comparing 2 day old cultures of the free sterol fraction of the control strain to the *dap1*Δ mutant strain, there was a greater change in some sterol. Zymosterol was present in about twice the quantity in the *dap1*Δ mutant strain as in the control strain. Ergosterol was diminished in the *dap1*Δ mutant strain to about 40% of control. As described above, the sum of the ergosta-tetraene peak eluting near ergosterol and the ergosterol in the *dap1*Δ mutant strain, is only 25% less in the *dap1*Δ mutant strain in 2 day old cultures. 4,4-dimethyl-cholesta-8,24(28)-trien-3β-ol was present in low quantities in each strain, but its relative proportion in the *dap1*Δ mutant strain was reduced to less than 20% of the

control strain at 2 days of culture. Ergosta-5,7,22,24(28)-tetraen-3β-ol, which was also present in low quantities in each strain, it was present in the *dap1*Δ mutant strain at about twice as much as in the control strain.

Comparing the steryl ester fraction of the control strain to the *dap1*Δ mutant strain, there was also significant differences between the sterol profiles. As with the free sterol fraction, there was also a much greater difference between 2 day old cultures than in 1 day old cultures.

Comparing 1 day old cultures in the steryl ester fraction of the control strain to the *dap1*Δ mutant strain, episterol and 4,4-dimethyl-cholesta-8,24(28)-trien-3β-ol exhibited the biggest difference between the strains. Episterol was about four-fold higher and 4,4-dimethyl-cholesta-8,24(28)-trien-3β-ol was present in about 2.5-fold higher in the control strain.

Comparing 2 day old cultures in the steryl ester fraction between the control strain and the *dap1*Δ mutant strain, almost all of the sterols exhibited significant changes. Most significantly, ergosta-5,7,24(28)-trien-3β-ol and ergosta-5,7,22,24(28)-tetraen-3β-ol were present in nearly twice the proportion in the *dap1*Δ mutant strain as in the control strain. But, ergosterol, which was increased in the *dap1*Δ mutant strain in 1 day old culture, was reduced in the *dap1*Δ mutant strain to ~60% of the control strain in 2 day old cultures, an ergosta-diene (peak #2) was reduced to about 25% of the control. An ergosta-ene isomer (peak #16) and an unidentified sterol (peak #17) also became reduced to about 50% of control levels, largely because these compounds increased 2-fold from 1 day to 2 day old cultures in the control strain, but not in the deletion strain.

Rescue Experiment

A rescue experiment was performed to see if the mutant sterol phenotype observed in the *dap1*Δ mutant strain could be restored upon the addition of Dap1p under the constitutive promoter Gpd. See Tables 9-10 and Figures 29-36.

With the addition of Dap1p to the *dap1*Δ mutant strain, the total sterol content increased slightly. The total sterol content was still lower than levels exhibited by the control strain, but higher than the levels exhibited by the *dap1*Δ mutant strain. The total free sterol fraction was between the levels of the control strain and the *dap1*Δ mutant strain. The total quantity of the steryl ester fractions matched the levels of steryl esters of the control strain.

Comparing the free sterol fractions among the *dap1*Δ +GPD:*DAP1* reconstituted strain, the *dap1*Δ mutant strain, and the control strain, the most striking feature is that the ambiguous ergosta-tetraene (peak #4) eluting just before ergosterol, present in the *dap1*Δ mutant strain but not in the control strain, was eliminated in the *dap1*Δ +GPD:*DAP1* cells. Ergosterol levels in the *dap1*Δ +GPD:*DAP1* strain were intermediate between the *dap1*Δ mutant strain and control strain levels, whereas the fecosterol level (peak #8) were restored to control levels in the 1-day old cultures, but fell well below the control of deletion strain levels in the 2-day old cultures. The *dap1*Δ +GPD:*DAP1* strain showed markedly elevated levels of several free sterol peaks compared to either the control of the *dap1*Δ mutant strain. These were ergosta-5,7,22,24(28)-tetraen-3β-ol (peak #1), an ambiguous ergosta-diene isomer (peak #2), ergosta-5,7,24- trien-3β-ol (peak #9), lanosterol (peak #11), an ambiguous ergosta-tetraene isomer (peak #12), an ambiguous lanosta-24-diene (peak #13), and an ambiguous ergosta-ene isomer (peak #16).

Conversely, the *dap1*Δ+GPD:*DAP1* strain had reduced levels, compared to either the control or the deletion strain, of zymosterol (peak #3), the sterol that may be either 4-methyl-cholestane-3-ol or a fully hydrogeneated ergosterol (peak #10), and an unidentified sterol (peak #17).

Comparing the steryl ester fractions, of the *dap1*Δ +GPD:*DAP1* strain had markedly elevated levels of two ambiguous sterols. A sterol identified as either 4-methylcholestane-3-ol or a fully hydrogenated ergosterol (peak #10) and an ergosta-ene isomer (peak #16) were present in the *dap1*Δ +GPD:*DAP1* strain at levels up to 3-fold higher than in either the control or the *dap1*Δ mutant strain. In fact, these two peaks accounted for ~13% and ~28% of the total esterified sterols, respectively, in this strain. Two sterols were present in lower quantities, as compared to the control strain. These were episterol (peak #7), which was present in ~20% of the amount present in the control strain in one-day cultures, an ambiguous ergosta-tetraene (peak #12), and ergosterol (peak #5).

Hpr6.6 Homologue Experiment

Experiments were performed to test the effects of introducing Hpr6.6, the human homologue of *DAP1*, on the sterol profiles of the control strain and the *dap1*Δ mutant strain. If Hpr6.6 has a similar role in human cells as Dap1p in yeast cells, then we would expect Hpr6.6 to be able to rescue the *dap1*Δ mutant phenotype and restore sterol profiles to resemble the control strain. Hpr6.6 was under the control of the copper promoter, CUP1. These data are shown in Tables 11-14 and Figures 31-34.

No significant differences were seen between the sterol profiles of the control strain with the addition of Hpr6.6 and the *dap1*Δ mutant strain with the addition of

Hpr6.6. There was a slight increase in total sterol content as a result of Hpr6.6 expression in both the control strain and the *dap1*Δ mutant strain.

The strains expressing Hpr6.6 showed a large increase in ergosterol in both the free sterol and steryl ester fractions. This was true for both the control strain and the *dap1*Δ mutant strain. Compared to the control strain there was about a 30-50% increase in ergosterol in the free sterol fraction and greater than 500% increase in the steryl ester fraction. Relative to the *dap1*Δ mutant strain, ergosterol increased about 200% in the free sterol fraction and about 500% in the steryl ester fraction.

The *dap1*Δ+CUP1:Hpr6.6 strain resembled the *dap1*Δ+GPD:*DAP1* strain in that both strains eliminated the ambiguous ergosta-tetraene isomer (peak #4) prominent in the parental *dap1*Δ mutant strain. The two strains differed in that most of the free sterols that were increased relative to control in the *dap1*Δ+GPD:*DAP1* strain were either reduced or comparable to controls in the *dap1*Δ+CUP1:Hpr6.6 strain. The most prominent of these were fecosterol (peak #8) at day 1 of culture, lanosterol (peak #11), a lanosterol isomer (peak #13), and an ergosta-diene isomer (peak #2).

In the esterified sterols, the *dap1*Δ+CUP1:Hpr6.6 strain differed from the *dap1*Δ+GPD:*DAP1* strain and the control strain in that the ergosterol was about 6-fold higher and most other sterols were significantly reduced. Whereas the *dap1*Δ+GPD:*DAP1* strain contained greatly elevated levels of either 4-methylcholestane-3β-ol or a fully hydrogenated ergosterol (peak #10) and an ergosta-ene isomer (peak #16), the *dap1*Δ+CUP1:Hpr6.6 strain had reduced levels of these sterols relative to the control strain.

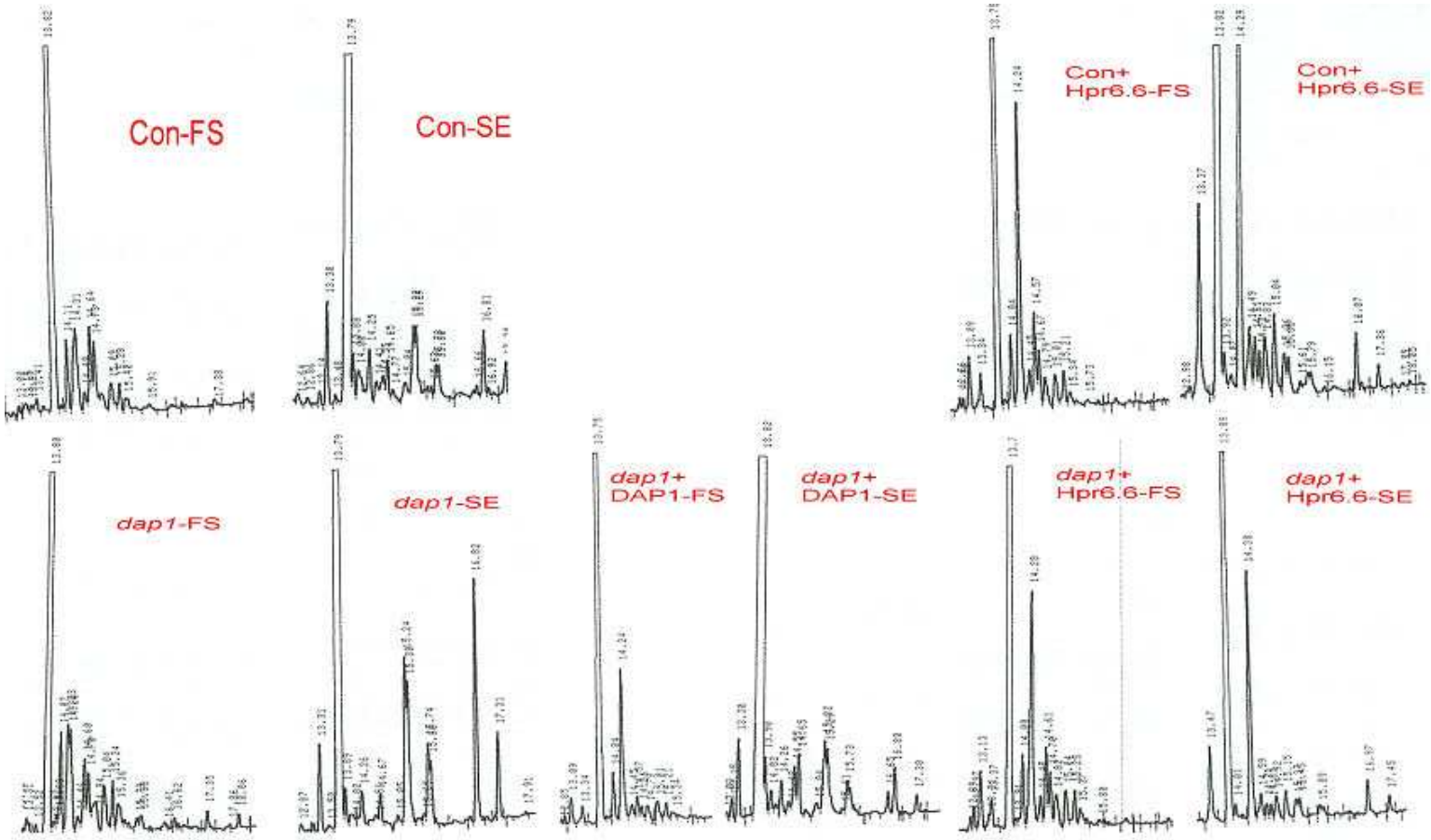

Figure 26. Representative of GC runs from each strain, experiment and fraction. GC runs are not a 1:1 correlation; peaks have to be normalized to the cholesterol peak. Cholesterol peak is the first large peak to the left in each GC run. Strain and fraction are designated to the right of each GC run. Con: control strain, dap1: *dap1* deletion mutant strain, DAP1: strains over-expressing the DAP1 gene, Hpr6.6: strains over-expressing the Hpr6.6 gene, FS: free sterol fraction, SE: steryl ester fraction.

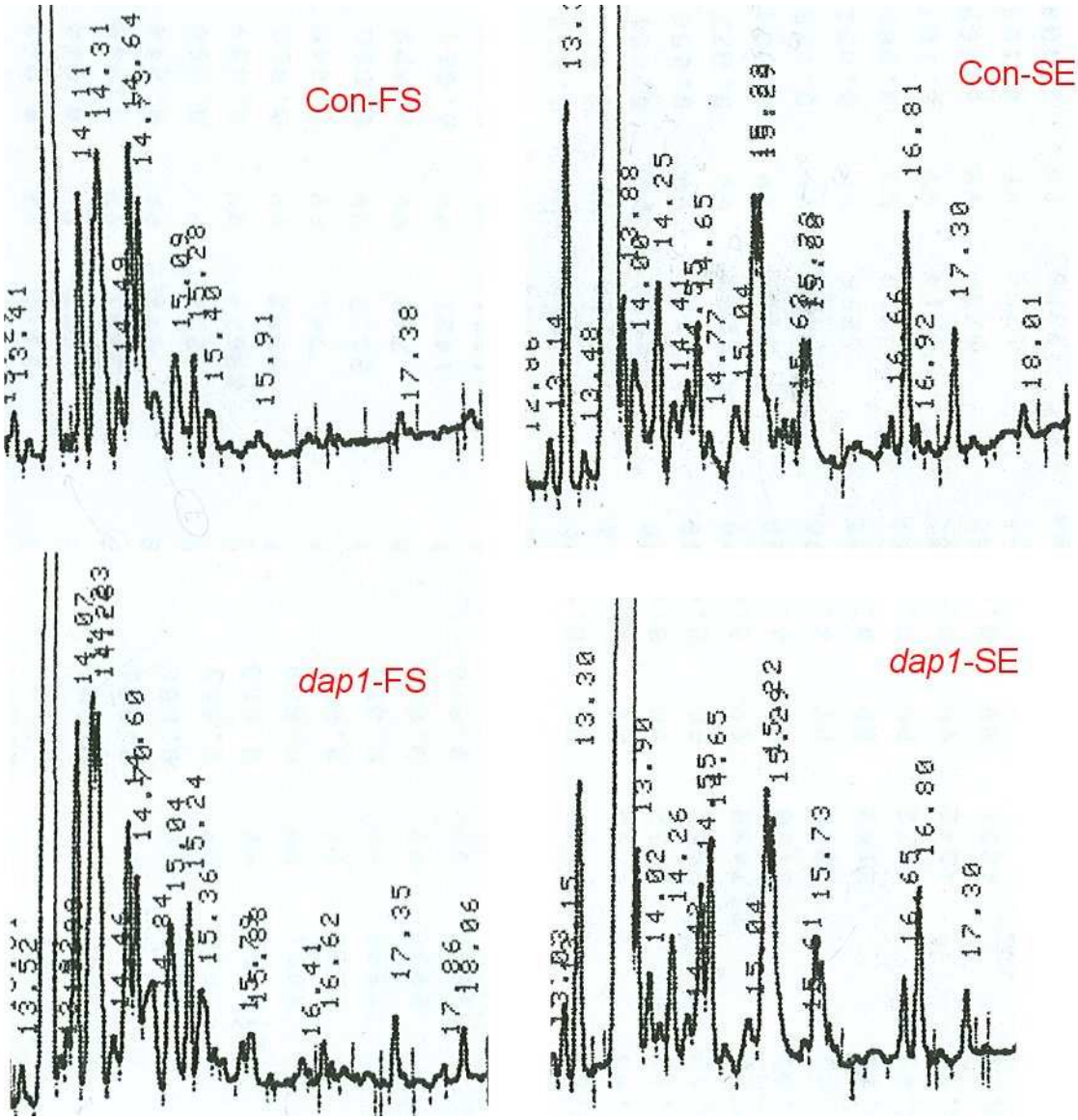

Figure 27. Magnified representative GC runs from the control strain and the *dap1*Δ mutant strain, free sterol and steryl ester fraction. Large peak to the left of each GC run is the added standard cholesterol. Con: control strain, dap1: *dap1*Δ mutant strain, FS: free sterol fraction, SE: steryl ester fraction.

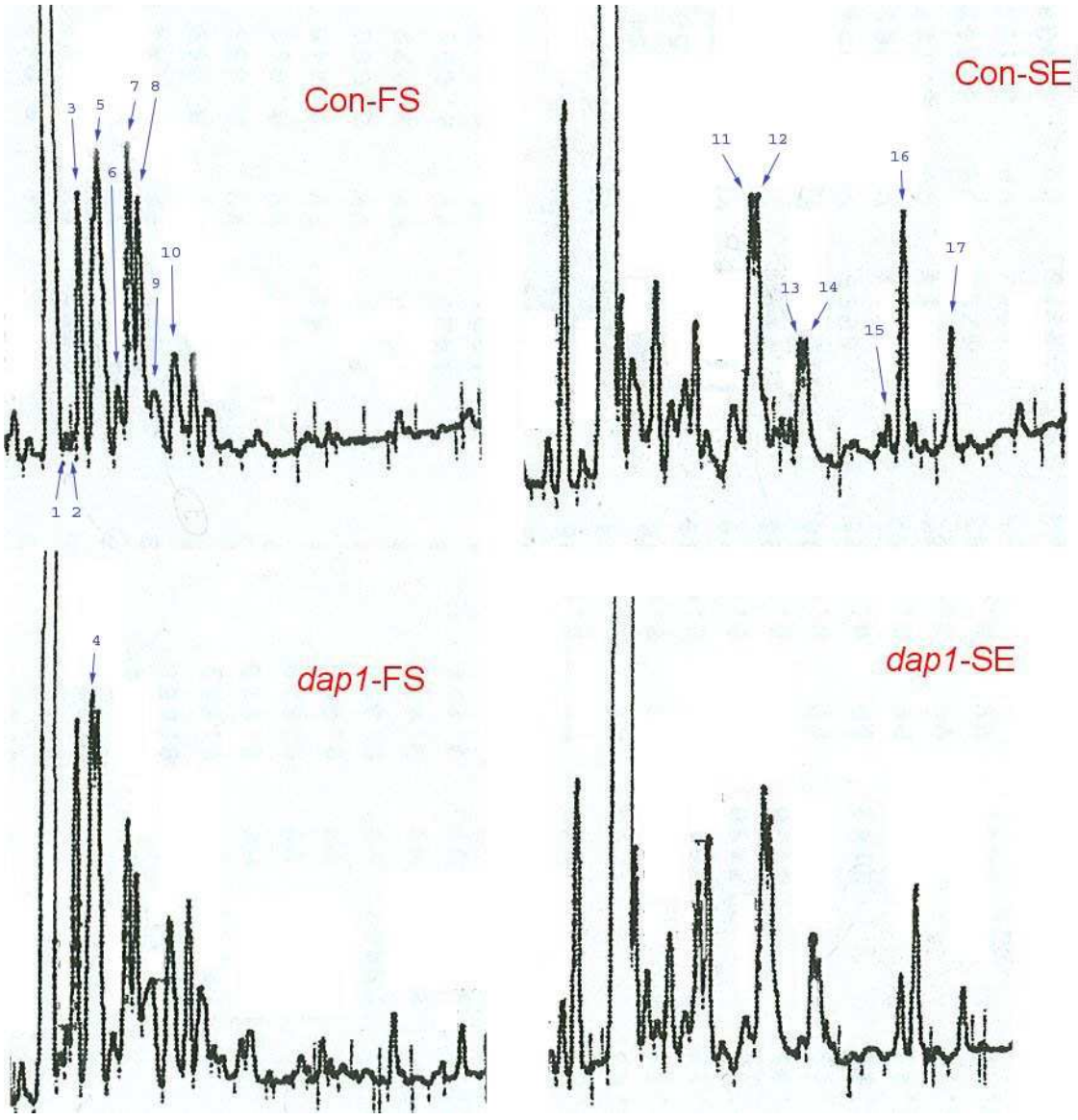

Figure 28. GC run peak numbers. Large peak to the left of each GC run is the added standard cholesterol. Notice the presence of extra peak # 4 in the dap1-FS run. Con: control strain, dap1: *dap1*Δ mutant strain, FS: free sterol fraction, SE: steryl ester fraction.

TABLE 5. Free Sterol Composition of Control Strain

Peak#	Identity	RRT[a]	1 Day Quantity[b]	1 Day Percent[c]	2 Day Quantity[b]	2 Day Percent[c]
	Estrone*	0.729				
	Cholesterol*	1.000				
1.	Ergosta-5,7,22,24-tetraen-3β-ol	1.009	ND	0	0.018	1.07
2.	Ergosta-diene-3β-ol isomer**	1.015	0.023	1.25	0.015	0.86
3.	Zymosterol	1.020	0.204	11.32	0.176	10.34
4.	Ergosta-tetraene-3β-ol isomer**	1.030	ND	0	ND	0
5.	Ergosterol	1.035	0.482	26.73	0.563	33.10
6.	4,4-Dimethylcholesta-8,24-dien-3β-ol	1.048	0.074	4.09	0.077	4.53
7.	Episterol	1.059	0.296	16.42	0.269	15.83
8.	Fecosterol	1.066	0.238	13.19	0.162	9.51
9.	Ergosta-5,7,24-trien-3β-ol	1.075	0.071	3.92	0.095	5.58
10.	4-methyl-cholestane/fully hydrogenated ergosterol**	1.091	0.129	7.16	0.121	7.12
11.	Lanosterol	1.105	0.102	5.66	0.093	5.48
12.	Ergosta-tetraene-3β-ol isomer**	1.114	0.078	4.29	0.037	2.19
13.	Lanosta-diene-3β-ol isomer**	1.143	0.028	1.57	0.017	0.98
14.	Lanosta-diene-3β-ol isomer**	1.150	0.054	3.00	0.023	1.34
15.	Ergosta-ene-3β-ol isomer**	1.205	ND	0	0.014	0.80
16.	Ergosta-ene-3β-ol isomer**	1.221	ND	0	ND	0
17.	3 compounds**	1.257	0.026	1.41	0.022	1.27

* Estrone and Cholesterol were added as surrogate marker and internal standard, respectively

**See MS interpretation for detailed discussion of possible double bond locations

RRT – Relative Retention Time

ND – None detected

[a] – Relative to cholesterol at an RRT of 1.000

[b] – $\mu g/10^8$ cells

[c] – percent based on total detectable compounds that are listed in the table

TABLE 6. Steryl Ester Composition of Control Strain

Peak#	Identity	RRT[a]	1 Day Quantity[b]	1 Day Percent[c]	2 Day Quantity[b]	2 Day Percent[c]
	Estrone*	0.729				
	Cholesterol*	1.000				
1.	Ergosta-5,7,22,24-tetraen-3β-ol	1.009	0.063	6.57	0.053	4.48
2.	Ergosta-diene-3β-ol isomer**	1.015	0.042	4.36	0.039	3.30
3.	Zymosterol	1.020	0.036	3.73	0.035	2.92
4.	Ergosta-tetraene-3β-ol isomer**	1.030	ND	0	ND	0
5.	Ergosterol	1.035	0.080	8.42	0.103	8.68
6.	4,4-Dimethylcholesta-8,24-dien-3β-ol	1.048	0.033	3.41	0.042	3.50
7.	Episterol	1.059	0.077	8.03	0.050	4.22
8.	Fecosterol	1.066	0.082	8.57	0.066	5.57
9.	Ergosta-5,7,24-trien-3β-ol	1.075	0.022	2.31	0.020	1.70
10.	4-methyl-cholestane/fully hydrogenated ergosterol**	1.091	0.043	4.52	0.050	4.23
11.	Lanosterol	1.105	0.125	13.12	0.158	13.30
12.	Ergosta-tetraene-3β-ol isomer**	1.114	0.127	13.29	0.149	12.59
13.	Lanosta-diene-3β-ol isomer**	1.143	0.046	4.79	0.067	5.67
14.	Lanosta-diene-3β-ol isomer**	1.150	0.047	4.88	0.083	7.02
15.	Ergosta-ene-3β-ol isomer**	1.205	0.007	0.68	0.011	0.93
16.	Ergosta-ene-3β-ol isomer**	1.221	0.088	9.21	0.182	15.35
17.	3 compounds**	1.257	0.040	4.13	0.078	6.57

* Cholesterol and Estrone were added as surrogate marker and internal standard, respectively

**See MS interpretation for detailed discussion of possible double bond locations

RRT – Relative Retention Time

ND – None detected

[a] – Relative to cholesterol at an RRT of 1.000

[b] – $\mu g/10^8$ cells

[c] – percent based on total detectable compounds that are listed in the table

TABLE 7. Free Sterol Composition of *dap1*? Mutant Strain

Peak#	Identity	RRT[a]	1 Day Quantity[b]	1 Day Percent[c]	2 Day Quantity[b]	2 Day Percent[c]
	Estrone*	0.729				
	Cholesterol*	1.000				
1.	Ergosta-5,7,22,24-tetraen-3β-ol	1.009	0.025	1.51	0.032	2.02
2.	Ergosta-diene-3β-ol isomer**	1.015	0.035	2.15	0.038	2.39
3.	Zymosterol	1.020	0.193	11.79	0.332	20.73
4.	Ergosta-tetraene-3β-ol isomer**	1.030	0.204	12.47	0.206	12.84
5.	Ergosterol	1.035	0.252	15.41	0.201	12.52
6..	4,4-Dimethylcholesta-8,24-dien-3β-ol	1.048	0.046	2.82	0.014	0.87
7.	Episterol	1.059	0.167	10.21	0.190	11.87
8.	Fecosterol	1.066	0.122	7.48	0.138	8.62
9.	Ergosta-5,7,24-trien-3β-ol	1.075	0.145	8.90	0.077	4.82
10.	4-methyl-cholestane/fully hydrogenated ergosterol**	1.091	0.146	8.90	0.096	6.01
11.	Lanosterol	1.105	0.102	6.25	0.098	6.11
12.	Ergosta-tetraene-3β-ol isomer**	1.114	0.073	4.48	0.063	3.96
13.	Lanosta-diene-3β-ol isomer**	1.143	0.032	1.93	0.022	1.37
14.	Lanosta-diene-3β-ol isomer**	1.150	0.043	2.63	0.036	2.27
15.	Ergosta-ene-3β-ol isomer**	1.205	0.016	0.97	0.015	0.96
16.	Ergosta-ene-3β-ol isomer**	1.221	ND	0	ND	0
17.	3 compounds**	1.257	0.035	2.11	0.043	2.65

* Estrone and Cholesterol were added as surrogate marker and internal standard, respectively

**See MS interpretation for detailed discussion of possible double bond locations

RRT – Relative Retention Time

ND – None detected

[a] – Relative to cholesterol at an RRT of 1.000

[b] – $\mu g/10^8$ cells

[c] – percent based on total detectable compounds that are listed in the table

TABLE 8. Steryl Ester Composition of *dapl*? Mutant Strain

Peak#	Identity	RRT[a]	1 Day Quantity[b]	1 Day Percent[c]	2 Day Quantity[b]	2 Day Percent[c]
	Estrone*	0.729				
	Cholesterol*	1.000				
1.	Ergosta-5,7,22,24-tetraen-3β-ol	1.009	0.066	8.31	0.092	9.32
2.	Ergosta-diene-3β-ol isomer**	1.015	0.036	4.48	0.011	1.12
3.	Zymosterol	1.020	0.032	3.95	0.035	3.60
4.	Ergosta-tetraene-3β-ol isomer**	1.030	ND	0	ND	0
5.	Ergosterol	1.035	0.091	11.33	0.056	5.68
6.	4,4-Dimethylcholesta-8,24-dien-3β-ol	1.048	0.011	1.39	0.023	2.30
7.	Episterol	1.059	0.017	2.09	0.060	6.13
8.	Fecosterol	1.066	0.071	8.90	0.097	9.89
9.	Ergosta-5,7,24-trien-3β-ol	1.075	0.030	3.71	0.032	3.29
10.	4-methyl-cholestane/fully hydrogenated ergosterol**	1.091	0.039	4.92	0.041	4.15
11.	Lanosterol	1.105	0.092	11.53	0.149	15.12
12.	Ergosta-tetraene-3β-ol isomer**	1.114	0.121	15.16	0.070	7.13
13.	Lanosta-diene-3β-ol isomer**	1.143	0.055	6.93	0.109	11.10
14.	Lanosta-diene-3β-ol isomer**	1.150	0.042	5.31	0.098	10.00
15.	Ergosta-ene-3β-ol isomer**	1.205	0.005	0.66	ND	0
16.	Ergosta-ene-3β-ol isomer**	1.221	0.061	7.59	0.079	8.04
17.	3 compounds**	1.257	0.030	3.75	0.031	3.15

* Cholesterol and Estrone were added as surrogate marker and internal standard, respectively

**See MS interpretation for detailed discussion of possible double bond locations

RRT – Relative Retention Time

ND – None detected

[a] – Relative to cholesterol at an RRT of 1.000

[b] – $\mu g/10^8$ cells

[c] – percent based on total detectable compounds that are listed in the table

TABLE 9. Free Sterol Composition of *dap1*? + pUGpd-*DAP1* Strain

Peak#	Identity	RRT[a]	1 Day Quantity[b]	1 Day Percent[c]	2 Day Quantity[b]	2 Day Percent[c]
	Estrone*	0.729				
	Cholesterol*	1.000				
1.	Ergosta-5,7,22,24-tetraen-3β-ol	1.009	0.036	2.14	0.042	2.55
2.	Ergosta-diene-3β-ol isomer**	1.015	0.077	4.53	0.074	4.52
3.	Zymosterol	1.020	0.110	6.46	0.153	9.30
4.	Ergosta-tetraene-3β-ol isomer**	1.030	ND	0	ND	0
5.	Ergosterol	1.035	0.335	19.61	0.366	22.47
6.	4,4-Dimethylcholesta-8,24-dien-3β-ol	1.048	0.027	1.57	0.058	3.58
7.	Episterol	1.059	0.176	10.28	0.159	9.77
8.	Fecosterol	1.066	0.239	13.98	0.039	2.42
9.	Ergosta-5,7,24-trien-3β-ol	1.075	0.221	12.96	0.169	10.40
10.	4-methyl-cholestane/fully hydrogenated ergosterol**	1.091	0.071	4.13	0.076	4.68
11.	Lanosterol	1.105	0.173	10.13	0.236	14.52
12.	Ergosta-tetraene-3β-ol isomer**	1.114	0.090	5.27	0.135	8.27
13.	Lanosta-diene-3β-ol isomer**	1.143	0.080	4.70	0.043	2.63
14.	Lanosta-diene-3β-ol isomer**	1.150	0.027	1.57	0.041	2.52
15.	Ergosta-ene-3β-ol isomer**	1.205	0.013	0.76	0.023	1.43
16.	Ergosta-ene-3β-ol isomer**	1.221	0.020	1.16	0.016	0.95
17.	3 compounds**	1.257	0.013	0.76	ND	0

* Estrone and Cholesterol were added as surrogate marker and internal standard, respectively

**See MS interpretation for detailed discussion of possible double bond locations

RRT – Relative Retention Time

ND – None detected

[a] – Relative to cholesterol at an RRT of 1.000

[b] – $\mu g/10^8$ cells

[c] – percent based on total detectable compounds that are listed in the table

TABLE 10. Steryl Ester Composition of *dap1*? +pUGpd-*DAP1* Strain

Peak#	Identity	RRT[a]	1 Day Quantity[b]	1 Day Percent[c]	2 Day Quantity[b]	2 Day Percent[c]
	Estrone*	0.729				
	Cholesterol*	1.000				
1.	Ergosta-5,7,22,24-tetraen-3β-ol	1.009	0.065	6.48	0.071	5.98
2.	Ergosta-diene-3β-ol isomer**	1.015	0.034	3.34	0.034	3.15
3.	Zymosterol	1.020	0.032	3.21	0.064	5.41
4.	Ergosta-tetraene-3β-ol isomer**	1.030	ND	0	ND	0
5.	Ergosterol	1.035	0.041	4.06	0.066	5.60
6.	4,4-Dimethylcholesta-8,24-dien-3β-ol	1.048	0.013	1.33	0.045	3.83
7.	Episterol	1.059	0.015	1.52	0.024	2.03
8.	Fecosterol	1.066	0.063	6.32	0.101	8.57
9.	Ergosta-5,7,24-trien-3β-ol	1.075	0.031	3.05	0.021	1.78
10.	4-methyl-cholestane/fully hydrogenated ergosterol**	1.091	0.134	13.32	0.161	13.60
11.	Lanosterol	1.105	0.112	11.19	0.107	9.03
12.	Ergosta-tetraene-3β-ol isomer**	1.114	0.078	7.82	0.083	6.99
13.	Lanosta-diene-3β-ol isomer**	1.143	0.047	4.64	0.056	4.73
14.	Lanosta-diene-3β-ol isomer**	1.150	0.040	3.94	0.027	2.28
15.	Ergosta-ene-3β-ol isomer**	1.205	0.017	1.68	0.006	0.48
16.	Ergosta-ene-3β-ol isomer**	1.221	0.282	28.10	0.314	26.53
17.	3 compounds**	1.257	ND	0	ND	0

* Cholesterol and Estrone were added as surrogate marker and internal standard, respectively

**See MS interpretation for detailed discussion of possible double bond locations

RRT – Relative Retention Time

ND – None detected

[a] – Relative to cholesterol at an RRT of 1.000

[b] – $\mu g/10^8$ cells

[c] – percent based on total detectable compounds

TABLE 11. Free Sterol Composition of Control + pmCUP1-Hpr6.6 Strain

Peak#	Identity	RRT[a]	Low Cu		High Cu	
			Quantity[b]	Percent[c]	Quantity[b]	Percent[c]
	Estrone*	0.729				
	Cholesterol*	1.000				
1.	Ergosta-5,7,22,24-tetraen-3β-ol	1.009	0.026	1.33	0.038	1.89
2.	Ergosta-diene-3β-ol isomer**	1.015	0.018	0.94	ND	0
3.	Zymosterol	1.020	0.159	8.23	0.237	11.81
4.	Ergosta-tetraene-3β-ol isomer**	1.030	ND	0	ND	0
5.	Ergosterol	1.035	0.929	47.99	0.950	47.35
6.	4,4-Dimethylcholesta-8,24-dien-3β-ol	1.048	0.112	5.77	0.117	5.84
7.	Episterol	1.059	0.217	11.19	0.144	7.18
8.	Fecosterol	1.066	0.111	5.76	0.076	3.78
9.	Ergosta-5,7,24-trien-3β-ol	1.075	0.100	5.15	0.124	6.19
10.	4-methyl-cholestane/fully hydrogenated ergosterol**	1.091	0.097	5.01	0.145	7.23
11.	Lanosterol	1.105	0.088	4.53	0.096	4.76
12.	Ergosta-tetraene-3β-ol isomer**	1.114	0.046	2.36	0.055	2.75
13.	Lanosta-diene-3β-ol isomer**	1.143	0.024	1.25	0.007	0.36
14.	Lanosta-diene-3β-ol isomer**	1.150	0.007	0.38	0.008	0.41
15.	Ergosta-ene-3β-ol isomer**	1.205	ND	0	0.009	0.46
16.	Ergosta-ene-3β-ol isomer**	1.221	ND	0	ND	0
17.	3 compounds**	1.257	0.003	0.13	ND	0

* Estrone and Cholesterol were added as surrogate marker and internal standard, respectively

**See MS interpretation for detailed discussion of possible double bond locations

RRT – Relative Retention Time

ND – None detected

[a] – Relative to cholesterol at an RRT of 1.000

[b] – $\mu g/10^8$ cells

[c] – percent based on total detectable compounds that are listed in the table

TABLE 12. Steryl Ester Composition of Control + pmCUP1-Hpr6.6 Strain

Peak#	Identity	RRT[a]	Low Cu		High Cu	
			Quantity[b]	Percent[c]	Quantity[b]	Percent[c]
	Estrone*	0.729				
	Cholesterol*	1.000				
1.	Ergosta-5,7,22,24-tetraen-3β-ol	1.009	0.016	1.54	0.032	2.79
2.	Ergosta-diene-3β-ol isomer**	1.015	ND	0	ND	0
3.	Zymosterol	1.020	0.012	1.18	0.024	2.05
4.	Ergosta-tetraene-3β-ol isomer**	1.030	ND	0	ND	0
5.	Ergosterol	1.035	0.554	53.19	0.677	58.58
6.	4,4-Dimethylcholesta-8,24-dien-3β-ol	1.048	0.064	6.12	0.075	6.45
7.	Episterol	1.059	0.048	4.58	0.039	3.39
8.	Fecosterol	1.066	0.031	2.99	0.030	2.58
9.	Ergosta-5,7,24-trien-3β-ol	1.075	0.051	4.89	0.059	5.08
10.	4-methyl-cholestane/fully hydrogenated ergosterol**	1.091	0.063	6.02	0.059	5.08
11.	Lanosterol	1.105	0.044	4.19	0.029	2.51
12.	Ergosta-tetraene-3β-ol isomer**	1.114	0.038	3.61	0.027	2.31
13.	Lanosta-diene-3β-ol isomer**	1.143	0.015	1.48	0.024	2.07
14.	Lanosta-diene-3β-ol isomer**	1.150	0.019	1.78	0.026	2.23
15.	Ergosta-ene-3β-ol isomer**	1.205	0.005	0.51	0.002	0.14
16.	Ergosta-ene-3β-ol isomer**	1.221	0.054	5.18	0.039	3.35
17.	3 compounds**	1.257	0.029	2.78	0.016	1.39

* Cholesterol and Estrone were added as surrogate marker and internal standard, respectively

**See MS interpretation for detailed discussion of possible double bond locations

RRT – Relative Retention Time

ND – None detected

[a] – Relative to cholesterol at an RRT of 1.000

[b] – $\mu g/10^8$ cells

[c] – percent based on total detectable compounds that are listed in the table

TABLE 13. Free Sterol Composition of *dap1*? + pmCUP1-Hpr6.6 Strain

Peak#	Identity	RRT[a]	Low Cu		High Cu	
			Quantity[b]	Percent[c]	Quantity[b]	Percent[c]
	Estrone*	0.729				
	Cholesterol*	1.000				
1.	Ergosta-5,7,22,24-tetraen-3β-ol	1.009	0.021	1.19	0.007	0.38
2.	Ergosta-diene-3β-ol isomer**	1.015	0.025	1.42	0.005	0.28
3.	Zymosterol	1.020	0.169	9.71	0.166	9.16
4.	Ergosta-tetraene-3β-ol isomer**	1.030	ND	0	ND	0
5.	Ergosterol	1.035	0.739	42.50	0.788	43.51
6.	4,4-Dimethylcholesta-8,24-dien-3β-ol	1.048	0.095	5.45	0.108	5.97
7.	Episterol	1.059	0.194	11.14	0.152	8.39
8.	Fecosterol	1.066	0.118	6.81	0.065	3.61
9.	Ergosta-5,7,24-trien-3β-ol	1.075	0.117	6.70	0.161	8.87
10.	4-methyl-cholestane/fully hydrogenated ergosterol**	1.091	0.106	6.08	0.181	9.99
11.	Lanosterol	1.105	0.093	5.34	0.088	4.86
12.	Ergosta-tetraene-3β-ol isomer**	1.114	0.054	3.11	0.080	4.39
13.	Lanosta-diene-3β-ol isomer**	1.143	0.006	0.32	0.006	0.34
14.	Lanosta-diene-3β-ol isomer**	1.150	0.004	0.22	0.005	0.25
15.	Ergosta-ene-3β-ol isomer**	1.205	ND	0	ND	0
16.	Ergosta-ene-3β-ol isomer**	1.221	ND	0	ND	0
17.	3 compounds**	1.257	ND	0	ND	0

* Estrone and Cholesterol were added as surrogate marker and internal standard, respectively

**See MS interpretation for detailed discussion of possible double bond locations

RRT – Relative Retention Time

ND – None detected

[a] – Relative to cholesterol at an RRT of 1.000

[b] – $\mu g/10^8$ cells

[c] – percent based on total detectable compounds that are listed in the table

TABLE 14. Steryl Ester Composition of *dapl*? +pCUP1-Hpr6.6 Strain

Peak#	Identity	RRT[a]	Low Cu Quantity[b]	Low Cu Percent[c]	High Cu Quantity[b]	High Cu Percent[c]
	Estrone*	0.729				
	Cholesterol*	1.000				
1.	Ergosta-5,7,22,24-tetraen-3β-ol	1.009	0.021	2.21	0.022	2.06
2.	Ergosta-diene-3β-ol isomer**	1.015	ND	0	ND	0
3.	Zymosterol	1.020	0.010	1.12	0.005	0.47
4.	Ergosta-tetraene-3β-ol isomer**	1.030	ND	0	ND	0
5.	Ergosterol	1.035	0.574	61.32	0.588	55.58
6.	4,4-Dimethylcholesta-8,24-dien-3β-ol	1.048	0.044	4.66	0.061	5.78
7.	Episterol	1.059	0.025	2.67	0.024	2.28
8.	Fecosterol	1.066	0.020	2.16	0.026	2.49
9.	Ergosta-5,7,24-trien-3β-ol	1.075	0.051	5.42	0.060	5.66
10.	4-methyl-cholestane/fully hydrogenated ergosterol**	1.091	0.040	4.22	0.050	4.73
11.	Lanosterol	1.105	0.030	3.20	0.042	3.96
12.	Ergosta-tetraene-3β-ol isomer**	1.114	0.029	3.07	0.039	3.68
13.	Lanosta-diene-3β-ol isomer**	1.143	0.014	1.52	0.024	2.29
14.	Lanosta-diene-3β-ol isomer**	1.150	0.014	1.52	0.019	1.76
15.	Ergosta-ene-3β-ol isomer**	1.205	ND	0	ND	0
16.	Ergosta-ene-3β-ol isomer**	1.221	0.044	4.66	0.068	6.41
17.	3 compounds**	1.257	0.021	2.27	0.030	2.87

* Cholesterol and Estrone were added as surrogate marker and internal standard, respectively

**See MS interpretation for detailed discussion of possible double bond locations

RRT – Relative Retention Time

ND – None detected

[a] – Relative to cholesterol at an RRT of 1.000

[b] – $\mu g/10^8$ cells

[c] – percent based on total detectable compounds

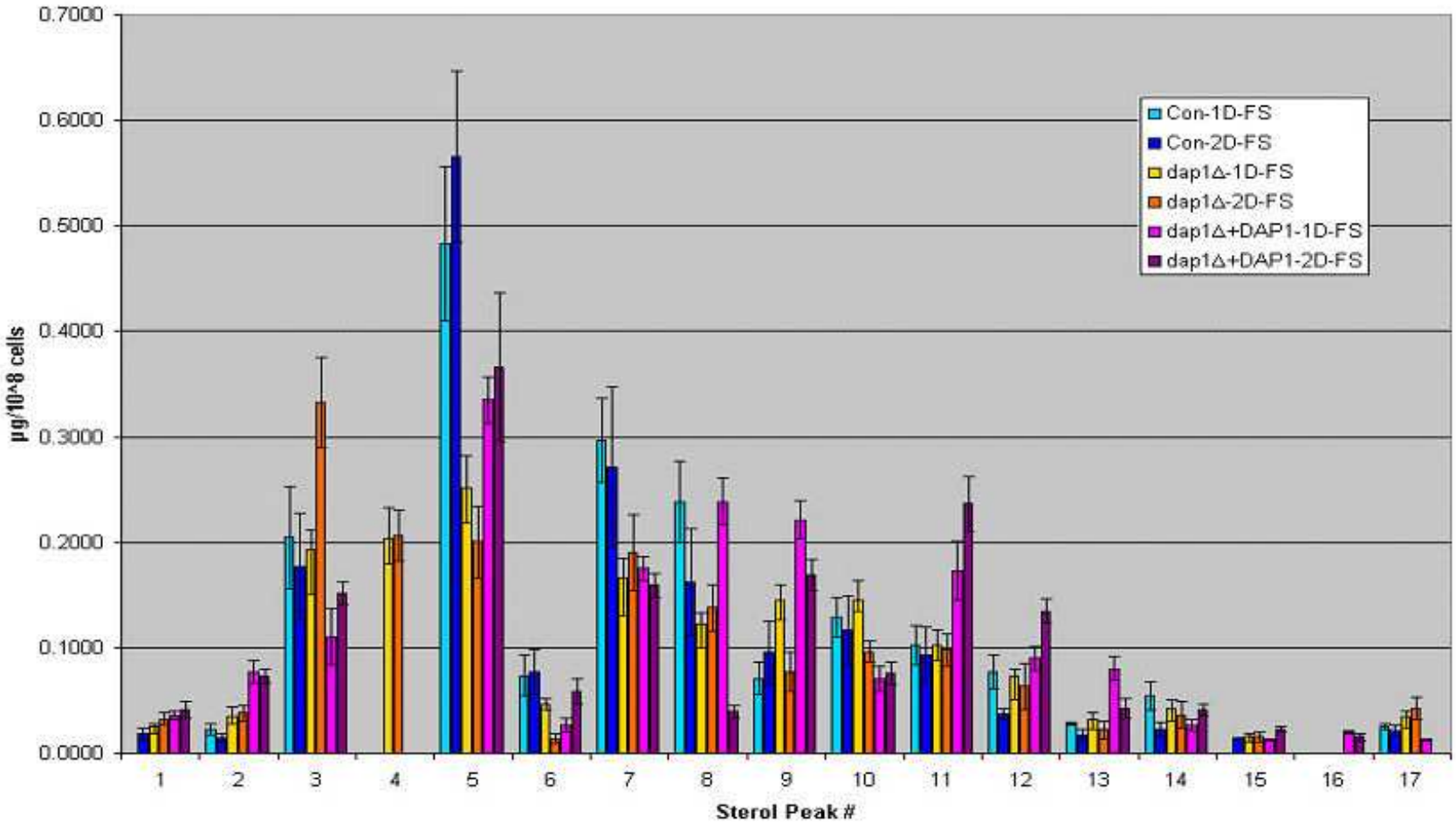

Figure 29. Free Sterol Distribution Comparison: Control Strain versus *dap1* Mutant Strain versus *dap1* + pUGpd-*DAP1* Strain in µg/10^8 cells. Error bars represent standard deviation. Control strain is for 4 replicates, all other strains are for 2 replicates.

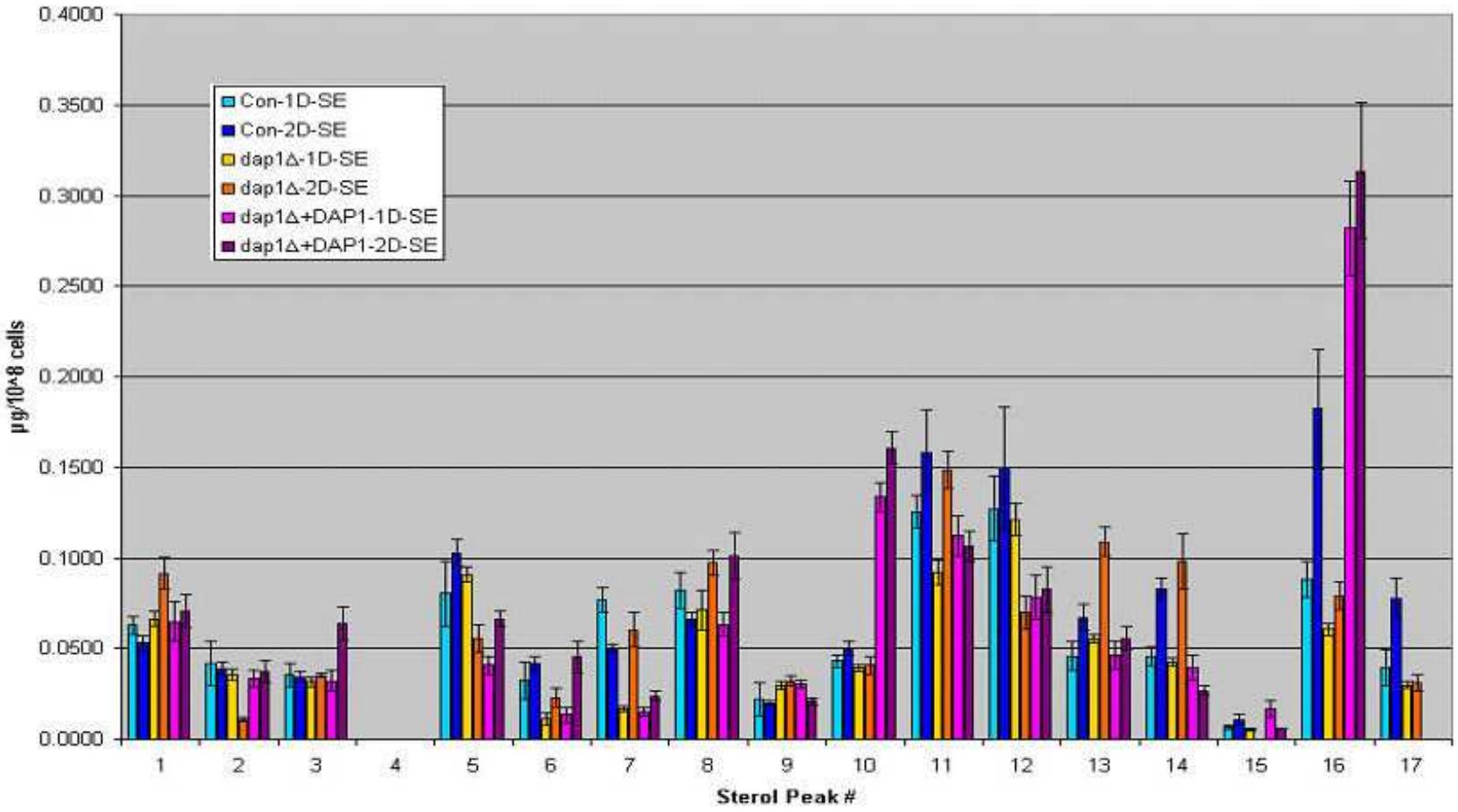

Figure 30. Steryl Ester Distribution Comparison: Control Strain versus *dap1* Mutant Strain versus *dap1* + pUGpd-*DAP1* Strain in µg/10^8 cells. Error bars represent standard deviation. Control strain is for 4 replicates, all other strains are for 2 replicates.

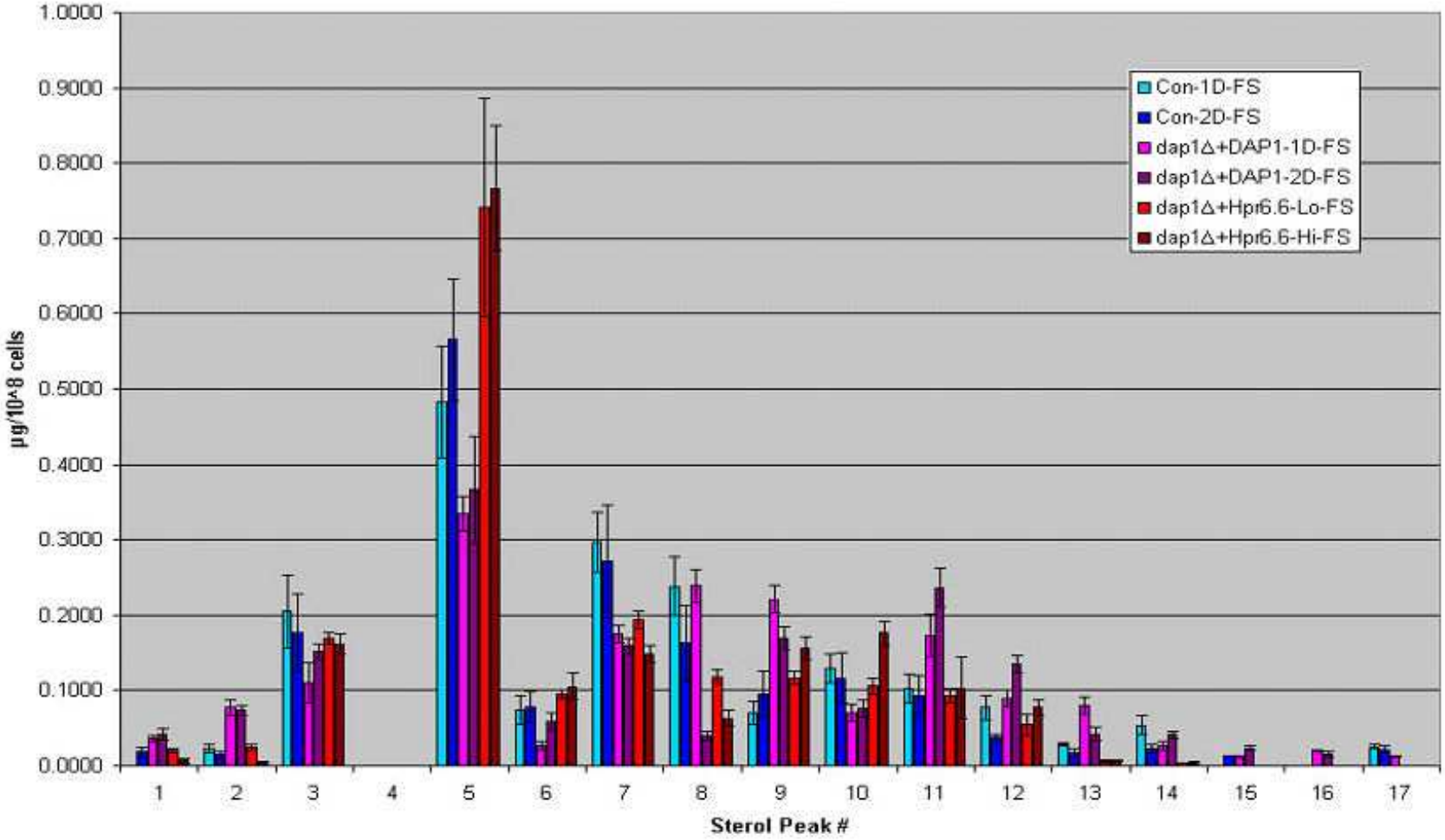

Figure 31. Free Sterol Distribution Comparison: Control Strain versus *dap1* + pUGpd-*DAP1* Strain versus *dap1* + pCUP1-Hpr6.6 Strain in µg/10^8 cells. Error bars represent standard deviation. Control strain is for 4 replicates, all other strains are for 2 replicates.

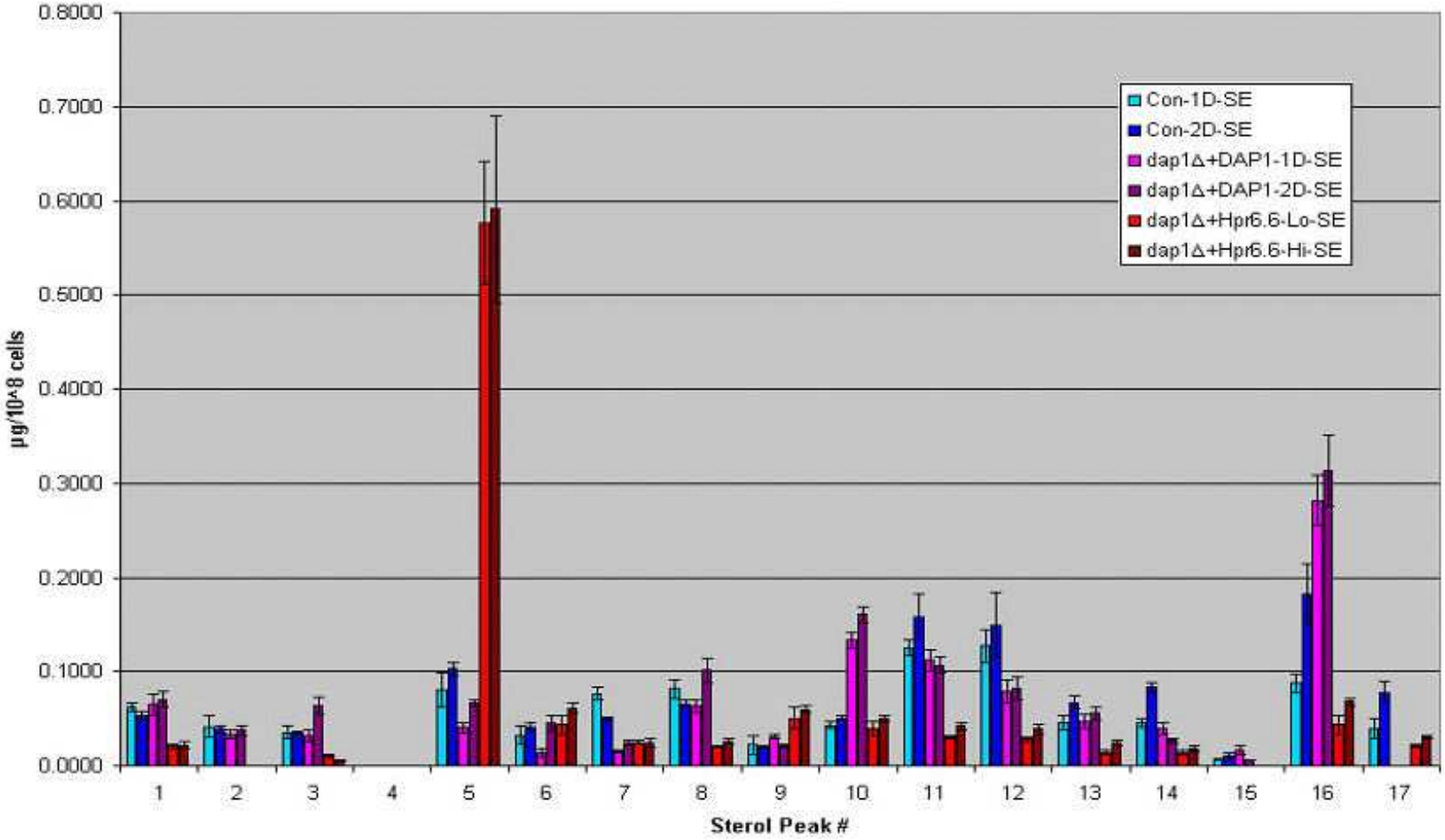

Figure 32. Steryl Ester Distribution Comparison: Control Strain versus *dap1* + pUGpd-*DAP1* Strain versus *dap1* + pCUP1-Hpr6.6 Strain in µg/10^8 cells. Error bars represent standard deviation. Control strain is for 4 replicates, all other strains are for 2 replicates.

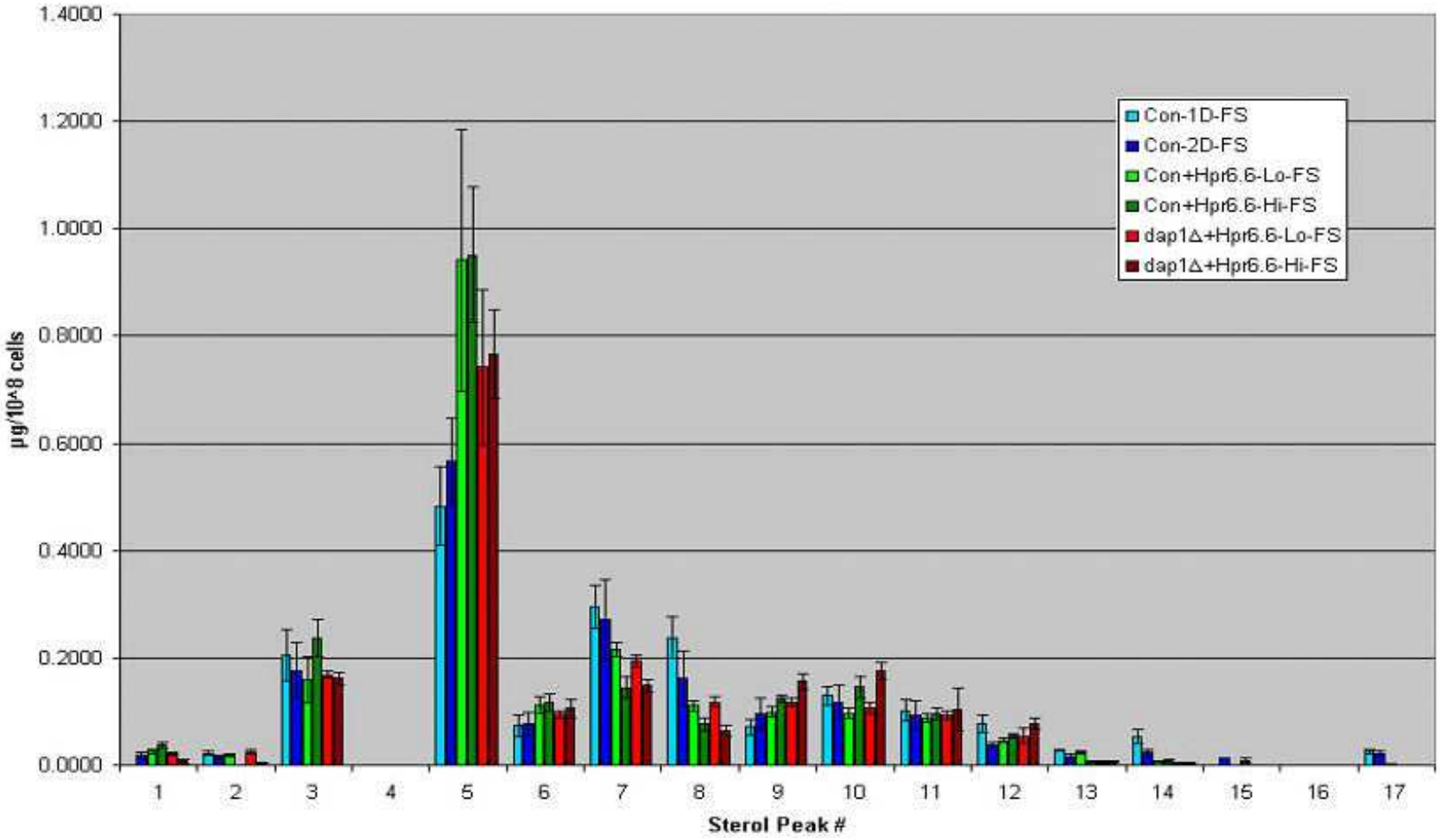

Figure 33. Free Sterol Distribution Comparison: Control Strain versus Control + pCUP1-Hpr6.6 Strain versus *dap1* + pCUP1-Hpr6.6 Strain in µg/10^8 cells. Error bars represent standard deviation. Control strain is for 4 replicates, all other strains are for 2 replicates.

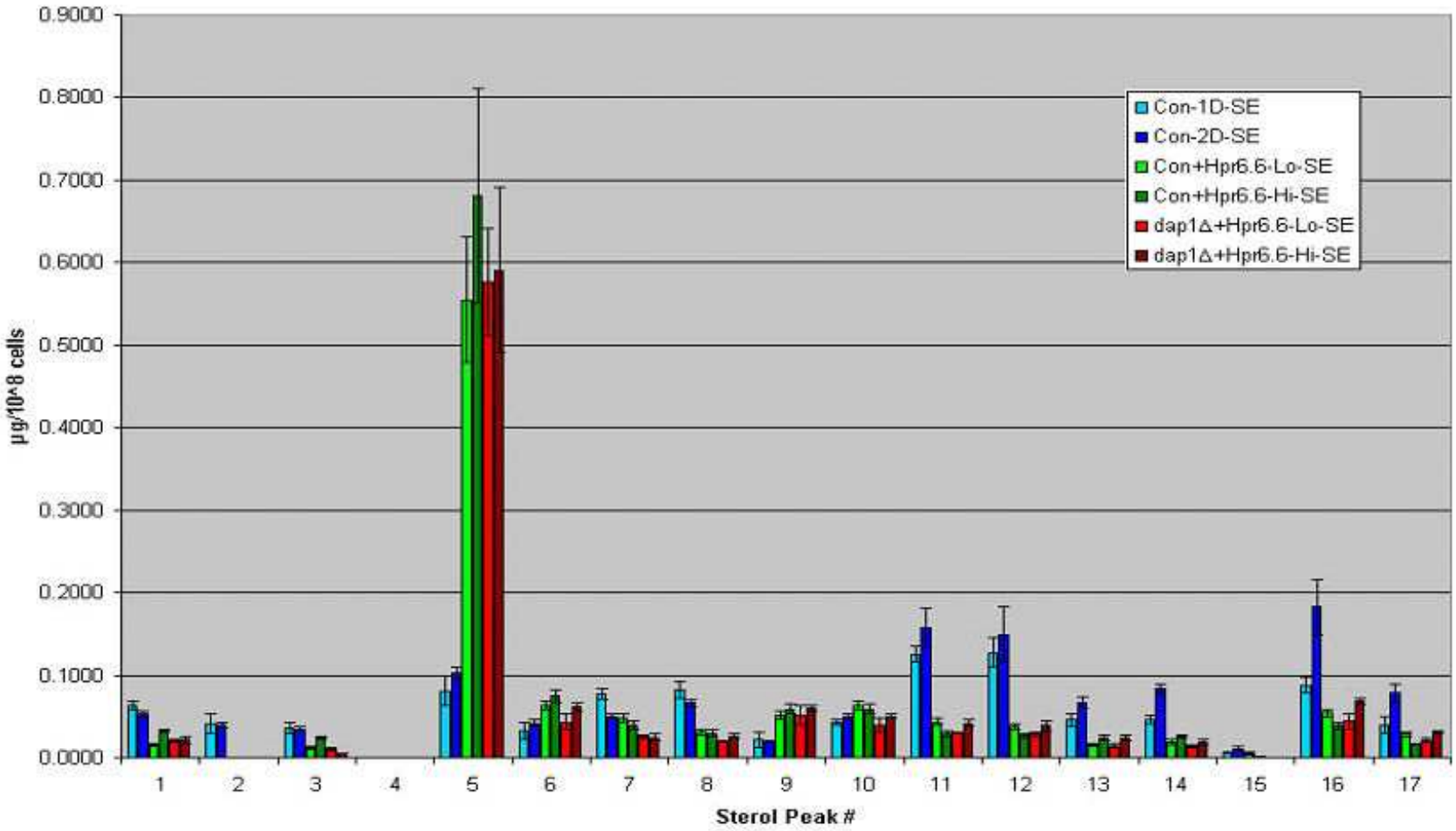

Figure 34. Steryl Ester Distribution Comparison: Control Strain vs. Control + pCUP1-Hpr6.6 Strain vs. *dap1* + pCUP1-Hpr6.6 Strain in µg/10^8 cells. Error bars represent standard deviation. Control strain is for 4 replicates, all other strains are for 2 replicates.

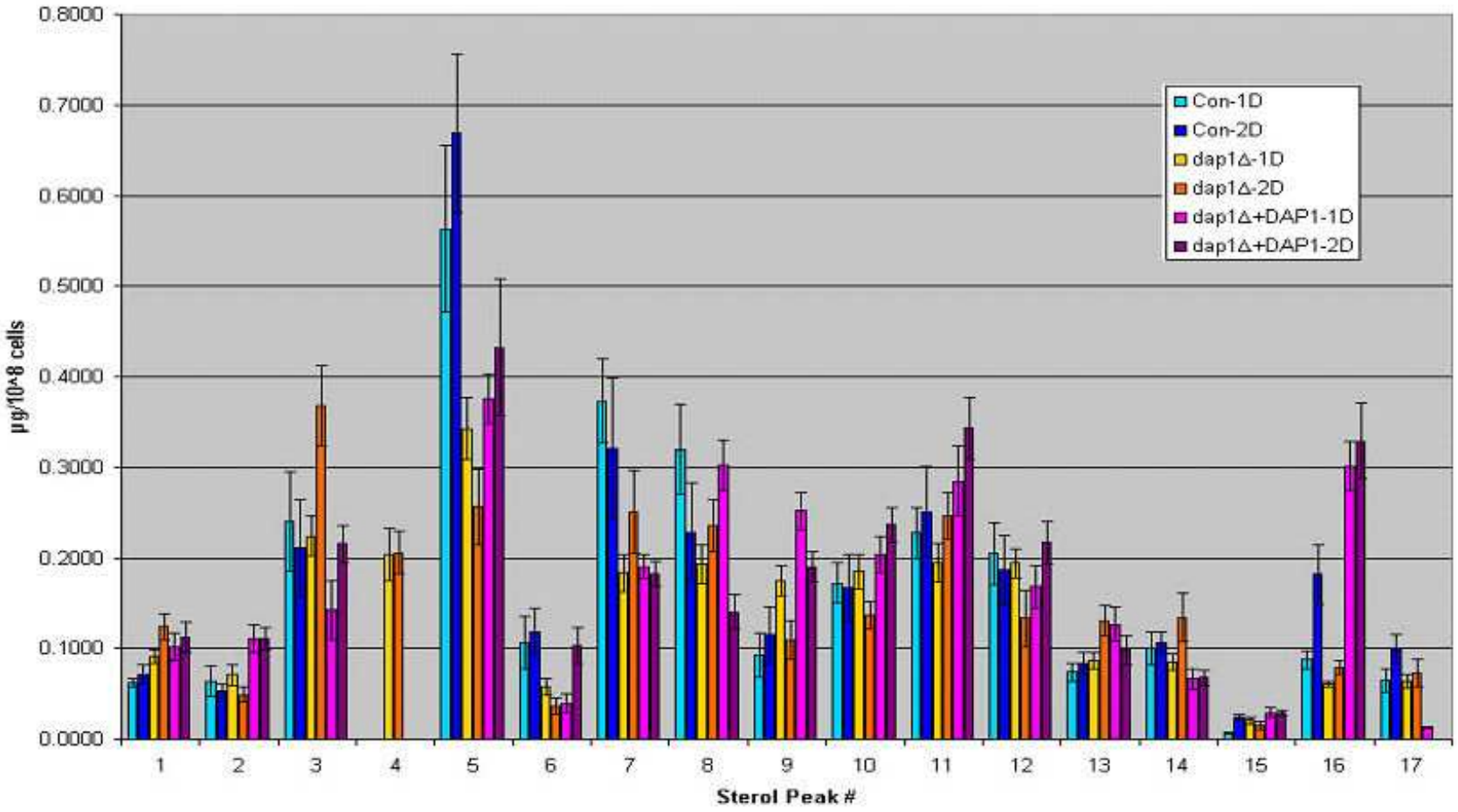

Figure 35. Total Sterol Content Comparison: Control Strain versus *dap1* Mutant Strain versus *dap1* + pUGpd-*DAP1* Strain in $\mu g/10^8$ cells. Error bars represent standard deviation. Control strain is for 4 replicates, all other strains are for 2 replicates.

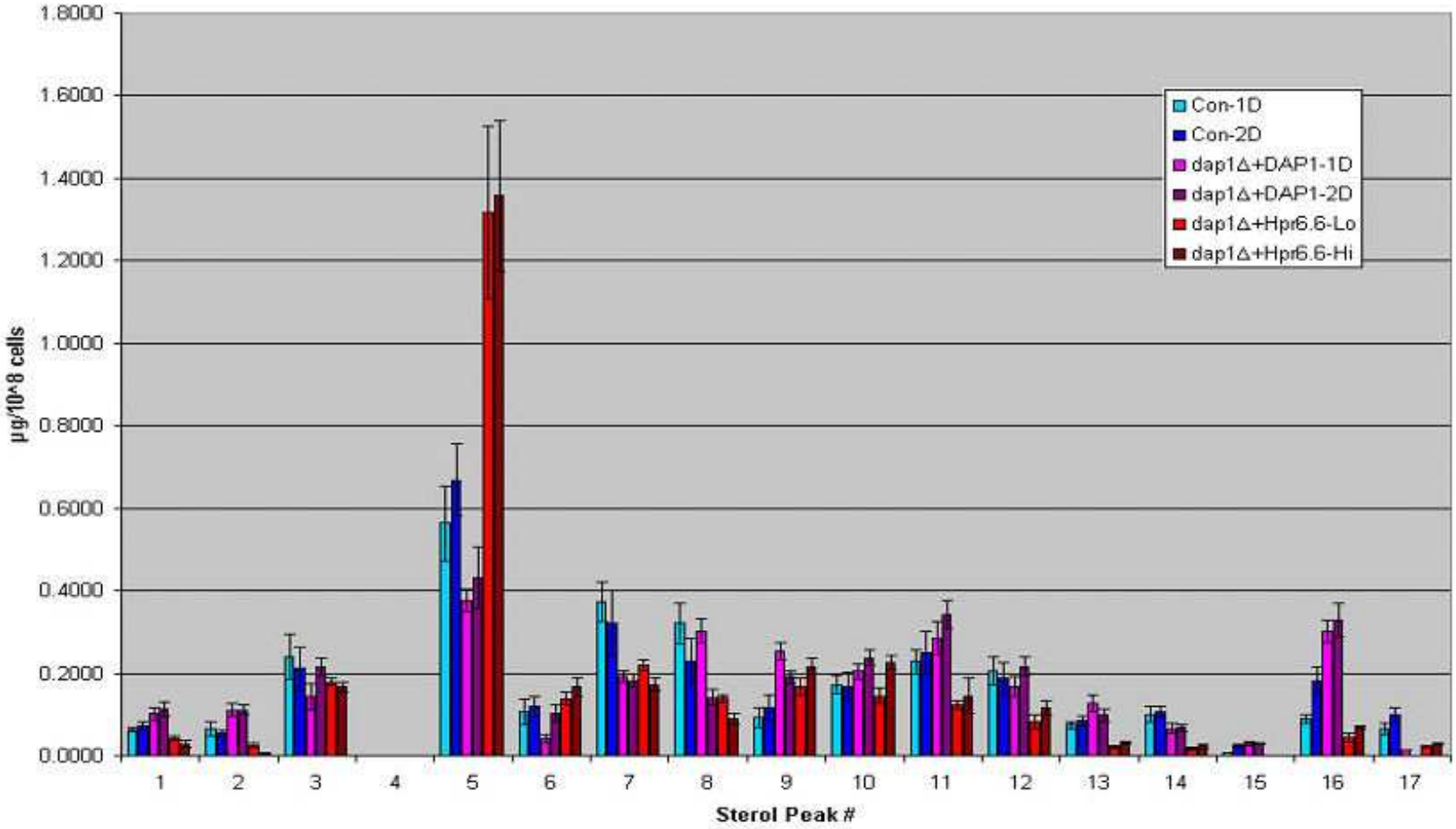

Figure 36. Total Sterol Content Comparison: Control Strain versus *dap1* Mutant Strain versus *dap1* + pCUP1-Hpr6.6 Strain in µg/10^8 cells. Error bars represent standard deviation. Control strain is for 4 replicates, all other strains are for 2 replicates.

DISCUSSION

Growth Curves

Growth of cells of the *dap1*Δ mutant strain, the *ypr118w*Δ mutant strain, and cells of the *dap1*Δ/ *ypr118w*Δ double mutant strain did not grow at a significantly different rate than cells of the control strain when grown separately in YPD medium, see Figure 2. Growth of cells of the *dap1*Δ mutant strain and the *ypr118w*Δ mutant strain did not outcompete the control strain in short term or moderately long term in YPD culture, see Figures 3-6. YPD is a very nutrient rich media. This environment does not allow for slight phenotypic defects in growth to become apparent. Only after 50 days of culture was there a slight increase in the proportions of the *dap1*Δ mutant strain and the *ypr118w*Δ mutant strain as compared to control. This change was noted after 14 days of continuous culture, in which no cells were transferred to fresh media. Under such conditions, it is hard to tell if indeed the strains were acting metabolically similar to the initial culture or if any secondary mutations had occurred after so many generations.

The growth curves in SLAD media, conversely, exhibited a marked change in growth patterns. SLAD media is a nitrogen starving media. The *dap1*Δ mutant strain had a significant increase in growth in competition experiment, almost outcompeting the control strain altogether, see Figure 7. After 15 days of culture, the percentage of the *dap1*Δ mutant strain ranged from about 70% to about 99% of cells in culture.

The growth of the *ypr118w*Δ mutant strain in SLAD exhibited almost the complete opposite pattern. The control strain significantly outcompeted the *ypr118w*Δ mutant strain after about 7 days of culture, see Figure 8. This continued until no cells of

the *ypr118w*Δ mutant strain were seen in culture. This is perhaps not entirely unforeseen. Ypr118w has been known to have sequence similarity to the regulatory subunits of the eukaryotic initiation factor two beta (eIF-IIβ) which has been recently found to be a methylthioribose-1-phospate isomerase [86]. It is involved in amino acid metabolism, specifically the methionine salvage pathway. It is required to grow on S-methylthioadenosine in the absence of methionine. It catalyzes the conversion of 5-methylthioribose-1-phosphate into 5-methylthioribulose-1-phosphate.

The competition experiment in SPD, which is a low nitrogen media, demonstrated that this media had no significant effect on the growth rate of the *dap1*Δ mutant strain as compared to the control strain, see Figure 9. Once again, only after about 50 days of continuous culture did the *dap1*Δ mutant strain exhibit a slight competitive edge over the control.

The growth of the *ypr118w*Δ mutant strain in SPD maintained its limitations in fidelity in a nitrogen limiting environment. The *ypr118w*Δ mutant strain exhibited a significant reduction in its ability to compete with the control strain in this nitrogen limiting media, see Figure 10. The proportion of cells of the *ypr118w*Δ mutant strain decreased until it seemed to stabilize around 25% of cells in culture.

Petite growth experiments

It was observed that there were a greater number of small colonies from the *dap1*Δ mutant strain when streaked out from glycerol stock and incubated at 30ºC overnight. These smaller colonies could be slow growers or they could have lost mitochondrial function. Those smaller colonies that have lost mitochondrial function are

ambiguously assigned the characteristic of petite. To test whether these cells were actually petite or to see whether the cells were just slow growing, a phenotypic experiment was performed. The designation petite is related to loss of mitochondrial function. Functional mitochondria are determined by the yeast cells ability to respire on a non-fermentable carbon source. A number of mutations can account for this phenotype, with a different designation for each. There can be mutations in the nuclear genome or mutation in the mitochondrial DNA, unknown mutations or specific known gene mutations. A designation of Nfs^- is a general phenotypic description and denotes lack of growth on non-fermentable substrates. Therefore, the phenotype of petite described here, should be designated as such, in the strict sense.

The sterol content of mitochondria has been reported to be, generally, low [64]. In yeast, most of the mitochondrial sterol content is located in the inner membrane [1]. During import into mitochondria, sterols have been detected in the contact sites between the outer and inner membranes, supporting an idea that these zones are sites for intramitochondrial lipid translocation [65]. Ergosterol translocation from cytosol to mitochondria was enhanced by the presence of a transfer protein at non-limiting concentrations, *in vitro* [65]. The transfer protein, phosphatidylserine transfer protein, is known to translocate sterols between isolated membranes, *in vitro*, and only hypothesized *in vivo* [64].

It was not the purpose of the study to determine the genetic or biochemical nature of the cause for the cells becoming petite, only to determine if cells had lost mitochondrial function or were slow growers. Therefore, a simple experiment was performed. Cells from each strain were grown overnight on separate YPD plates and the

next day colonies were replica-plated onto YPG plates. YPG is media containing glycerol as the only carbon source. Cells without functioning mitochondria are not able to ferment on glycerol, and hence can not grow. This would distinguish between slow growers and petites.

The experiment demonstrated that there was about a two-fold increase in the number of petites in the *dap1*Δ mutant strain as compared to the control strain, see Figures 11 and 12. This difference disappeared after the first serial transfer, implying that the growth medium composition played a role in petite formation. Since, only those cells that were able to utilize glycerol were used for subsequent generations. Cells of the *ypr118w*Δ mutant strain exhibited no significant difference from the control strain, see Figure 13. This suggests a more active role for Dap1p than ypr118wp in respiration. Cells of the *dap1*Δ*/ypr118w*Δ double mutant strain acted similar to cells of the *dap1*Δ mutant strain, exhibiting about a two-fold increase in petites over control strain, see Figure 14, reinforcing the possibility that Dap1p plays a more central role in respiration than Ypr118wp.

It could be hypothesized that the reason for the increase in the loss of mitochondrial function, and therefore a greater number of petites in the *dap1*Δ mutant strain, has to do with an altered sterol makeup in the mitochondria. Since, there is an altered overall sterol profile in the *dap1*Δ mutant strain, it is reasonable to assume there is an altered sterol profile in the mitochondria. This could lead to a reduction of respiratory function. Furthermore, a physical connection exists between Dap1p and mitochondria in yeast. It has been demonstrated that Dap1p interacts with GUF1, a mitochondrial GTPase of unknown function [87]. GTPases specifically bind and hydrolyse GTP in a

cyclic mechanism that activates and inactivates the GTPase protein [88]. In this cycle, the GTPase passes through three conformational states [89]. Initially, the GTPase is inactive and is not bound to any nucleotide. After binding GTP, the protein becomes active and changes conformation, so that it has a changed affinity for effector molecules or other enzymes. GTP is then hydrolyzed simultaneously, with an effect being generated on the target of the GTPase. Subsequently, GDP is released from the inactive GTPase, so that the protein returns to the empty state. This cyclic reaction usually involves several other factors that either catalyze the hydrolysis step of the GTPase cycle or catalyze the release of bound GDP from the inactive state of the GTPase [90]. Guf1p function in the mitochondria is still unclear.

Furthermore, Ypr118wp has been demonstrated to interact with Atp14p [91]. Ypr118wp has been demonstrated to interact with Dap1p through a yeast two-hybrid interaction and demonstrated to co-localize with Dap1p. Atp14p is located on the mitochondria membrane and functions in respiration as subunit H in the ATP synthase complex [92]. F_1F_2 ATP synthase is responsible for the synthesis of ATP from ADP and P_i at the expense of the proton chemical gradient generated by the respiratory chain [93]. The null mutant is unable to respire on glycerol as the only carbon source [92].

These two interaction coupled with an altered sterol profile could presumable account for the elevation in petite formation. It is unclear how this proteins interact with one another and how this interaction negatively affects respiration.

Growth on MMS

It has been reported that haploid cells of the *dap1*Δ mutant strain are sensitive to treatment with MMS [66] and even hypersensitive by the same lab [103]. MMS is a DNA damaging agent. It causes double stranded DNA to be methylated, causing the replication fork to stall during S phase, leading to double stranded DNA breaks. To verify this sensitivity and to determine how cells of the *ypr118w*Δ mutant strain and cells of the *dap1*Δ*/ypr118w*Δ double mutant strain reacted to treatment with MMS, a sensitivity experiment was performed. It was observed that cells of the *dap1*Δ mutant strain are slightly sensitive, but not hyper-sensitive, to MMS treatment, see Figure 15. Cells of the *dap1*Δ mutant strain exhibited a slight sensitivity to media containing 0.01% MMS (v/v) and marked sensitivity to media containing 0.025% MMS (v/v) as compared to control cells grown on same media. Cells of the *ypr118w*Δ mutant strain did not exhibit any significant deviation from cells of the control strain. Cells of the *dap1*Δ*/ypr118w*Δ double mutant strain were about equally sensitive as cells of the *dap1*Δ mutant strain.

One could propose the reason for this has to do with DNA damage repair, however further work would have to be done in this area to verify or specify this functionality for Dap1p. It has been reported that Dap1p does in fact have some role in DNA damage repair [66], hence its name, that Dap1p is required in order to progress through the G_1-S transition following MMS induced DNA damage. Further evidence supports this view; it has been demonstrated that Dap1p interacts with Tfb1p [94], a component of the RNA polymerase II transcription initiation factor TFIIH, which is involved in nucleotide excision repair and transcription [95].

Localization of Proteins

Dap1p-GFP localizes to the cytosol; see Figures 16 and 17. This protein was seen mostly in lipid bodies, which is consistent with previous studies done on Dap1p [22,66,69], but here evidence is presented that suggest it can also be localized to the E.R. The protein-GFP studies done at UCSF support this claim that Dap1p is localized to both lipid bodies and the ER [69]. Most of the enzymes involved in the ergosterol biosynthetic pathway are localized to the ER, but several of the enzymes are also localized to lipid particles, in particular, Erg1p, Erg7p, and Erg6p. Also, there is evidence to suggest that Erg27p interacts with Erg7p in the ER and also in lipid particles. The localization pattern of Dap1p-GFP, as seen under the confocal microscope, suggest that it can localize peri-nuclearly; see Figures 21 and 22. Furthermore, it has been demonstrated that Dap1p interacts with Erg11p [96], a protein located on the ER. Erg11p is an enzyme in the ergosterol biosynthetic pathway that functions as a squalene epoxidase, catalyzing the conversion of squalene into squalene epoxide.

Ypr118w-RFP2 localizes to the cytosol, is present in lipid bodies (see Figures 18 and 19), and also co-localizes with Dap1p-GFP when the two proteins are expressed together; see Figures 23 and 24. The co-localization is not mutually inclusive; there can be the presence of one protein without the presence of the other, but major overlap is seen.

Upon treatment of MMS, Dap1p-GFP is still localized to the cytosol, but a greater proportion became localized peri-nuclearly; see Figures 21 and 22. The percentage seems to change between 10 and 15 minutes and the highest percentage seemed to be produced between 15 and 30 minutes of treatment with MMS, but was still apparent after

60 minutes of treatment; see Table 3. Location was termed peri-nuclear and not nuclear since limitations do exist with the confocal; however overlap was seen on the confocal microscope. The nucleus in yeast is about 1-2μm and the smallest focal cell of the confocal used is about 1μm. Accordingly, overlap appears to have occurred between the two; however in reality they could be adjacent, and not coinciding. The patterns of localizations of Dap1p-GFP exhibited in these yeast cells do not suggest the protein is localized to the nucleus, although overlap is indeed seen on the confocal microscope.

Hpr6.6 was localized on the ER in HeLa cells; see Figure 25. Which is consistent with studies done with the porcine MAPR homologue, mPR, which localized on the ER [67,68]. Treatment with MMS did not cause any differential location as seen in the yeast MAPR homologue Dap1p-GFP. The reason for this difference is unclear. Perhaps, the reason is simply that Hpr6.6 is already located on the ER and not located in lipid bodies. Therefore Hpr6.6 does not need to translocate, in order to achieve its role, if any, in DNA damage response. Or perhaps even simpler, it has nothing to do with DNA damage, even though its yeast homologue Dap1p does. It is thought the trans-membrane region in the N-terminal on Hpr6.6p is responsible for its specific localization.

Sterol Profiles

As compared to the control strain the *dap1*Δ mutant strain exhibited a significant alteration of sterol profile. The most striking noticeable difference was the appearance of an additional unidentified sterol peak very close in retention time to ergosterol. Mass fragmentation pattern analysis identified this compound to have a molecular ion of m/z = 466; an ergosterol skeleton with four double bonds. Two of these double bonds were localized to the side chain, presumably the positions can be assumed as 22E, 24(28) since

ergosta-5,7,22E,24(28)-tetraen-3-ol is the only intermediate in the ergosterol biosynthetic pathway which has two double bonds in the side chain. The localization of the two double bonds in the rings remains to be elucidated. This peak disappears upon rescue with Dap1p under the constitutive promoter Gpd, and with the human MAPR homologue Hpr6.6 under the control of the copper promoter, CUP1. Perhaps of particular importance, this compound was only present in the free sterol fraction and not the steryl ester fraction. The question needs to be addressed as to why it is only present in the free sterol form. Further experiments will need to be done in order to verify if the localization of this molecule is constant throughout the cell or specific to either the plasma membrane or to any internal membranes. Also, the significance of the absence of Dap1p in the formation of this compound needs to be addressed.

As compared to the control strain the *dap1*Δ mutant strain exhibited an 11.8% and a 10.5% decrease in total sterol content for 1 and 2 day old cultures, respectively. This decrease was mostly due to the steryl ester fraction which exhibited a decrease of 16.4% and 17.2% of sterol content for 1 and 2 day old cultures, respectively. Not only was the total sterol content affected, but the profile of individual sterols was also affected. In the free sterol fraction, the most significant changes include zymosterol which increased to almost double the amount in 2 day old cultures. Fecosterol was decreased in the *dap1*Δ mutant strain. In the ergosterol biosynthetic pathway, Erg6p catalyzes the conversion of zymosterol into fecosterol. Erg6p is located in lipid particles, where Dap1p is predominantly located, which suggests a connection between Erg6p function and Dap1p. The fact that sterol conversion does not stop at zymosterol, suggest that Erg6p can function without the help of Dap1p, although in a reduced capacity.

In the steryl ester fraction, the most significant differences were in the unidentified sterols, particularly peak #13, #14 which was increased in the *dap1*Δ mutant strain, and #16 which was decreased. The significance of this notable change in the unidentified sterols remains to be elucidated. Significant differences were also seen in ergosta-5,7,24,(28)-trien-3β-ol and ergosta-5,7,22,24,(28)-tetraen-3β-ol which were increased, ergosterol is also increased in 1 day old cultures, but decreased significantly in 2 day old cultures. These are the last three sterols in the ergosterol biosynthetic pathway. Couple this with a slight increase of ergosta-5,7,24,(28)-trien-3β-ol and ergosta-5,7,22,24,(28)-tetraen-3β-ol in the free sterol fraction with a decrease of ergosterol, suggests the production of ergosterol is being hindered at the very last step in the pathway. This also suggests that these intermediates were being stored instead of being used for membrane biogenesis. The fact that esterified ergosterol was similar to the control strain in 1 day old cultures, but significantly decreased in 2 day old cultures suggests a lag time response for this process.

Rescue Experiment

When Dap1p was expressed in the *dap1*Δ mutant strain under the constitutive promoter, Gpd, the sterol profile once again changed, but did not match the control strain exactly; see Figures 29 and 30. Partial rescue of the altered sterol profile might be caused by two reasons; use of a constitutive promoter and plasmid loss. The addition of Dap1p to the *dap1*Δ mutant strain was not done using its native promoter, but a constitutive promoter overexpressing *DAP1*, this difference in level could account for differences in sterol levels. Also, *DAP1* was introduced via a plasmid. Evidence suggests up to 30% of

cells can achieve plasmid loss in liquid cultures even under stringent selective media. This is a more likely scenario as to why sterol levels did not match the control levels. With the addition of Dap1p, zymosterol levels decreased significantly and fecosterol levels increased, once again suggesting a connection between Dap1p and Erg6p. Lanosterol also increased significantly. In the *dap1*Δ mutant strain, lanosterol levels matched the control strain very well in both the free sterol fraction and the steryl ester fraction. Lanosterol production is under the control of Erg7p, which is also localized to lipid particles. This suggests a connection between Dap1p and Erg7p. In fact, in 1 day old cultures every sterol in the free sterol fraction was increased or maintained similar levels upon addition of Dap1p in the *dap1*Δ mutant strain, with the exception of zymosterol which was severely decreased. This holds true for 2 day old cultures as well, with the exception of fecosterol, the sterol made directly from zymosterol. Taking this a step further, Erg6p is the first enzyme in the ergosterol biosynthetic pathway that is not essential for viability, meaning that cells can survive with zymosterol and not ergosterol as the primary sterol. This suggests zymosterol could possibly be used as an indicator sterol like ergosterol for sterol production; reduction of zymosterol levels could promote either enzyme transcription or post-transcriptional up-regulation of these enzymes through phosporylation, see references [97,98] for this kind of sterol regulation in mammalian cells. This could explain why every other sterol was present in a greater quantity, when zymosterol was decreased.

In the steryl ester fraction, the most significant changes occur in the unidentified peaks #10 and #16, upon addition of Dap1p in the *dap1*Δ mutant strain. Mass spectral analysis revealed unidentified peak #10 to have a molecular ion at m/z = 474, a

completely hydrated ergosterol skeleton, and unidentified peak #16 to have a molecular ion at m/z = 472, with one double bond in the side chain. Most of the other sterols maintain very similar quantitative levels. The significance that only these two peaks change significantly in the steryl ester fraction remains to be elucidated.

Hpr6.6 Homologue Experiment

Upon addition of Hpr6.6 to the control strain and the *dap1*Δ mutant strain, there was a very significant increase in ergosterol levels in both the free sterol fraction and the steryl ester fraction, see Figures 31 and 32. This accompanied a corresponding decrease in the quantity of all the other sterols, with a few exceptions. Interestingly in the control strain, ergosta-5,7,24,(28)-trien-3β-ol; ergosta-5,7,22,24,(28)-tetraen-3β-ol; which are the last two sterols before ergosterol; and 4,4-dimethylcholesta-8,24(28)-dien-3β-ol increased slightly. This was mirrored in the *dap1*Δ mutant strain, with the exception of ergosta-5,7,22,24,(28)-tetraen-3β-ol.

The fact that Hpr6.6 does not mirror the role *DAP1* has upon sterol synthesis perhaps has to do with the N-terminal transmembrane region in Hpr6.6, which Dap1p does not possess. The N-terminal transmembrane domain may cause retention of Hpr6.6 in the ER, whereas Dap1p localizes to lipid particles as well as the ER.

CONCLUSION

Dap1p belongs to a family of proteins that, although it has not been rigorously demonstrated *in vivo* or *in vitro*, is strongly suggestive of binding to certain steroids/sterols. Enzymes involved in the ergosterol biosynthetic pathway are located mostly in the ER, but some (Erg1p, Erg7p, Erg6p, and Erg27p) are also located in lipid bodies. Steryl esters are stored in lipid particles. Steryl ester hydrolases have the highest specific activity on the plasma membrane. Steryl esters somehow arrive at the plasma membrane where they are hydrolyzed to form the free sterol manifestation. It was not noticed that Dap1p-GFP localized to the plasma membrane. But, it has been demonstrated that Dap1p interacts with Pma1p [99] a plasma membrane H^+-ATPase that serves to regulate intracellular pH and generate the membrane potential across the plasma membrane [100]. The proteins and/or the process(s) that move the sterols from the ER to lipid bodies and back again, or from lipid bodies to the plasma membrane, or from the ER to the various cellular membranes are not known. Furthermore, the elements responsible for the translational and post-translational regulation of the enzymes directly involved in ergosterol production are also largely unknown.

The data presented here demonstrate that Dap1p localized to lipid particles and suggest it also localized to the ER, both sites of sterol synthesis. The data presented in this study demonstrates that Dap1p was involved in sterol processing, although its specific role is unknown. Two possible scenarios are proposed; one where Dap1p is involved in regulating the flux of sterols from one internal membrane to another, and another where Dap1p is involved in aberrant sterol pathways.

A number of structural isomers of known yeast sterols were identified in this study in both the control strain and to a greater extent in the *dap1*Δ mutant strain; see pp 105-113. Evidence for aberrant sterol production pathways in yeast has been recently verified [104]. The possible double bond positions in the aberrant sterols found in this study are consistent with the positions of the double bonds in the aberrant sterol pathways. Further work needs to be done to determine if Dap1p is directly involved in these aberrant sterol pathways or if the absence of Dap1p causes the upregulation of these pathways.

BIBLIOGRAPHY

1. **Zinser, E., Sperka-Gottlieb, C.D.M., Fasch, E.V., Kohlwein, S.D., Paltauf, F. and Daum, G.,** (1991) Phospholipid synthesis and lipid composition of subcellular membranes in the unicellular eukaryote *Saccharomyces cerevisiae*. *J. Bacteriol*. **173**:2026-2034.

2. **Zinser, E., Paltauf, F. and Daum, G.,** (1993) Sterol composition of yeast organelle membranes and subcellular distribution of enzymes involved in sterol metabolism. *J. Bacteriol*. **175**:2853-2858.

3. **Clark, L.H., Watson, C., Upchurch, S., McCormack, S., Padykula, H., Markaverich, B., and Hardin, J.W.,** (1980) Estrogen action in normal and abnormal cell growth In McLachlan J.A. Ed. Estrogen in the Enviroment. Amsterdam: Elsevier North Holland, Inc., p53.

4. **Mangeisdorf, D.J., Thummel, C., Beato, M., Herrlich, P., Schutz. G., Umesono, K., Blumberg, B., Kastner, P., Mark, M., Chambon, P., and Evans, R.M.,** (1995) The nuclear receptor superfamily: The second decade. *Cell* **83**:835-839.

5. **Groner, B., Hynes, N.E., Rahmsdorf, U., and Ponta, H.,** (1983) Transcription initiation of transfected mouse mammary tumor virus LTR DNA is regulated by glucocorticoid hormones. *Nucleic Acids Res.* **11**:4713-4725.

6. **Parks, L.W.,** (1978) Metabolism of sterols in yeast. *CRC Crit. Rev. Microbiol.* **6**:301-341.

7. **Seyle, H.,** (1941) Anaesthetic effects of steroid hormones. *Proc Soc Biol Med.* **46**:116-118.

8. **Falkenstein, E, Norman, A.W., and Wehling, M.,** (2000) Mannheim classification of nongenomically initiated (rapid) steroid actions. *J Clin Endocr Metab.* **85**:2072-2075.

9. **Evans, R.M.,** (1998) The steroid and thyroid hormone receptor superfamily. *Science* **240**:889-895.

10. **Williams, S.P., and Sigler, P.B.,** (1998) Atomic structure of progesterone complexed with its receptor. *Nature* **393**:392-396.

11. **Blackmore, P.F., Beebe, S.J., Danforth, D.R., and Alexander, M.,** (1990) Progesterone and 17 alpha-hydroxyprogesterone. Novel stimulators of calcium influx in human sperm. *J. Biol. Chem.* **265**:1376-1380.

12. **Turner, K.O., and Meizel, S.,** (1995) Progesterone-mediated efflux of cytosolic chloride during human sperm acrosome reaction. *Biochem. Biophys. Res. Commun.* **213**:774-780.

13. **Waldegger, S., Beisse, F., Apfel, H., Breit, S., Kolb, H.A., Haussinger, D., and Lang, F.,** (1995) Electrophysical effects of progesterone on hepatocytes. *Biochim. Biophys. Acta* **1266**:186-190.

14. **Wasserman, W.J., Pinto, L.H., O'Conner, C.M., and Smith, L.D.,** (1980) Progesterone induces a rapid increase in $[Ca^{2+}]_{in}$ of *Xenopus laevis* oocytes. *Proc. Natl. Acad. Sci.* USA. **77**:1534-1536.

15. **Lan, N.C., Bolger, M.B., and Gee, K.W.,** (1991) Identification and characterization of a pregnane steroid recognition site that is functionally coupled to an expressed $GABA_A$ receptor. *Neurochem. Res.* **16**:347-356.

16. **Grazzini, E., Guillon, G., Mouillac, B., and Zingg, H.H.,** (1998) Inhibition of oxytocin receptor function by direct binding of progesterone. *Nature.* **392**:509-512.

17. **Wehling, M.,** (1995) Looking beyond the dogma of genomic steroid action: insights and facts of the 1990s. *J. Mol. Med.* **73**:439-447.

18. **Falkenstein, E., Meyer, C., Eisen, C., Scriba, P.C., and Wehling, M.,** (1996) Full-lentgh cDNA sequence of a progesterone membrane-binding protein from porcine vascular smooth muscle cells. *Biochem. Biophys. Res. Commum.* **229**:86-89.

19. **Gerdes, D., Wehling, M., Leube, B., and Falkenstein, E.,** (1998) Cloning and tissue expression of two putative steroid membrane receptors. *Biol Chem.* **379**:907-911.

20. **Nolte, I., Jeckel, D., Wieland, F.T., and Sohn, K.,** (2000) Localization and topology of ratp28, a member of a novel family of putative steroid-binding proteins. *Biochem. Biophys. Acta* **1543**:123-130.

21. **Kwon, S., Lunn, R.M., O'Brien, D.A., Bell, D.A., and Eddy, E.M.,** (1998) *Biol. Reprod. Supplement* 1, p. 78.

22. **Gray, P.N.,** (2001) Characterization of the membrane associated progesterone receptor (MAPR) homologues in *Saccharomyces cerevisiae* and *Arabidopsis Thaliana*. Thesis, Georgia Institute of Technology.

23. **Mifsud, W., and Bateman, A.,** (2002) Membrane-bound progesterone receptors contain a cytochrome b5-like ligand-binding domain. *Genome Biology* **3**(12):1-5.

24. **Falkenstein, E., Heck, M., Gerdes, D., Grube, D., Christ, M., Weigel, M., Buddhikot, M., Meizel, S., and Wehling, M.,** (1999) Specific progesterone binding to a membrane protein and related nongenomic effects on Ca^{2+} fluxes in sperm. *Endocrinology* **140**:5999-6002.

25. **Meyer, C., Schmid, R., Scriba, P.C., and Wehling, M.,** (1996) Purification and partial sequencing of high-affinity progesterone-binding site(s) from porcine liver membranes. *Eur. J. Biochem.* **239**:726-731.

26. **Buddhikot, M., Falkenstein, E., Wehling, M., and Meizel, S.,** (1999) Recognition of a human sperm surface protein involved in the progesterone-initiated acrosome reaction by antisera against an endomembrane progesterone binding protein from porcine liver. *Mol. Cell Endocrinol.* **158**:187-193.

27. **Falkenstein, E., Schmibding, K., Lange, A., Meyer, C., Gerdes, D., Welsch, U., and Wehling, M.,** (1998) Localization of a putative progesterone membrane binding protein in porcine hepatocytes. *Cell. Mol. Biol.* **44**:571-578.

28. **Krebs, C.J., Jarvis, E.D., Chan. J., Lydon. J.P., Ogawa, S., and Pfaff. D.W.,** (2000) A membrane-associated progesterone-binding protein, 25-Dx, is regulated by progesterone in brain regions involved in femaile reproductive behaviors. *Proc. Nat. Acad. Sci.* USA **97**:12816-12821.

29. **Runko, E., Wideman, C., and Kaprielian, Z.,** (1999) Cloning and Expression of VEMA: A Novel Ventral Midline Antigen in the Rat CNS. *Mol. Cell. Neuro.* **14**:428-443.

30. **Raza, F.S., Takemori, H., Tojo, H., Okamoto, M., Vinson, G.P.**, (2001) Identification of the rat adrenal zona fsciculata/reticularis specific protein, inner zone antigen (IZAg), as the putative membrane progesterone receptor. *Eur. J. Biochem.* **268**:2141-2147.

31. **Radisky, E., and Poulter, C.D.,** (2000) Squalene synthase: steady-state, pre-state, and isotope-trapping studies. *Biochem.* **39**: 1748-1760.

32. **Gemmerich, A.R.,** (1981) Ultrastructure and enzymatic studies on the development of microbodies in germinating spores of the fern *Anemia phyllitidis*. *Z. Pflanzenphysiol*. **226**:497-509.

33. **Jayaram, A., Bal, A.K.,** (1991) Oleosomes (lipid bodies) in nitrogen-fixing peanut nodules. *Plant Cell Environ.* **14**:195-203.

34. **Christiansen, K., and Jensen, P.K.,** (1972) Membrane bound lipid particles from beef heart. Chemical composition and structure. *Biochim. Biophys. Acta* **260**:449-459.

35. **Clausen, M.K., Christiansen, K., Jensen, P.K., and Behnke, O.,** (1974) Isolation of lipid particles from baker's yeast (*Saccharomyces cerevisiae*). *FEBS Lett.* **43**:176-179.

36. **Athenstaedt, K., Zweytick, D., Jandrositz, A., Kohlwein, S.D., and Daum, G.,** (1999) Identification and characterization of major lipid particle proteins of the yeast *Saccharomyces cerevisiae*. *J. Bacteriol.* **181**:6441-6448.

37. **Schatz, G.,** (1979) How mitochondria import proteins from the cytoplasm. *FEBS Lett.* **103**:203-211.

38. **Neupert, W., and Schatz, G.,** (1981) How proteins are transported into mitochondria. *Trends Biochem. Sci*. **6**:1-4.

39. **Gasser, S.M., Daum, G., and Schatz, G.,** (1982) *J. Biol. Chem.* **257**:13034-13041.

40. **Scheiter, R.,** (1999) Electrospray ionization tandem mass spectrometry (E.S.I.-M.S./M.S.) analysis of the lipid molecular species composition of yeast subcellular membranes reveals acyl chain-based sorting/remodeling of distinct molecular species en route to the plasma membrane. *J. Cell Biol*. **146**:741-754.

41. **Lees, N.D., Bard, M., and Kirsch, D.R.,** (1999) Biochemistry and molecular biology of sterol synthesis in *Saccharomyces cerevisiae*. *Crit. Rev. Biochem. Mol. Biol.* **34**:33-47.

42. **Nes, W.D., Xu, S.H., and Haddon, W.F.** (1989) Evidence for similarities and differences in the biosynthesis of fungal sterols. *Steroids* **53**:533-558.

43. **Arthington, B.A., Bennett, L.G., Skatrud, P.L., Guyun, C.J., Barbuch, R.J., Ulbright, C.E., and Bard, M.,** (1991) Cloning, disruption and sequence of the gene encoding yeast C-5 sterol desaturase. *Gene* **102**:39-44.

44. **Barton, D.H.R., Ganatilaka, A.A.L., Jarman, T.R., Widdowson, D.A., Bard, M., and Woods, R.A.,** (1975) Biosynthesis of terpenes and steroids. Part X. The sterols of some yeast mutants doubly defective in ergosterol biosynthesis. *J. Chem. Soc,* Perkin 1, 88-92.

45. **Ashman, W.H., Barbuch, R.J., Ulbright, C.E., Jarret, H.W., and Bard, M.,** (1991) Cloning and disruption of the yeast C-8 sterol isomerase gene. *Lipids* **26**:628-632.

46. **Lorentz, R.T., and Parks L.W.,** (1991) Physiological effects of fenpropimorph on wild-type *Saccharomyces cerevisiae* and fenpropimorph-resistant mutants. *Antimicrob. Agents Chemother* **35**:1532-1537.

47. **Campagnoni, C., Holmlumd, C.E., and Whittaker, N.,** (1977) The effect of triparanol on the composition of free and esterified sterols of *Saccharomyces cerevisiae*. *Arch. Biochem. Biophys.* **184**:555-560.

48. **Rodriguez, R.J., and Parks, L.W.,** (1983) Structural and physiological features of sterols necessary to satisfy bulk membrane and sparking requirements in yeast sterol auxotrophs. *Arch. Biochem. Biophys.* **225**:861-871.

49. **Munn, A.L., HeesePeck, A., Stevenson, B.J., Pichler, H., and Riezman, H.,** (1999) Specific sterols required for the internalization step of endocytosis in yeast. *Mol. Biol. Cell* **10**:3943-3957.

50. **Rietveld, A., and Simons, K.,** (1998) The different miscibility of lipids as the basis for the formation of functional membrane rafts. *Biochem. Biophys. Res. Commun.* **1376**:467-479.

51. **Bagnat, M., Keranen, S., Shevchenko, A., and Simons, K.,** (2000) Lipid rafts function in biosynthetic delivery of proteins to the cell surface in yeast. *Proc. Natl. Acad. Sci.* USA **97**:3254-3259.

52. **Reinhart, M.P.,** (1990) Intracellular sterol trafficking. *Experientia* **46**:599-611.

53. **Colbeer, T., and Threfall, D.R.,** (1989) Biosynthesis of terpenoid lipids, p. 116, In C. Ratledge and S.G. Wilkinson (ed.) Microbial lipids, Academic Press, Inc., New York.

54. **Taylor, F.R., and Parks, L.W.,** (1978) Metabolic interconversion of free sterols and steryl esters in *Saccharomyces cerevisiae*. *J. Bacteriol.* **136**:531-537.

55. **Zweytick, D., Hrastnik, C., Kohlwein, S.D., and Daum, G.,** (2000) Biochemical characterization and subcellular localization of the sterol C-24(28) reductase, Erg4p, from the yeast *Saccharomyces cerevisiae*. *FEBS Lett.* **470**:83-87.

56. **Paultauf, F., Kohlwein, S.D., and Henry, S.A.,** (1992) The Molecular and Cellular Biology of the Yeast *Saccharomyces cerevisiae*: Gene Expression, pp. 415-500, Cold Spring Harbor Laboratory Press, Cold Spring Harbor.

57. **Leber, R., Zinser, E., Zellnig, G., Paltauf, F., and Daum, G.,** (1994) Characterization of the lipid particles of the yeast, *Saccharomyces cerevisiae*. *Yeast* **10**:1421-1428.

58. **Lewis, T.A., Rodriguez, R.J., and Parks, L.W.,** (1987) Relationship between intracellular sterol content and sterol esterification and hydrolysis in *Saccharomyces cerevisiae*. *Biochim. Biophys. Acta* **921**:205-212.

59. **Billheimer, J.T., and Reinhart, M.P.,** (1990) In Subcellular Biochemistry-Intracellular Transfer of Lipid Molecules (Hilderson, H.J., ed.), pp. 301-331, Plenum Press, New York.

60. **Reinhart, M.P.,** (1990) Intracellular sterol trafficking. *Experientia* **46**:599-611.

61. **Leber, R., Zinser, E., Hrastnik, C., Paltauf, F., and Daum, G.,** (1995) Export of steryl esters from lipid particles and release of free sterols in the yeast, *Saccharomyces cerevisiae*. *Biochim. Biophys. Acta* **1234**:119-126.

62. **Bailey, R.B., and Parks, L.W.,** (1975) Yeast sterol esters and their relationship to the growth of yeast. *J. Bacteriol.* **124**:606-612.

63. **Zweytick, D., Leitner, E., Kohlwein, S.D., Yu, C., Rothblatt, J., and Daum, G.,** (2000) Contribution of Are1p and Are2p to steryl ester synthesis in the yeast *Saccharomyces cerevisiae*. *Eur. J. Biochem.* **267**:1075-1082.

64. **Daum, G.,** (1985) Lipids of mitochondria. *Biochem. Biophys. Acta* **822**:1-42.

65. **Tuller, G., and Daum, G.,** (1995) Import of sterols into mitochondria of the yeast *Saccharomyces cerevisiae*. *FEBS Lett.* **372**:29-32.

66. **Hand, R.A., Jia, N., Bard, M., and Craven, R.J.,** (2003) *Saccharomyces cerevisiae* Dap1p, a novel DNA damage response protein related to the mammalian membrane-associated progesterone receptor. *Eukary. Cell* 2:306-317.

67. **Ke, F.C., and Ramirez, V.D.,** (1990) Binding of progesterone to nerve cell membranes of rat brain using progesterone conjugated to 125I-bovine serum albumin as a ligand. *Biol. Reprod.* **49**:980-988.

68. **Ozaki, T., Nakamura, Y., Enomoto, H., Hirose, M., and Sakiyama, S.,** (1995) *Cancer Res.* **55**:895-900.

69. Yeast protein-GFP localization study at UCSF. http://yeastgfp.ucsf.edu/getOrf.php?orf=YPL170W

70. **Leber, R., Landl, K., Zinser, E., Ahorn, H., Spök, A., Kohlwein, S.D., Turnowsky, F., and Daum, G.,** (1998) Dual localization of squalene epoxidase, Erg1p, in yeast reflects a relationship between the endoplasmic reticulum and lipid particles. *Mol. Biol. Cell* **9**: 375-386.

71. **Milla, P., Athenstaedt, K., Viola, F., Oliaro-Bosso, S., Kohlwein, S.D., Daum, G., and Balliano, G.,** (2002) Yeast oxidosqualene cyclase (Erg7p) is a major component of lipid particles. *J. Biol. Chem.* **277**:2406-2412.

72. **Leber, R., Zenz, R., Shröttner, K., Fuchsbichler, S., Pühringer, B., and Turnowsky, F.,** (2001) A novel sequence element is involved in the transcriptional

regulation of expression of the *ERG1* (squalene epoxidase) gene in *Saccharomyces cerevisiae*. *Eur. J. Biochem.* **268**: 914-924.

73. **Daum, G., Lees, N.D., Bard, M., and Dickson, R.,** (1998) Biochemistry, Cell Biology and Molecular Biology of Lipids of *Saccharomyces cerevisiae*. *Yeast* **14**: 1471-1510.

74. **Smith, S.J., and Parks. L.W.,** (1993) The *ERG3* gene in *Saccharomyces cerevisiae* is required for the utilization of respiratory substrates and in heme-deficient cells. *Yeast* **9**:1177-1187.

75. **Smith, S.J., and Parks. L.W.,** (1997) Requirements of heme to replace the sparking sterol function in the yeast *Saccharomyces cerevisiae*. *Biochim. Biophys. Acta* **1345**:71-76.

76. **Dahl, C., Biemann, H.P., and Dahl, J.,** (1987) A protein kinase antigenically related to pp60 *src* possibly involved in yeast cell cycle control: positive *in vivo* regulation of sterol. *Proc. Natl. Acad. Sci.* USA **84**:4012-4016.

77. **Lorenz, R.T., Rodriguez, R.J., Lewis, T.A., and Parks, L.W.,** (1986) Characteristics of sterol uptake in *Saccharomyces cerevisiae*. *J. Bacteriol.* **167**: 981-985.

78. Yeast protein-GFP localization study at UCSF. http://yeastgfp.ucsf.edu/getOrf.php?orf=YHR007C

79. Yeast GRID resource http://biodata.mshri.on.ca/yeast_grid/servlet/SearchResults?keywords=YHR007C

80. **Kontoyiannis, D.P.,** (2000) Modulation of fluconazole sensitivity by the interaction of mitochondria and Erg3p in *Saccharomyces cerevisiae*. *J. Antimicro. Chemo.* **46**: 191-197.

81. **Mo, C., Milla, P., Athenstaedt, K., Ott, R., Balliano, G., Daum, G., and Bard, M.,** (2003) In yeast sterol biosynthesis the 3-keto reductase protein (Erg27p) is required for oxidosualene cyclase (Erg7p) activity. *Biochim. Biophys. Acta* **1633**: 68-74.

82. **Mo, C., Valachovic, M., Bard, M.,** (2004) The *ERG28*-encoded protein, Erg28p, interacts with both the sterol C-4 demethylation enzyme complex as well as the late biosynthetic protein, the C-24 sterol methyltransferase (Erg6p). *Biochim. Biophys. Acta* Atricle in Press.

83. **Bard, M., Bruner, D.A., Pierson, C.A., Lees, N.D., Biermann, B., Frye, L., Koegel, C., and Barbuch, R.,** (1996) Cloning and chatacterization of *ERG25*, the *Saccharomyces cerevisiae* gene encoding C-4 sterol methyl oxidase. *Proc. Natl. Acad. Sci.* USA **93**: 186-190.

84. **Bard, M., Downing, J.F.,** (1981) Genetic and biochemical aspects of yeast sterol regulation involving 3-hydroxy-3-methylglutaryl coenzyme A reductase. *J. Gen. Microbiol.* **125**: 415-20.

85. **Bitter, G.A., and Egan, K.M.,** (1984) Expression of heterologous genes in *Saccharomyces cerevisiae* from vectors utilizing the glyceraldehydes-3-phosphate dehydrogenase gene promoter. *Gene* **32**: 263-274.

86. **Bumann, M., Djafarzadeh, S., Oberholzer, A.E., Bigler, P., Altmann, M., Trachsel, H., Baumann, U.,** (2004) Crystal Structure of Yeast Ypr118w, a Methylthioribose-1-phosphate Isomerase Related to Regulatory eIF2B Subunits. *J. Biol. Chem.* **279**: 37087-37094.

87. Yeast GRID resource http://biodata.mshri.on.ca/yeast_grid/servlet/SearchResults?keywords=DAP1

88. **Bourne, H.R., Sanders, D.A., and McCormick, F.,** (1991) The GTPase superfamily: conserved structure and molecular mechanism. *Nature* **349**: 117-127.

89. **Caldon, C.E., Yoong, P., and March, P.E.,** (2001) Evolution of a molecular switch: universal bacterial GTPase regulate ribosome function. *Mol. Micro.* **41**: 289-297.

90. **Bourne, H.R.,** (1995) GTPase: a family of molecular switches and clocks. *Phil. Trans. R. Soc. London* **349**: 283-289.

91. Yeast GRID resource http://biodata.mshri.on.ca/yeast_grid/servlet/SearchResults?keywords=ypr118w

92. **Arselin, G., Vaillier, J., Graves, P., and Velours, J.,** (1996) ATP Synthase of Yeast Mitochondria. *J. Biol. Chem.* **271**: 20284-20290.

93. **Senior, A.E.,** (1988) *Physiol. Rev.* **68**: 177-231.

94. Yeast GRID resource http://biodata.mshri.on.ca/yeast_grid/servlet/SearchResults?keywords=DAP1

95. **Feaver, W.J., Henry. N.L., Wang, Z., Wu, X., Svejstrup, J.Q., Bushnell, D.A., Friedberg, E.,C., and Kornberg, R.D.,** (1997) Genes for Tfb2, Tfb3, and Tfb4 Subunits of Yeast Transcription/Repair Factor IIH. *J. Biol. Chem.* **272**: 19319-19327.

96. Yeast GRID resource http://biodata.mshri.on.ca/yeast_grid/servlet/SearchResults?keywords=DAP1

97. **Brown, M.S., and Goldstein, J.L.,** (1999) A proteolytic pathway that controls the cholesterol content of membranes, cells, and blood. *Proc. Natl. Acad. Sci.* USA **96**: 11041-11048.

98. **Goldstein, J.L., and Brown, M.S.,** (1990) Regulation of the mevalonate pathway. *Nature* **343**: 425-430.

99. Yeast GRID resource http://biodata.mshri.on.ca/yeast_grid/servlet/SearchResults?keywords=DAP1

100. **Gong, X., and Chang, A.,** (2001) A mutant plasma membrane ATPase, Pma1-10, is defective in stability at the yeast cell surface. *Proc. Natl. Acad. Sci.* USA **98**: 9104-9109.

101. **Bligh, E.G., and Dyer, W.J.,** (1959) A rapid method of total lipid extraction and purification. *Can. J. Physiol.* **37**: 911-917.

102. **Folch, J, Lees, M., Sloane, Stanley G.H.,** (1957) A simple method for the isolation and purification of total lipides from animal tissues. *J. Biol. Chem.* **226**: 497-509.

103. **Hand, R.A., and Craven, R.J.,** (2003) Hpr6.6 mediates cell death in oxidative damage in MCF-7 human breast cancer cells. *J. Cell. Biochem.* **90**: 534-547.

104. **Ruan, B., Lai, P.S., Yeh, C.W., Wilson, W.K., Pang, J., Xu, R., Matsuda, S.P.T., and Schroepfer, G.J.,** (2002) Alternative pathways of sterol synthesis in yeast: Use of C27 sterol tracers to study aberrant double-bond migrations and evaluate their relative importance. *Steroids* **67**: 1109-1119.

105. **Nes, W.D., McCourt, B.S., Marshall, J.A., Ma, J., Dennis, A.L., Lopez, M., Li, H., and He, L.,** (1999) Site-directed mutagenesis of the sterol methyl transferase active site from *Saccharomyces cerevisiae*: results in formation of novel 24-ethyl sterols. *J. Org. Chem.* **64**: 1535-1542.

106. **Min, L., Takemori, H., Nonaka, Y., Katoh, Y., Doi, J., Horike, N., Osamu, H., Raza, F.S., Vinson, G.P., and Okamoto M.,** (2004) Characterization of the adrenal-specific antigen IZA (inner zone antigen) and its role in the steroidogenesis. *Mol. Cell. Endocrin.* **215**: 143-148.

107. ACD/NIST MS Database. http://www.acdlabs.com/products/spec_lab/exp_spectra/spec_libraries/nist_ms.html

108. Palisade complete MS Library 600K. http://www.palisade-ms.com/complete.htm

109. **Gerst, N., Ruan, B., Pang, J., Wilson, W.K., and Schroepfer, Jr., G.J.,** (1997) An updated look at the analysis of unsaturated C27 sterols by gas chromatography and mass spectrometry. *J. Lipid Res.* **38**: 1685-1701.

110. **Sakamoto, H., Ukena, K., Takemori, H., Okamoto, M., Kawata, M., and Tsutsui, K.,** (2004) Expression and localization of 25-Dx, a membrane-associated putative progesterone-binding protein, in the developing Purkinje cell. *Neuroscience* **126**: 325-334.

111. **Ho, Y., Gruhler, A., Heilbut, A., Bader, G.D., Moore, L., Adams, S.L., Millar, A., Taylor, P., Bennett, K., Boutilier, K., Yang, L., Wolting, C., Donaldson, I., Schandorff, S., Shewnarane, J., Vo, M., Taggart, J., Goudreault, M., Muskat, B., Alfarano, C., Dewar, D., Lin, Z., Michalickova, K., Willems, A.R., Sassi, H., Nielsen, P.A., Rasmussen, K.J., Andersen, J.R., Johansen, L.E., Hansen, L.H., Jespersen, H., Podtelejnikov, A., Nielsen, E., Crawford, J., Poulsen, V., Sorensen, B.D., Matthiesen, J., Hendrickson, R.C., Gleeson, F., Pawson, T., Moran, M.F., Durocher, D., Mann, M., Hogue, CW., Figeys, D., and Tyers, M.,** (2002) Systematic identification of protein complexes in Saccharomyces cerevisiae by mass spectrometry. *Nature* **415**:180-183.

112. **Parsons, A.B,, Brost, R.L., Ding, H., Li, Z., Zhang, C., Sheikh, B., Brown, G.W., Kane, P.M., Hughes, T.R., Boone, C.,** (2004) Integration of chemical-genetic and genetic interaction data links bioactive compounds to cellular target pathways. *Nat. Biotechnol.* **22**:62-69.

113. **Ito, T., Chiba, T., Ozawa, R., Yoshida, M., Hattori, M., and Sakaki, Y.,** (2001) A comprehensive two-hybrid analysis to explore the yeast protein interactome. *Proc. Natl. Acad. Sci.* U S A **98**:4569-4574.

114. **Gasch, A.P., Spellman, P.T., Kao, C.M., Carmel-Harel, O., Eisen, M.B., Storz, G., Botstein, D., Brown, P.O.,** (2000) Genomic expression programs in the response of Yeast cells to environmental changes. *Mol. Biol. Cell* **11**:4241-4257.

115. **Gaber, R.F., Copple, D.M., Kennedy, B.K., Vidal, M., Bard, M.,** (1989) The yeast gene ERG6 is required for normal membrane function but is not essential for biosynthesis of the cell-cycle-sparking sterol. *Mol. Cell. Biol.* **9**:3447-3456.